Supercontinental Inheritance and its Influence on Supercontinental Breakup: The Central Atlantic Magmatic Province and the Breakup of Pangea

Lisa M. Whalen

Thesis submitted to the faculty of the Virginia Polytechnic Institute and State University in partial fulfillment of the requirements for the degree of

Master of Science
In
Geosciences

Esteban Gazel
Mark J. Caddick
Phillip Prince

June 10th, 2016
Blacksburg, VA

Keywords: Large igneous province, Pangea, continental break-up, supercontinent

Supercontinental Inheritance and its Influence on Supercontinental Breakup: The Central Atlantic Magmatic Province and the Breakup of Pangea

Lisa M. Whalen

ABSTRACT

The Central Atlantic Magmatic Province (CAMP) is the large igneous province (LIP) that coincides with the breakup of the supercontinent Pangea. Major and trace element data, Sr-Nd-Pb radiogenic isotopes, and high-precision olivine chemistry were collected on primitive CAMP dikes from Virginia (VA). These new samples were used in conjunction with a global CAMP data set to elucidate different mechanisms for supercontinent breakup and LIP formation. On the Eastern North American Margin, CAMP flows are found primarily in rift basins that can be divided into northern or southern groups based on differences in tectonic evolution, rifting history, and supercontinental inheritance. Geochemical signatures of CAMP suggest an upper mantle source modified by subduction processes. We propose that the greater number of accretionary events, or metasomatism by sediment melts as opposed to fluids on the northern versus the southern Laurentian margin during the formation of Pangea led to different subduction-related signatures in the mantle source of the northern versus southern CAMP lavas. CAMP samples have elevated Ni and low Ca in olivine phenocrysts indicating a significant pyroxenite component in the source, interpreted here as a result of subduction metasomatism. Different collisional styles during the Alleghanian orogeny in the North and South may have led to the diachroneity of the rifting of Pangea. Furthermore, due to a low angle of subduction, the Rheic Plate may have underplated the lithosphere then delaminated, triggering both the breakup of Pangea and the formation of CAMP.

Dedication

This thesis is dedicated to my husband for reading me his geology textbook when I couldn't fall asleep in the hope that it would help. I've been wide-awake ever since with my mind stimulated by the wonderful complexity of our planet.

Acknowledgements

I would like to thank my husband, William Whalen for his support and encouragement at every step – I couldn't have done this without you. My brother, Daniel Ashley showed me that graduate school could be done and was worth it. My dad, Rick Ashley supported me through tough times and gave great advice. My mom, Laurie Ashley supported me early on in my college endeavor and instilled in me a love of the outdoors and science at an early age.

I would like to thank my advisor, Esteban Gazel for all of his encouragement and support. Thank you for giving an undergraduate such an interesting project!

I would also like to thank my co-authors and committee members Chris Vidito, John Puffer, Bill Henika and Mark Caddick as well as Phillip Prince for their wisdom, help and input.

A big thank you to the members of VT Volcanoes: Jarek Trela, Sarah Mazza, Pilar Madrigal, Denis Zamboni and Lowell Moore for their comments, instruction and guidance which helped me transition from an undergraduate to a graduate student.

Attributions

This thesis was published in the journal *Geochemistry, Geophysics, Geosystems* as "Whalen L, Gazel E, Vidito C, Puffer J, Bizimis M, Henika W, Caddick MJ (2015) Supercontinental inheritance and its influence on supercontinental breakup: The Central Atlantic Magmatic Province and the breakup of Pangea."

L. Whalen prepared sample powders that were then sent for analysis for major and trace elements at the GeoAnalytical Lab at Washington State University and at the Center for Elemental Mass Spectrometry at the University of South Carolina by M. Bizimis for radiogenic isotopes. L.Whalen also prepared samples to be sent to the New Mexico Geochronology Research Laboratory for age dating. L. Whalen mapped thick sections that were then analyzed with the electron microprobe for olivine phenocryst data by C. Vidito at Rutgers University. J. Puffer and B. Henika provided samples and valuable input on sample locations. L. Whalen drafted the manuscript and figures. All co-authors provided input on the drafting of the manuscript and figures. All interpretation and modeling of the data was done by L. Whalen and E. Gazel.

Table of Contents

List of Figures

List of Tables

Introduction

1.1 Large Igneous Provinces

Wilson cycles, or the formation and breakup of supercontinents, are an integral part of plate tectonics [Wilson, 1965, 1966]. However, a mechanism or trigger for initiating the breakup of the continental lithosphere is a fundamental missing piece of this unifying theory. Although large igneous province (LIP) formation has been linked to supercontinent breakup [Storey, 1995; Courtillot et al., 1999], the formation mechanisms of LIPs are still debated [King and Anderson, 1995; Lustrino, 2005; Campbell, 2007]. Nevertheless, some of the most significant mass extinction events in Earth's history correlate with LIPs [Courtillot and Renne, 2003] making LIP formation important not only for understanding mantle dynamics, but also for elucidating relationships between geological and biological processes during the evolution of our planet.

1.2 The Central Atlantic Magmatic Province

The Central Atlantic Magmatic Province (CAMP, Figure 1) is the LIP temporally related to the breakup of Pangea ~200 Ma [Marzoli et al., 1999; Blackburn et al., 2013] and is one of the largest LIPs in the geologic record, with a volume of 2.3 x 10^5 km^3 and a surficial area of 10^7 km^2 [McHone, 2003]. Thus, understanding the formation mechanism of CAMP can provide explanations for the formation of LIPs that share similar characteristics. Assessing the role of CAMP in the breakup of Pangea can also help to clarify the triggering mechanism responsible for the breakup of supercontinents. Some models for CAMP suggest that it may have formed from the impingement of a mantle plume on the lithosphere [e.g., May, 1971; Morgan, 1983; Anderson, 1982; White and McKenzie, 1989; Hill, 1991; Wilson, 1997; Courtillot et al., 1999; Ernst and Buchan, 2002; Fokin, 2003]. In this scenario, a hot mantle upwelling impacts the lithosphere, the plume head undergoes decompression, melts, and emplaces the LIP [e.g., White and McKenzie, 1989; Wilson, 1997]. This mechanism is problematic for CAMP because no active hot spot or hot spot trail can be linked to the province, nor are there clear geochemical signatures to indicate plume activity or excess mantle potential temperatures [McHone, 2000; Puffer, 2001; Herzberg and Gazel, 2009]. Thus, alternative explanations such as edge-driven convection (EDC) [King and Anderson, 1995] have also been proposed for CAMP initiation [McHone, 2000; Deckart et al., 2005; Merle et al., 2011].

EDC relies on the difference in thickness between the thinner edge of the continent and the thicker interior, forming a temperature gradient that drives small-scale convection cells [King and Anderson, 1995]. Delamination is another shallow formation mechanism that has been proposed for some continental LIPs [Lustrino, 2005]. Delamination occurs when denser lower crust, lithospheric mantle, or underplated material separates or breaks away as either a planar feature or a Rayleigh-Taylor instability and sinks into the asthenospheric mantle [Bird, 1979; Houseman et al., 1981; Conrad and Molnar, 1997; Houseman and Molnar, 1997; Kay and Kay, 1993; Schott and Schmeling, 1998]. The resulting influx of hot asthenosphere will melt due to decompression, producing uplift, extension, and rifting [Bird, 1979; Houseman et al., 1981; Conrad and Molnar, 1997; Houseman and Molnar, 1997; Kay and Kay, 1993; Schott and Schmeling, 1998].

The goal of this study was to provide a viable formation mechanism for CAMP that explains the large volume of melt produced, the relatively cool mantle potential temperatures, temporal and chemical evolution, as well as the relationship of this LIP to the breakup of Pangea. Despite the large amount of data available for some parts of CAMP there are limited data available for CAMP in Virginia. Therefore, diabase dikes were sampled from different locations around the Danville Triassic rift basin and in the Shenandoah Valley in southwest Virginia (GPS locations in Table 1). Our new data were combined with a more complete data set to address the formation mechanism of CAMP and its relationship to both the assembly and the breakup of Pangea. Additionally, our new samples from Virginia were used to assess the source components of CAMP using high-precision olivine chemistry [Sobolev et al., 2007] never applied to the LIP before.

1.3 Previous Work

Any attempt at assessing how Pangea broke up must examine if any of the inherited structures and/or chemical signatures from the breakup of the previous supercontinent, Rodinia, or protracted subduction leading to the formation of Pangea played a role. While previous authors [Schlische et al., 2003; Hatcher, 2010; Hibbard et al., 2010] have made huge strides toward a large-scale, integrated view of the breakup of Pangea, we combined their conclusions with some relatively new, relevant geophysical results [Benoit et al., 2014] and the results from our characterization of the source composition of CAMP samples from Virginia, allowing for a new look at the formation mechanism for CAMP and the breakup of Pangea.

1.4 Formation of Pangea: Differences in the Northern and Southern Appalachians

The Paleozoic Appalachian Orogeny records the multistage formation of the most recent supercontinent, Pangea through several accretionary events [Hatcher, 2010]. After the Middle Ordovician-age Taconic Orogeny [e.g., Hibbard et al., 2007; van Staal et al., 2009; Hatcher, 2010; Hibbard et al., 2010] these accretionary events are not evenly distributed across the Laurentian margin, thus Hibbard et al. [2010] suggested the use of the New York promontory as the division between the northern and southern Appalachians. During the Late Ordovician through the Early Devonian, the northern margin records the accretion of the Ganderia and Avalonia terranes while the southern margin records the accretion of the Carolina terrane [van Staal et al., 2009; Hibbard et al., 2010]. The terminal step in the formation of Pangea was the Alleghanian Orogeny that occurred during the Carboniferous period when Gondwana collided obliquely with the northern portion of the Laurentian margin, then rotated clockwise eventually resulting in a head-on collision between Gondwana and the southern portion of the Appalachians. This resulted in the accretion of the Meguma Terrane in the North and the Suwannee Terrane in the South [Hatcher, 2002].

1.5 Timing and Age Progression of CAMP Magmatism

Recent work by Blackburn et al. [2013] using high-precision U-Pb geochronology on zircons from CAMP basalts definitively linked CAMP with the End-Triassic Extinction as well as constrained the initiation of CAMP to the North as opposed to the South, as previously thought [Wilson, 1997; Schlische et al., 2003]. Furthermore, CAMP lavas decrease in age from North to South. High-titanium quartz normative lavas represent the first pulse of CAMP magmatism with an age of 201.566 6 0.031 (North Mt. Basalt, Fundy, Nova Scotia) [Blackburn et al., 2013]. Olivine normative lavas, found mostly in the South, are the youngest pulse and have an age of 200.916 6 0.064 (Butner intrusive, Deep River Basin, North Carolina) [Blackburn et al., 2013]. The rifting of Pangea proceeded in the opposite direction to CAMP magmatism, beginning first in the South [Schlische et al., 2003] (Figure 2).

1.6 Breakup of Pangea and CAMP Emplacement: Differences Between the Northern and Southern Appalachians

A series of fault-bounded rift basins related to the initial rifting of Pangea exist along the eastern margin of North America and the western margin of Africa [Olsen, 1997]. Significant differences between the basin history of the northern versus the southern Appalachians are evident through a comparison of the timing of sediment deposition between rift basins (Figure 2) [Olsen, 1997; Schlische et al., 2003]. In general, rifting began in the South and ended prior to the emplacement of CAMP basalts, depositing only Late Triassic-age strata [Schlische et al., 2003]. In the North, most CAMP flows thicken toward the upper border faults of rift basins indicating that they are late synrift flows [e.g., Olsen et al., 1989; Withjack et al., 1995]. Strata in the northern basins span the Triassic and Early Jurassic [Olsen et al., 1989; Olsen, 1997] with accelerated rates of sedimentation in the Jurassic [Olsen et al., 1989; Schlische and Olsen, 1990].

1.7 Supercontinental Inheritance From Rodinia

Rodinia, the supercontinent preceding Pangea, formed during the Grenville Orogeny (1.2–0.9 Ga) [Hatcher, 2010] and broke up over a 200 myr timespan, during which rifting occurred along what would become the eastern Laurentian margin [McClellan and Gazel, 2014]. Supercontinental inheritance, the geologic history of a previous supercontinent directing the evolution of its successor, is observed in the rifting record of the Newark, Gettysburg, Culpepper and Barboursville basins (Figures 1 and 2). Similarities between these basins have led to the suggestion that they represent one continuous basin [Faill, 2003] and collectively share specific traits with both the northern and southern rift basins. Like the southern basins, deposition in the Newark, Gettysburg, and Culpepper basins began in the Late Triassic, but in common with the northern basins they also contain Jurassic-age strata and synrift CAMP flows [Olsen, 1997].

These basins are located adjacent to the Pennsylvania salient, where the central Appalachian Mountains undergo a drastic change in strike [e.g., Lefort and Van der Voo, 1981; Wise, 2004; Ong et al., 2007]. Hibbard et al. [2010] suggested that the New York promontory, which separates first order distinctions between the two portions of the Appalachian orogen, might reflect an inherited structure related to the Neoproterozoic rifting of Rodinia. A failed Neoproterozoic rift was recently imaged adjacent to the Pennsylvania salient using wide-angle reflection and temporary broadband seismic data [Benoit et al., 2014]. The Scranton Rift is buried in the subsurface and based on adjacent fold and fault geometry, may have acted as a collisional ‘‘backstop’’ during the Alleghanian accretionary event, effectively shaping the Appalachian Orogeny [Benoit et al., 2014].

This Rodinia-related relic rift and associated underplated dense material [Benoit et al., 2014] were probably responsible for the change from oblique collision in the North to rotation and eventual head-on collision in the South during the Alleghanian Orogeny.

Furthermore, we propose that the transitional nature of the Newark, Gettysburg, and Culpepper basin histories [Schlische et al., 2003] are also due to this subsurface inherited feature which acted as a rigid ‘‘buffer’’ and effectively negated much of the uplift, which may have affected the northern and southern Appalachians throughout the Mesozoic [Frizon de Lamotte et al., 2015]. In this study we use the Scranton Rift to separate northern CAMP (located to the north of the Scranton Rift) [Dostal and Durning, 1998; Marzoli et al., 2011; Merle et al., 2013], southern CAMP (located to the south of the Scranton Rift [Callegaro et al., 2013; Mazza et al., 2014] and transitional CAMP (located within or nearby the Newark, Gettysburg, and Culpepper basins) [Marzoli et al., 2011; Merle et al., 2013].

Materials and Methods

2.1 Methods for Collected Data

Sample SPG-111 was selected for $^{40}Ar/^{39}Ar$ geochronology because it contained ample biotite, an ideal mineral to date with this method. The sample was crushed, and sieved. Biotite was separated using a magnetic separator, heavy liquids, and hand picking. After being washed with HCl, phenocryst biotite separates and the standard Fish Canyon tuff sanidine (FC-2) (assigned age = 28.02 Ma [Renne et al., 1998]) were irradiated for 40 hours at the USGS TRIGA reactor in Denver, Colorado. Bulk separates were analyzed using the incremental heating age spectrum method (15 steps per analysis) utilizing a Argus VI mass spectrometer and a defocused 50 watt diode laser at the New Mexico Geochronology Research Laboratory.

Rock chips free of alteration (oxides, zeolites, etc.) were selected under a stereoscopic microscope and powdered in an alumina mill at Virginia Tech. Samples were analyzed for major (wt. %) and trace elements (ppm) at the GeoAnalytical Lab at Washington State University. Major elements were collected by x-ray fluorescence (XRF) on a ThermoARL XRF following standard XRF procedures [Johnson et al., 1999]. Trace elements were collected on solutions by an Agilent model 4500 ICP-MS. Data from two additional samples (042 Singers Glen and 12DJ Mosque 1) are from [Mazza et al., 2014].

Analyses of Sr, Nd, and Pb radiogenic isotope ratios were carried out at the Center for Elemental Mass Spectrometry, University of South Carolina following established techniques for this lab [e.g., Bizimis et al., 2013; Khanna et al., 2014].

Sample powders from the same aliquots used for major and trace elements were digested in sub-boiling Teflon-distilled 3:1 HF:HNO_3 (v/v) mixture, and the isotopes were analyzed on aliquots of a single digestion. Pb was separated on an anion resin in HBr, HNO_3 acids [e.g. Mahnes et al., 1984]. Sr and REE were separated from the bulk rock washes of the Pb chemistry on a cation resin in HCl. Sr was further purified on a Sr-spec resin and Nd on an Ln-resin (both from EICHROM, USA). The radiogenic isotope ratios were determined on a Thermo Neptune multi collector ICPMS with the PLUS upgrade. Sample introduction was with an APEX enhanced sensitivity spray chamber and high sensitivity cones (JET and X-skimmer configuration) resulting in Nd sensitivities in the order of 1400-1500 V / ppm. The NIST SRM-987 Sr standard was determined at $^{87}Sr/^{86}Sr$ = 0.710320 ± 0.000012 (n=12) using $^{87}Sr/^{86}Sr$ = 0.1194 for instrumental fractionation correction. All Sr-isotope ratios are reported relative to the $^{87}Sr/^{86}Sr$ = 0.710250 for the NIST standard to correct for instrument bias. The LaJolla Nd standard was determined at $^{144}Nd/^{146}Nd$ of 0.511858 ± 0.000007 (n = 10) using $^{144}Nd/^{146}Nd$ = 0.7219 for fractionation correction. Pb isotope ratios were determined using the TI-addition technique [White et al., 2000]. The standard NBS-981 was determined at $^{206}Pb/^{204}Pb$ = 16.936 ± 0.001, $^{207}Pb/^{204}Pb$ = 15.940 ±00.1, $^{208}Pb/^{204}Pb$ = 36.694 ±0.003 (n=13).

A modified version of the high precision method of [Sobolev et al., 2007] was used to analyze 71 olivine phenocrysts from 7 different dikes in Virginia using only the most primitive, unfractionated (samples in olivine control) basalts. Data was collected at Rutgers University on a JEOL JXA-8200 Superprobe. Many of the olivine phenocrysts exhibited compositional zoning so 4-point traverses were done on several phenocryts from each sample (resulting in 247 individual analyzes). A focused beam (~1 um) of 20 kV and 300 nA was used with peak count times: Si: 50s; Mg: 80s; Fe: 100s; Ni: 150s; Ca: 150s and Mn: 150s. To correct for instrumental drift the San Carlos olivine standard was analyzed at regular intervals during each analysis. Primary standards, statistics for the secondary standards and statistics for the olivine analyses are given in Tables 6 and 7. The average relative 2σ error for major and trace elements were: Si ~0.14%, Mg ~0.15%, Fe ~0.19% and Ni ~0.74%, Mn ~1.85, and Ca 1.39%. Detection limits (3σ) for the major and trace elements were: Si ~0.004%, Mg ~0.004%, Fe ~0.003%, Ni ~0.001%, Mn ~0.002% and Ca ~0.002%. 2 standard errors for the San Carlos olivine standard (n=48) were Si ~0.17%, Mg ~0.12%, Fe ~0.08% and Ni 40 ppm, Mn 33 ppm, and Ca 15 ppm.

2.2 Data from the Literature

Our new data were incorporated into the geochemical data set from the literature for CAMP dikes and flows collected in Africa, Europe, and North and South America (Figure 1) [Bertrand, 1991; Dostal and Durning, 1998; Puffer and Volkert, 2001; Cebria et al., 2003; Jourdan et al., 2003; Marzoli et al., 2004; Deckart et al., 2005; Verati et al., 2005; Mahmoudi and Bertrand, 2007; Martins et al., 2008; Marzoli et al., 2011; Merle et al., 2011; Callegaro et al., 2013; Merle et al., 2013; Callegaro et al., 2014; Mazza et al., 2014]. We also compiled available radiogenic isotope data for the Coastal New England Magmatic Province (CNE) that overlaps with the onset of CAMP [McHone and Butler, 1984; McHone, 1992; Pe-Piper et al., 1992; Pe-Piper and Reynolds, 2000] and for the accreted terrenes where CAMP was emplaced [Pettingill et al., 1984; Sinha et al., 1996; Currie et al., 1998; Pe-Piper and Piper, 1998].

Results

3.1 Age Data

A single $^{40}Ar/^{39}Ar$ age was obtained for sample SPG111, making this the first CAMP sample dated in southwest Virginia. After evaluating the mean calculated age of 202.81±0.55 Ma with the inverse isochron technique, the calculated age was 201±2 Ma (Figure 3). This confirms the connection of this dike with the CAMP event of 201.566±0.031 Ma [Blackburn et al., 2013].

3.2 Major and Trace Elements

New major and trace element data are reported in Table 1, 2 and 3. Following nomenclature originally defined for CAMP lavas [Weigand and Ragland, 1970], the samples analyzed consist of low-Ti tholeiites: olivine normative and quartz normative basalts, which we will call here low-Ti basalts and basaltic andesites, respectively. The low-Ti basalt samples have primitive Mg#s ([molar MgO/FeO1MgO]*100) ranging from 64 to 73. SiO_2, CaO and Al_2O_3 decrease with increasing MgO, while the opposite occurs for NiO, suggesting that olivine was the main fractionating phase. A primary magma was calculated from the most primitive low-Ti basalt sample, SPY681 (that required <10% olivine addition). Liquid lines of descent (LLDs) were modeled for CAMP low-Ti basalts using Petrolog3 [Danyushevsky and Plechov, 2011] showing that they are in olivine control (Figure 4a–4c). The Mg#s of the low-Ti basaltic andesites range from 42 to 53. CaO decreases with decreasing MgO, while K_2O increases and Al_2O_3 remains relatively unchanged, suggesting a cotectic crystallization of olivine and clinopyroxene (Figure 4), followed by other phases (e.g., plagioclase) as fractionation proceeded. The same primary starting composition used for the Petrolog3 LLD models was too low in silica to replicate the trends of the low-Ti basaltic andesites. Primary magmas of varying degrees of enrichment in silica were estimated and then modeled in Petrolog3. A primary magma with 50.0 wt.% SiO_2 and 0.5 21.0 wt.% H_2O replicated the low-Ti basaltic andesite trends the best (Figure 4g–4i).

Our new CAMP samples, plotted in a primitive mantle normalized multi-element diagram [McDonough and Sun, 1995] (Figure 5) show relative high field strength element (e.g., Nb, Ta and Ti) depletions as well as large-ion lithophile element (LILE) enrichments. As expected, the low-Ti basaltic andesites are more enriched in trace elements relative to the basalts as a result of fractional crystallization discussed above.

3.3 Radiogenic Isotopes

Measured radiogenic isotope ratios, associated errors, and age-corrected isotope ratios (corrected to 200 Ma) are reported in Table 4. Age corrected isotope ratios are plotted in Figure 6. The basalts have lower $^{143}Nd/^{144}Nd_{200Ma}$ (0.51221–0.51234), $^{206}Pb/^{204}Pb_{200Ma}$ (18.27–18.37), $^{207}Pb/^{204}Pb_{200Ma}$ (15.60–15.63), $^{208}Pb/^{204}Pb_{200Ma}$ (38.21–38.27) and higher $^{87}Sr/^{86}Sr_{200Ma}$ ratios (0.70587– 0.71075) than the basaltic andesites, which have $^{143}Nd/^{144}Nd_{200Ma}$: 0.51230–0.51243; $^{206}Pb/^{204}Pb_{200Ma}$: 18.52–18.65; $^{207}Pb/^{204}Pb_{200Ma}$: 15.60–15.64; $^{208}Pb/^{204}Pb_{200Ma}$: 38.20–38.44; $^{87}Sr/^{86}Sr_{200Ma}$: 0.70489–0.70625. Both the low-Ti basalts and basaltic andesites from Virginia sampled for this study plot in the range of published southern CAMP [Callegaro et al., 2013; Mazza et al., 2014] except for one basalt (sample PHT911Table 4), which has a high $^{87}Sr/^{86}Sr_{200Ma}$

value of 0.71075. Sample BLR531B, a low-Ti basaltic andesite increases the range of $^{206}Pb/^{204}Pb_{200Ma}$ for southern CAMP to 18.65. Sample STS971, also a low-Ti basaltic andesite is a radiogenic end-member for southern CAMP as it has a $^{207}Pb/^{204}Pb_{200Ma}$ value of 15.64, and a $^{208}Pb/^{204}Pb_{200Ma}$ value of 38.44.

3.4 Mineral Data

New high-precision major and trace element data from olivine phenocrysts (Figure 7 and Table 5) show elevated Ni and Fe/Mn as well as low Ca and Mn relative to the values expected for peridotite derivative magmas [Sobolev et al., 2007; Qin and Humayun, 2008; Herzberg, 2011; Foley et al., 2013].

Discussion

4.1. Trace Element Signatures of CAMP Magmas

CAMP samples from Virginia analyzed for this study are similar to CAMP samples from the literature from all along the Eastern North American Margin [Dostal and Durning, 1998; Puffer and Volkert, 2001; Marzoli et al., 2011; Callegaro et al., 2013; Merle et al., 2013; Mazza et al., 2014] in that they display large-ion lithophile element (LILE) (e.g., Ba, Pb, K, Figure 5) and light rare earth element (LREE) enrichments and high-field strength element (HFSE) (e.g., Nb and Ta, Figure 5) depletions typical of arc magmas. Elevated LREE/heavy rare earth element (HREE) ratios alone do not necessarily imply a subduction-modified source, but taken together with low HFSE contents and no significant differences in melt fraction [Herzberg and Gazel, 2009], enrichment in LREE compared to HREE can be used as evidence of mantle metasomatism in subduction systems [Pearce and Peate, 1995]. This signature suggests, in accordance with Puffer [2001] that from a geochemical perspective CAMP lavas are broadly more arc-like than plume-like.

Subduction-sensitive Th/Yb and fluid-immobile Nb/Yb element ratios are particularly useful for distinguish- ing between subduction and mantle plume influenced environments. In Figure 8a, these element ratios from CAMP samples are compared to the mantle array as defined by global mid-ocean ridge basalt (MORB) and intraplate ocean island basalt (OIB) data. Like lavas from the Lesser Antilles, Marianas and Cascades arcs, most CAMP lavas (including the new samples from Virginia) plot above the mantle array, suggesting a subduction-modified source. We divide CAMP terranes (Figure 1) into northern, southern and transitional groups based on their location with respect to the Scranton Rift. Southern CAMP lavas plot nearest to or within the mantle array indicating less of a subduction component in the South. High Th/Yb and Nb/Yb ratios of transitional and northern CAMP suggest mixing between relatively depleted and enriched arc- modified sources. Ce/Yb ratios of CAMP lavas show an increase in Ce/Yb from South to transitional to North (Figure 8b). In terms of Nb/U, another trace element ratio that is indicative of source compositions, northern and transitional CAMP have lower values than southern CAMP samples (Figure 8b) placing them in the same Nb/U space as lavas from an arc-modified source (Nb/U < 20) [Hofmann et al., 1986; Hofmann, 2007]. Southern CAMP spans the entire range of Nb/U ratios including those derived from nonsubduction modified sources such as MORB and OIB [Hofmann et al., 1986; Hofmann, 2007]. Most of the new samples from Virginia plot within the bounds of published southern CAMP [Callegaro et al., 2013], with the exception of a few low-Ti basaltic andesites that plot at slightly higher Th/Yb and Nb/Yb ratios suggesting a stronger subduction influence for these samples. In Nb/U - Ce/Yb space, the low-Ti basalts collected in Virginia for this study plot within the confines of published southern CAMP data, with the low-Ti basaltic andesites plotting as the high Ce/Yb end-member of southern CAMP.

4.2 Sr-Nd-Pb Radiogenic Isotope Signatures of CAMP Magmas

Radiogenic isotopes do not fractionate by melting or crystallization processes, thus they provide key information about the geochemical signature of the melt source components. We age-corrected Sr-Nd-Pb radiogenic isotopic ratios to 200 Ma for our new data (Table 4) as well as for northern, transitional and southern CAMP, and for

CAMP sampled in Africa, Europe, and South America. Additionally, we included Sr-Nd-Pb radiogenic isotope ratios for the accreted terranes of Avalonia [PePiper and Piper, 1998], Meguma [Currie et al., 1998], and Carolina [Pettingill et al., 1984; Sinha et al., 1996]. We also included, in this isotopic comparison data from the Coastal New England magmatic province (CNE) [McHone and Butler, 1984; McHone, 1992; Pe-Piper et al., 1992; Pe-Piper and Reynolds, 2000] because its age range (255 - 202 Ma) broadly overlaps with the onset of CAMP magmatism at 200 Ma.

Northern and transitional CAMP lavas have higher $^{143}Nd/^{144}Nd_{200Ma}$ and Pb isotopic ratios while southern CAMP covers a wider range for both $^{87}Sr/^{86}Sr_{200Ma}$ ratios, $^{143}Nd/^{144}Nd_{200Ma}$ and Pb isotopic ratios (Figures 6a–6c). CAMP lavas plot in a mixing line between depleted MORB mantle (DMM) (Figure 6a), an enriched source and a HIMU-like (high $\mu = {}^{238}U/{}^{204}Pb$) component (Figures 6b and 6c). South American CAMP also plots toward a HIMU component along with the Coastal New England lavas on a $^{87}Sr/^{86}Sr_{200Ma}$ - $^{143}Nd/^{144}Nd_{200Ma}$ diagram (Figure 6a), however these high-Ti tholeiites may represent a younger pulse of CAMP magmatism recording the transition to oceanic crust [Deckart et al., 2005].

In $^{143}Nd/^{144}Nd_{200Ma}$ - $^{206}Pb/^{204}Pb_{200Ma}$, as well as in Pb isotope space, northern and transitional CAMP plot alongside the Meguma and Avalonia terranes (Figure 9), while the Carolina terrane plots closer to southern CAMP. Erosion of the Avalonia, Meguma and Carolina terranes prior to accretion could have led to sediment input during subduction, which would then be incorporated into the upper mantle through the input of sediment melts into the overlying mantle wedge beneath Laurentia, accounting for the Nd and Pb isotopic composition of the northern and transitional CAMP lavas [Merle et al., 2013].

For northern and transitional CAMP this is evidence that the source of these magmas inherited their enriched continental-like trace element and radiogenic isotope composition from subduction-related processes as opposed to crustal contamination, which has been shown to represent a minimal contribution for any of the CAMP terranes [Puffer, 2001; Merle et al., 2011; Callegaro et al., 2013; Callegaro et al., 2014]. The low $^{187}Os/^{188}Os$ ratios of CAMP samples also argue against significant crustal contamination processes in the generation of this LIP [Merle et al., 2011; Callegaro et al., 2013].

Furthermore, assimilation-fractional-crystallization (AFC) calculations starting with an Atlantic plume [Holm et al., 2005] or MORB [Gale et al., 2013] composition that was then contaminated with local Blue Ridge basement (detailed in section 4.3) were unsuccessful in replicating the trace element and Sr-Nd-Pb compositions of the low-Ti basalts and basaltic andesites analyzed in this study.

AFC models by Merle et al. [2013] using both a plume and a MORB starting composition also argue against crustal contamination as the models require an unrealistic amount (up to 35%) of assimilation to get close to the radiogenic isotopes of CAMP samples while keeping primitive mantle-derived major element com- positions. On the other hand, calculations to reproduce northern CAMP lavas required only 3–5% sediment [Merle et al., 2013], which is within the range (2–6%) of the sediment budget of arc lavas [Plank, 2005].

As a current example of this process, the Lesser Antilles' highly radiogenic isotope signature has been attributed to sediment derived from the South American cratonic basement and transported by the Orinoco River [e.g., White and Dupr e, 1986] with Lesser Antilles basalts requiring a sediment component of up to 10% [Carpentier et al., 2008]. Transport of eroding sediment via rivers into the subduction trench, as well as by deep underwater currents may account for southern CAMP's isotopic range from the less evolved Carolina through Meguma and Avalonia. Alternatively sediment may have played less of a role in the metasomatization of the mantle beneath the southern margin of Laurentia.

4.3 Assimilation Fractional Crystallization Modeling

A database of local Blue Ridge basement in Virginia [*Pettingill et al.,* 1984; *Sinha et al.,* 1996] was compiled and used to assess the possible crustal contribution to our sample set. We limited our crustal samples to those with Sr, Nd and Pb radiogenic isotopes in order to check for consistency between systems. We used the average MORB composition calculated by *Gale et al.* [2013] and a basanite from Cape Verde [*Holm et al.,* 2005; *Millet et al.,* 2008] to model an Atlantic plume starting composition for modeling assimilation fractional crystallization (AFC)[*DePaolo,* 1981]. For all models using a MORB starting composition r (r = dMa/dfc) was 0.5 (Figure 10a-f). For models using a plume starting composition (Cape Verde) r = 0.7 Figure 10g-l). The majority of the partition coefficients used are from *Rollison* [1993] with Pb from *McKenzie and O'Nions* [1991]. All isotopes were age-corrected to 200 Ma.

Using MORB as the starting composition, sample H-13-81 and similar samples out of the Blue Ridge crust database are able to reproduce our sample set in $^{87}Sr/^{86}Sr$ –

$^{144}Nd/^{143}Nd$ space (Figure 10a). H-13-81 is a Grenville-age ferrodiorite from the Rose's Mill Pluton in the Blue Ridge [*Pettingill et al*., 1984]. However, AFC models using H-13-81 as a contaminate fail to reproduce the CAMP sample trends in Pb isotope space (Figure 10b-d). Only sample HP-24 as a contaminate produced AFC models capable of explaining the Pb isotopes of the basaltic andesites collected for this study as the rest of the database had much too low $^{206}Pb/^{204}Pb$ as well as most having too low $^{207}Pb/^{204}Pb$ and $^{208}Pb/^{204}pb$. Sample HP-24 is from the Roseland Anorthosite complex, a Grenville-aged anorthosite that forms the core of the Blue Ridge anticlinorium [*Pettingill et al.,* 1984]. Sample M32 was also able to explain some of the basaltic andesite's Pb isotope composition, though not as well as HP-24. Sample M32 is a felsic dike collected in the vicinity of basaltic sample PHT 911 near Philpott Lake. Muscovite separates from sample M32 gave an $^{40}Ar/^{39}Ar$ age of 332.6 ± 4.8 Ma. Both HP-24 and M32 fall short on a $^{206}Pb/^{204}Pb – ^{144}Nd/^{143}Nd$ diagram with M32 only replicating the samples when r is increased to 0.9, which is practically mixing. HP-24 also fails to explain the samples $^{87}Sr/^{86}Sr – ^{144}Nd/^{143}Nd$. Using a plume starting composition, only AFC (using r = 0.7) with H-13-81 as a contaminant could replicate the trend of the CAMP samples in $^{87}Sr/^{86}Sr – ^{144}Nd/^{143}Nd$ space (Figure 10g). However, models with H-13-81 still failed to replicate the trend of the CAMP samples in Pb isotope space (Figure 10h-j).

Trace element data was not available for the crust samples from the Blue Ridge, so upper, middle, lower and total crust values from *Rudnick and Gao* [2003] were used in addition to sample M32. Using a MORB starting composition, upper, middle, and total crust as well as M32 can replicate subsets of the trend of the basaltic andesites on a

Ce/Yb-Gd/Yb plot, while nothing replicates the basalts as they plot at much lower Gd/Yb values than the MORB starting composition (Figure 10e). However, on a Ce/Yb-Nb/U diagram only M32 replicates the trend of the basaltic andesites (as well as the basalts) (Figure 10f). All crustal compositions on a Ce/Yb- Nb/U plot can replicate a small subset of the basalts. Using a plume starting composition, AFC models for trace element ratios were completely unsuccessful in terms of replicating the trends of the CAMP samples (Figure 10k-l).

Beginning with either an average MORB or an Atlantic plume (Cape Verde) starting composition, no crustal composition that we tried adequately replicated the basalts, or the basaltic andesites in terms of Sr-Nd-Pb isotopes and trace elements confirming what others have found, that crustal contamination can not at this time be used to explain the geochemical trends of CAMP lavas [e.g. *Puffer,* 2001; *Merle et al*., 2011; *Callegaro et al*., 2013; *Callegaro et al*., 2014]. That the more successful models suggest not AFC, but rather mixing supports the conclusion that sediment from erosion of Grenville-age terranes may have been incorporated into the mantle through subduction [*Merle et al.,* 2013].

4.4 Discriminating Between Metasomatism by Fluids or Sediment Melt Components in CAMP

Magmas Merle et al. [2013] showed that northern and transitional CAMP were influenced by sediments or sediment melts based on LREE and Th/Yb coupled with initial Nd-isotopes [Woodhead et al., 2001]. On a Ba/La-Th/Yb diagram (Figure 11a), northern and transitional CAMP plot along the increasing Th/Yb trend observed for several arcs, which has been interpreted as incorporation of a sediment component [e.g., Class et al., 2000]. Northern and transitional CAMP also have higher middle rare earth element (MREE) contents relative to heavy rare earth elements (HREE) than southern CAMP as indicated by higher Dy/Yb values on a Dy/Yb - Dy/Dy* diagram (Dy/Dy* = $Dy_N/(La_N)^{4/13}*(Yb_N)^{9/13}$) (Figure 11b) [Davidson et al., 2013]. Dy/Dy* and Th/Yb correlate with $^{143}Nd/^{144}Nd_{200Ma}$ for northern (R^2 50.77, and 0.55, respectively) and transitional (R^2 5 0.91, 0.35, respectively) CAMP (Figures 11c and 11d). Taken as a group, Th/Yb and Dy/Dy* for northern and transitional CAMP also correlate with $^{143}Nd/^{144}Nd_{200Ma}$ (R^2 50.81, 0.55, respectively) (Figures 11c and 11d). Th/Yb for southern CAMP does not change as Ba/La increases (Figure 11a) suggesting a limited role for sediment melt input and more of a fluid-dominated influence [McCulloch and Gamble, 1991; Woodhead et al., 2001]. There is no correlation between $^{143}Nd/^{144}Nd_{200Ma}$ and Th/Yb (Figure 11c) and only a weak correlation between $^{143}Nd/^{144}Nd_{200Ma}$ and Dy/Dy* for southern CAMP (Figure 11d) (R^2 50.21).

On a Dy/Dy*-Dy/Yb plot, CAMP samples plot similarly to arc samples as they plot along the MORB array of Davidson et al. [2013], but offset toward lower Dy/Yb values (Figure 11b) [Davidson et al., 2013]. Davidson et al. [2013] suggested that the negative trend of arc data toward lower Dy/Dy* and higher Dy/Yb values as a possible influence of sediment melts. We suggest that the sediment signature was incorporated into the subcontinental mantle by sediment melts during the Paleozoic subduction that formed Pangea [Pegram, 1990; Puffer, 2001, 2003; De Min et al., 2003; Deckart et al., 2005; Dorais and Tubrett, 2008; Merle et al., 2011, 2013; Murphy et al., 2011; Callegaro et al., 2013]. This interpretation is strengthened by the Th/Yb and Ce/Yb trends (Figure 6) [Woodhead et al., 2001; Hawkesworth et al., 1993, 1997] as well as strong correlations between Dy/Dy* and $^{143}Nd/^{144}Nd_{200Ma}$ (Figure 11d) for northern and transitional CAMP.

Northern and transitional CAMP show positive trends between Dy/Dy* and Dy/Yb (Figure 11b). A subset of mostly southern CAMP (including the Virginia basalt samples analyzed for this study) plot within the lower lefthand corner of the diagram (Dy/Dy* < 1.0, Dy/Yb < 1.55) and also show a positive trend between Dy/Dy* and Dy/Yb. Samples that plot in this corner of the diagram have U-shaped REE patterns, which Davidson et al. [2013] suggested indicates amphibole or clinopyroxene fractionation. Nevertheless, in our samples there is no correlation between Dy/Dy* and MgO, and some of these samples are in an olivine control trend, indicating instead that these U-shaped REE patterns are a feature inherited from the source. U-shaped REE patterns from mantle xenolith samples (Figure 11b) have been interpreted as the result of melt-rock reaction [e.g., Chalot-Prat and Boullier, 1997; Lenoir et al., 2000; Zhang et al., 2012; Ackerman et al., 2013; Bénard and Ionov, 2013] due to melt migration through the mantle [Navon and Stolper, 1987; Ackerman et al., 2007, 2013].

4.5 CAMP Source Lithology Composition From High-Precision Olivine Chemistry and Modeled Primary Magmas

High-precision olivine chemistry has been used as a powerful tool for the evaluation of source lithology composition [Sobolev et al., 2005, 2007; Herzberg, 2011]. Several studies have attempted to include the effects of pressure and temperature in parameterizations of $D_{Ni}^{Ol/L}$ [e.g., Li and Ripley, 2010; Niu et al., 2011; Matzen et al., 2013] with varying degrees of success [Herzberg, 2011; Herzberg et al., 2013, 2014], however the Beattie et al. [1991] parameterization is only dependent on $D_{MgO}^{Ol/L}$, which effectively accounts for temperature and will be used here. The additional terms used by other studies [e.g., Li and Ripley, 2010; Niu et al., 2011; Matzen et al., 2013] to account for pressure and temperature negatively impacted the ability of the parameterization to replicate experimentally derived $D_{Ni}^{Ol/L}$ which may be due to these terms being model - dependent [Herzberg et al., 2013]. The Beattie et al. [1991] model has been the most reliable choice for replicating experimentally derived Ni values in olivine as this model produces the lowest root mean square error (RMSE=1.1) while the temperature dependent model from Matzen et al. [2013] yields a RMSE of 2.5 and the pressure dependent (0–3 GPa) model of Niu et al. [2011] yields a RMSE of 2.1 [Herzberg et al., 2014]. Ni systematics in olivine phenocrysts have therefore been shown to be a viable tool for evaluating source lithology [Sobolev et al., 2005, 2007; Wang and Gaetani, 2008; Herzberg, 2011].

CAMP olivine data collected from basalts in Virginia for this study show elevated Ni and low Ca concentrations relative to peridotite-derived olivines indicating a pyroxenite source component for CAMP [Sobolev et al., 2007; Herzberg, 2011]. CAMP olivine phenocrysts systematically plot alongside data from Mauna Kea or at transitional values between data from mid-ocean ridges and Mauna Kea (Figure 7). The data from Mauna Kea have been interpreted as coming from a second-stage pyroxenite source that formed from the reaction of a high-silica melt from eclogite with peridotite. Ca and Fe/Mn values obtained for olivine phenocrysts from CAMP plot between samples from Mauna Kea and MORB and may indicate both peridotite and pyroxenite source lithologies for CAMP [Sobolev et al., 2005]. Our new data contrast with those published by Callegaro et al. [2013], who suggested that it was unlikely that the source of CAMP contained a pyroxenite component based on their analyses of olivine phenocrysts. Our results, which utilize a modified high-precision method from Sobolev et al. [2007] indicate that a pyroxenite component probably contributed significantly to the source of CAMP.

In order to determine which type of pyroxenite was involved, CAMP primary magma compositions were calculated by taking the bulk rock compositions of lavas in olivine control and adding olivine until equilibrium with the maximum forsterite (Fo) content observed in CAMP magmas (Fo_{89}) [Callegaro et al., 2013] was achieved (using a variable Fe-Mg partition coefficient for olivine–liquid with an initial value of 0.32 [Roeder and Emslie, 1970; Toplis, 2005]) (Tables 8 and 9). These primary magma compositions contain 11.5–19.8 wt.% MgO, and 46.93–52.43 wt.% SiO_2. The modeled results are plotted in the pseudoternary system olivine-calcium Tschermak's (CATS)-pyroxene-quartz projected from diopside [O'hara, 1968] (Figure 12). CAMP primary magmas project onto the high-SiO_2 pyroxenite side of the pyroxene-garnet plane, which acts as a thermal divide [Kogiso et al., 2004]. Source lithologies with excess silica (olivine-free source) can produce primary magmas that plot on the high-SiO_2 side of the diagram [Herzberg, 2011]. This suggests that CAMP primary magmas likely melted from a silica-rich, olivine-free pyroxenite source lithology, which could be the result of high-silica melts formed from subducted material (sediment, subducting oceanic crust) that reacted with mantle peridotite, in a process similar to that suggested by Sobolev et al. [2005, 2007].

The new olivine data together with trace element signatures and radiogenic isotopes argue for a significant sediment component in the source of CAMP lavas. As the ratio of silica-rich melt to peridotite increases, the source will change from refertilized peridotite to olivine-bearing pyroxenite, and then to an olivine-free pyroxenite. Additionally, the Ni and Fe/Mn of olivine phenocrysts crystallizing from the primary melt will also increase, while Ca decreases [Herzberg et al., 2014]. Further supporting the possibility of high-silica pyroxenite, the modeled LLD for the basaltic andesites analyzed in this study require a primary magma rich in silica (Figure 4). Northern and transitional CAMP magmas have on average even higher SiO_2 contents suggesting the possibility of a higher contribution of pyroxenite-derived melt in the source than those from the South, which resulted in more evolved primary magmas no longer in an olivine-control trend.

4.6 Evaluation of Mechanisms for Pangea Breakup and the Generation of CAMP

Mantle plume activity has been suggested as the formation mechanism for LIPs [White and McKenzie, 1989], but because the plume model is inconsistent with the formation of CAMP alternative explanations such as edge-driven convection (EDC) [King and Anderson, 1995] have been invoked. However, EDC does not explain the observed differences between northern and southern CAMP. More crustal thickening occurred in the South during the Alleghanian Orogeny [Hatcher, 2002], which could lead to a greater difference in the thickness between the edge of the continental lithosphere and the orogenic root. A substantial difference in lithospheric thickness can cause a localized convection cell to form in the mantle, which could explain earlier rifting in the southern basins. However, EDC does not explain why rifting was accompanied by synrift magmatism in the North but not in the South as would be expected. Another issue with the EDC model is that Missenard and Cadoux [2012] show that EDC cannot persist if plate velocities exceed 1 cm a^{-1}. Absolute plate motions are not available for North America for the Triassic, but Ruiz-Martínez et al. [2012] calculated that Pangea was moving at an average speed of 8 cm/yr at 200 Ma, using Africa as a fixed reference in order to approximate absolute velocities. This suggests that EDC would not have been viable in the mantle beneath Pangea at the time of rifting.

Continental insulation of the mantle leading to elevated mantle temperatures and magmatism has been suggested as a formation mechanism for CAMP [Anderson, 1982; Verati et al., 2005; Coltice et al., 2007, 2009; Herzberg and Gazel, 2009; Hole, 2015]. Although this model is consistent with reported mantle potential temperatures, it does not explain why rifting is asynchronous with magmatism in the South, nor the age progression of CAMP magmatism. Geodynamic models indicate the magmatism induced by continental insulation would be tectonically controlled [Coltice et al., 2009], but dikes in the South cross- cut both pre and synrift structures, indicating that magmatism was not structurally controlled [Schlische et al., 2003].

Delamination could be a formation mechanism for LIPs [Lustrino, 2005]. Ductile delamination is controlled by phase changes in the lithosphere (resulting in density instabilities) as well as low viscosity [Conrad and Molnar, 1997; Houseman and Molnar, 1997; Schott et al., 2000; Tanton and Hager, 2000; Elkins-Tanton, 2005]. Delamination may be common during supercontinent formation [Kay and Kay, 1993] as it is likely to occur in areas that have undergone crustal shortening [e.g., Kay and Kay, 1993; Schott and Schmeling, 1998; Conrad, 2000; Morency et al., 2002]. The eastern margin of

Laurentia experienced subduction related to several collisional events [Hatcher, 2010; Hibbard et al., 2010]. Both the orogenic keels formed during these events and the subducting plates themselves are likely candidates for delamination.

Reduced crustal thicknesses at the center of the Appalachian orogenic belt in Newfoundland [Hall et al., 1998] could indicate delamination. A fossil anisotropy indicative of extension perpendicular to the Appalachian Orogeny was detected using shear-wave birefringence across the New England region [Levin et al., 2000]. The anisotropy may have resulted from Late Paleozoic delamination and extension [Levin et al., 2000]. Based on the uniformity of the anisotropy layer, it must post-date the Alleghanian Orogeny. There- fore, the proposed delamination event could be related to the formation of CAMP near the Triassic-Jurassic boundary.

Finally, CAMP is part of the group of continental LIPs with arc-like geochemical signatures [Puffer, 2001]. Similarities between the LIPs with arc affinities and arc magmas may be due to the melting of subduction- metasomatized mantle [Pegram, 1990; Puffer, 2001, 2003; De Min et al., 2003; Deckart et al., 2005; Dorais and Tubrett, 2008; Merle et al., 2011, 2013; Murphy et al., 2011; Callegaro et al., 2013]. Subduction-metasomatized lithosphere is also more likely to delaminate due to heating and hydration, which lower its viscosity [Elkins- Tanton, 2005] and melt emplacement [Jull and Kelemen, 2001] and removal, which can leave behind mafic residues that can lead to density instabilities [Herzberg et al., 1983; Kay and Kay, 1993; Elkins-Tanton, 2005].

4.7 Proposed Model for the Breakup of Pangea and CAMP

Using the Scranton Rift to demarcate northern, transitional, and southern CAMP groups, the geochemical variation between northern and southern CAMP could be attributed to a difference in the amount of subduction experienced by the northern and southern margins of Laurentia. While the Scranton Rift represents a possible structural and not a chemical control on the lavas themselves, this geochemical variation is less obvious, without separating out the CAMP flows preserved in the rift basins along the east coast of North America into groups based on their position relative to the Scranton Rift. If the Scranton Rift did act as a ‘‘collisional backstop,’’ causing a rotation in the direction of collision between Gondwana and Laurentia, this may have led to a change in the angle of subduction. This could affect the rate of subduction erosion [Keppie et al., 2009; Stern, 2011] and thus the amount of sediment incorporated into the mantle. Smaller angles of subduction favor subduction erosion of the upper plate [Keppie et al., 2009] and could explain the more prominent sediment signal in northern and transitional CAMP as opposed to southern CAMP.

We propose that differences in the accretionary history of the northern and southern Appalachians (Figure 13a) can account for the diachroneity in rifting, the chemical differences in CAMP lavas from the North and South, and could be responsible for triggering for the breakup of Pangea. Subduction of the Rheic Plate [Moran et al., 2007; Woodcock et al., 2007] at a very low angle (Figure 13b) may have resulted in the under- plating of the slab to the base of the lithosphere beneath Laurentia. During the Alleghanian collisional event, oblique subduction in the North may have led to a jamming of the subduction zone when the colli- sional front impacted the Scranton Rift and could no longer advance (Figure 13b). This blocking of the subduction zone may have led to a rotation of the subduction direction, as seen for example in the subduction of the Hikurangi Plateau beneath New Zealand [Davy, 2014], resulting in head-on collision in the South (Figure 13c).

The head-on collision of Gondwana with the southern portion of Laurentia (Figure 13c) possibly led to greater overthickening of the crust in the South than in the North. This resulted in a denser orogenic keel surrounded by a less dense asthenospheric mantle and to earlier orogenic collapse and delamination [Sacks and Secor, 1990; Samson et al., 1995] as documented by the onset of rifting in the South at 230 Ma, probably with a similar situation in the Fundy and Argana basins in the North. While the small episodes of earliest rifting in the North were relatively restricted to the Argana and Fundy basins, rifting in the South was widespread at 230 Ma, but unaccompanied by volcanism. This initial orogenic collapse in the South may have served to heat the upper mantle as hotter material ascended to replace the foundering material permitting magmatism closer to 200 Ma [Nelson, 1992]. Additionally, the upper mantle beneath Pangea may have been warmer due to continental insulation [Anderson, 1982; Coltice et al., 2009; Herzberg and Gazel, 2009; Hole, 2015].

Subduction of the Rheic Plate continued in the North, where the slab was not constricted by the Scranton Rift, straining and eventually tearing the slab (Figure 13e). A small tear in a subducting slab can propagate laterally due to slab pull [Wortel and Spakman, 2000]. Tectonic events leading to the formation of the Central Range of New Guinea and the Talamanca Range in Central America show that the jamming of a subduction zone can lead to a slab tear, delamination, and magmatism [Cloos et al., 2005; Gazel et al., 2011]. Potentially, a tear in the Rheic slab could have led to mantle upwelling, which over time heated and destabilized the underplated oceanic slab eventually resulting in delamination, which triggered more rifting in the North. In agreement with geodynamic models of lithospheric delamination, [Elkins-Tanton, 2005] approaching the eruption of CAMP and continuing into the Jurassic, there was active subsidence with an increase in the sedimentation rate right at the time of eruption (Figure 14) [Olsen, 1997; Schlische et al., 2003].

Uplift due to mantle upwelling could explain the hiatus in sedimentation in the Fundy Basin in Nova Scotia [Schlische et al., 2003] (Figures 2 and 14) during the Late Triassic (230–215 Ma). Thermal doming has been suggested to explain the Late Triassic unconformity in the CAMP basins in Nova Scotia and Morocco [Frizon de Lamotte et al., 2015]. Late Triassic alkaline Coastal New England (CNE) magmatism [McHone and Butler, 1984; McHone, 1992; Pe-Piper et al., 1992; Pe-Piper and Reynolds, 2000] peaks during the hiatus in sedimentation in the Fundy Basin (Figure 14) and could represent an early stage of rifting or uplift (Figure 13e) prior to the main phase of rifting [Ross, 1992; Swanson, 1992] as high-potassium silica-rich magmas preceding mafic, extensionally related magmas agrees with the delamination model of Kay and Kay [1993]. Alternatively CNE lavas may be from the slab tear itself, which acted as a trigger for the delamination event responsible for CAMP through heating of the underplated, now eclogitized slab, reducing its viscosity and increasing the likelihood of delamination (Figure 13e). The oldest $^{40}Ar/^{39}Ar$ age reported for CNE is 246±4 for a dike in Massachusetts [Ross, 2010]. While the youngest $^{40}Ar/^{39}Ar$ ages reported for CNE dikes are in Plymouth, Nova Scotia of 203±15 [Pe-Piper and Reynolds, 2000] with the oldest CAMP lava flows located nearby in the Fundy Basin, Nova Scotia. We suggest this decrease in age in the CNE dikes from closer to the Scranton Rift toward the site of the onset of CAMP magmatism may indicate the direction of the initial tear in the Rheic slab.

Continued heating due to mantle upwelling through the slab tear eventually led to slab foundering in the North, culminating in the upwelling that led to CAMP magmatism (beginning in the Fundy Basin on Laurentia and in the Argana Basin on Gondwana) (Figures 1 and 13f). The magmatism was voluminous and extensive due to heating from the upwelling asthenosphere, as well as the presence of a significant pyroxenite component derived from previous subduction events (Figure 13a). Subduction-related volatiles like H_2O added to the overlying mantle wedge by arc metasomatism helped to reduce the melting temperature [e.g., Hirschmann et al., 1999] increasing the amount of melting achieved at lower temperatures. Melts of the lithosphere that had been metasomatized during past subduction events could be responsible for the arc-like magmas typical of CAMP [Puffer, 2001, 2003], as well as the low $^{187}Os/^{188}Os$ combined with enriched Sr-Nd-Pb isotopic ratios [Callegaro et al., 2013; Merle et al., 2013]. Upwelling in the North propagated to the South, where earlier heating may have facilitated melting [Nelson, 1992]. This upwelling could have then facilitated the weakening of the remaining slab beneath the southern portion of the margin of Laurentia

Conclusions

The northern Appalachians are the product of at least four different orogenic events terminating with the accretion of Ganderia, Avalonia and Megmua, while the southern Appalachians resulted from the accretion of Carolina, and Suwannee terranes. The difference in the number and size of accretionary events is consistent with an increase in arc-modification of the mantle beneath Laurentia in the North. Different accretionary histories may have played a part in the different trace element chemistries of the resultant CAMP lavas while the isotopic signature of the lavas reflects the incorporation of eroded sediment from adjacent accreted terranes into the mantle by subduction, particularly in northern and transitional CAMP.

The Scranton Rift, as an example of supercontinental inheritance, may have influenced the formation of Pangea by acting as a collisional backstop and leading to a rotation of the direction of subduction. The Scranton Rift may have also influenced the breakup of Pangea as the underplated rift material may have had some structural control over the basins that formed nearby. Additionally, geochemical trends showing evidence of more metasomatism of the mantle by subducted sediment melts are observed in the CAMP basalts that were emplaced in the basins north of and adjacent to the Scranton Rift versus the basins located to the South.

Major and trace element chemistry from olivine phenocrysts indicate a pyroxenite component for CAMP basalts based on elevated Ni, low Ca and some elevated Fe/Mn values. Calculated CAMP primary magmas sug- gest that the source of CAMP may be the result of a reaction between a silica-rich melt and peridotite. Due to the ubiquitous arc signature in CAMP lavas we interpret this pyroxenite component as the result of metasomatism of the upper mantle by previous instances of subduction, possibly in the form of sediment melt.

We suggest that the combination of lithospheric delamination, slab break off, and mantle upwelling is the result of the protracted accretionary history of Pangea, although aspects of this model still require further exploration. For instance, the exact timing of delamination of the Rheic slab is complicated by the extensive erosion in the South and a general lack of consensus on the subduction direction during the final closure of Pangea.

Finally, CAMP is not responsible for the breakup of Pangea, but is itself the result of supercontinental inheritance. As supercontinents are the products of many different processes, it stands to reason that the breakup of each supercontinent will be as unique and complex as the events leading to their formation.

References

Anderson, D. L. (1982), Hotspots, polar wander, Mesozoic convection and the geoid, *Nature*, *297*(5865), 391-393.

Ackerman, L., N. Mahlen, E. JelÍnek, G. Medaris, J. Ulrych, L. Strnad, and M. MihaljeviČ (2007), Geochemistry and evolution of subcontinental lithospheric mantle in Central Europe: evidence from peridotite xenoliths of the Kozákov volcano, Czech Republic, *Journal of Petrology*, *48*(12), 2235-2260.

Ackerman, L., P. ŠpaČek, T. Magna, J. Ulrych, M. Svojtka, E. Hegner, and K. Balogh (2013), Alkaline and carbonate-rich melt metasomatism and melting of subcontinental lithospheric mantle: evidence from mantle xenoliths, NE Bavaria, Bohemian Massif, *Journal of Petrology*, 54, 2597-2633.

Beattie, P., C. Ford, and D. Russell (1991), Partition coefficients for olivine-melt and orthopyroxene-melt systems, *Contributions to Mineralogy and Petrology*, *109*(2), 212-224.

Bénard, A., and D. A. Ionov (2013), Melt–and fluid–rock interaction in supra-subduction lithospheric mantle: Evidence from andesite-hosted veined peridotite xenoliths, *Journal of Petrology*, 54, 2339-2378.

Benoit, M. H., C. Ebinger, and M. Crampton (2014), Orogenic bending around a rigid Proterozoic magmatic rift beneath the Central Appalachian Mountains, *Earth and Planetary Science Letters, 402, 197-208*.

Bird, P. (1979), Continental delamination and the Colorado Plateau, *Journal of Geophysical Research: Solid Earth (1978–2012)*, *84*(B13), 7561-7571.

Bertrand, H. (1991), The Mesozoic tholeiitic province of northwest Africa: a volcano-tectonic record of the early opening of Central Atlantic, in *Magmatism in extensional structural settings*, edited, pp. 147-188, Springer.

Bizimis, M., V. J. Salters, M. O. Garcia, and M. D. Norman (2013), The composition and distribution of the rejuvenated component across the Hawaiian plume: Hf-Nd-Sr-Pb isotope systematics of Kaula lavas and pyroxenite xenoliths, *Geochemistry, Geophysics, Geosystems*, *14*(10), 4458-4478.

Blackburn, T. J., P. E. Olsen, S. A. Bowring, N. M. McLean, D. V. Kent, J. Puffer, G. McHone, E. T. Rasbury, and M. Et-Touhami (2013), Zircon U-Pb geochronology links the end-Triassic extinction with the Central Atlantic Magmatic Province, *Science*, *340*(6135), 941-945.

Bullard, E., J. E. Everett, and A. G. Smith (1965), The fit of the continents around the Atlantic, *Philosophical Transactions of the Royal Society of London. Series A, Mathematical and Physical Sciences*, *258*(1088), 41-51.

Callegaro, S., A. Marzoli, H. Bertrand, M. Chiaradia, L. Reisberg, C. Meyzen, G. Bellieni, R. E. Weems, and R. Merle (2013), Upper and lower crust recycling in the source of CAMP basaltic dykes from southeastern North America, *Earth and Planetary Science Letters*, *376*, 186-199.

Callegaro, S., C. Rapaille, A. Marzoli, H. Bertrand, M. Chiaradia, L. Reisberg, G. Bellieni, L. Martins, J. Madeira, and J. Mata (2014), Enriched mantle source for the Central Atlantic magmatic province: new supporting evidence from Southwestern Europe, *Lithos*, *188*, 15-32.

Campbell, I. H. (2007), Testing the plume theory, *Chemical Geology*, *241*(3–4), 153-176.

Carpentier, M., C. Chauvel, and N. Mattielli (2008), Pb–Nd isotopic constraints on sedimentary input into the Lesser Antilles arc system, *Earth and Planetary Science Letters*, *272*(1), 199-211.

Cebriá, J. M., J. López-Ruiz, M. Doblas, L. T. Martins, and J. Munha (2003), Geochemistry of the Early Jurassic Messejana–Plasencia dyke (Portugal–Spain); Implications on the Origin of the Central Atlantic Magmatic Province *Journal of Petrology*, *44*(3), 21.

Chalot-Prat, F., and A.-M. Boullier (1997), Metasomatism in the subcontinental mantle beneath the Eastern Carpathians (Romania): new evidence from trace element geochemistry, *Contributions to Mineralogy and Petrology*, *129*(4), 284-307.

Class, C., D. M. Miller, S. L. Goldstein, and C. H. Langmuir (2000), Distinguishing melt and fluid subduction components in Umnak Volcanics, Aleutian Arc, *Geochemistry, Geophysics, Geosystems*, *1*(6).

Cloos, M., B. Sapiie, A. Q. van Ufford, R. J. Weiland, P. Q. Warren, and T. P. McMahon (2005), Collisional delamination in New Guinea: The geotectonics of subducting slab breakoff, *Geological Society of America Special Papers*, *400*, 1-51.

Coltice, N., B. Phillips, H. Bertrand, Y. Ricard, and P. Rey (2007), Global warming of the mantle at the origin of flood basalts over supercontinents, *Geology*, *35*(5), 391-394.

Coltice, N., H. Bertrand, P. Rey, F. Jourdan, B. R. Phillips, and Y. Ricard (2009), Global warming of the mantle beneath continents back to the Archaean, *Gondwana Research*, *15*(3), 254-266.

Coney, P. J., D. L. Jones, and J. W. Monger (1980), Cordilleran suspect terranes, *Nature*, *288*(5789), 329-333.

Conrad, C. P. (2000), Convective instability of thickening mantle lithosphere, *Geophysical Journal International*, *143*(1), 52-70.

Conrad, C. P., and P. Molnar (1997), The growth of Rayleigh—Taylor-type instabilities in the lithosphere for various rheological and density structures, *Geophysical Journal International*, *129*(1), 95-112.

Courtillot, V., C. Jaupart, I. Manighetti, P. Tapponnier, and J. Besse (1999), On causal links between flood basalts and continental breakup, *Earth and Planetary Science Letters*, *166*(3–4), 177-195.

Courtillot, V. E., and P. R. Renne (2003), On the ages of flood basalt events, *Comptes Rendus Geoscience*, *335*(1), 113-140.

Currie, K., J. Whalen, W. Davis, F. Longstaffe, and B. Cousens (1998), Geochemical evolution of peraluminous plutons in southern Nova Scotia, Canada—a pegmatite-poor suite, *Lithos*, *44*(3), 117-140.

Danyushevsky, L. V., and P. Plechov (2011), Petrolog3: Integrated software for modeling crystallization processes, *Geochemistry, Geophysics, Geosystems*, *12*(7).

Davidson, J., S. Turner, and T. Plank (2013), Dy/Dy*: variations arising from mantle sources and petrogenetic processes, *Journal of Petrology*, *54*(3), 525-537.

Davy, B. (2014), Rotation and offset of the Gondwana convergent margin in the New Zealand region following Cretaceous jamming of Hikurangi Plateau large igneous province subduction, *Tectonics*, *33*(8), 1577-1595.

De Min, A., E. M. Piccirillo, A. Marzoli, G. Bellieni, P. R. Renne, M. Ernesto, and L. S. Marques (2003), The Central Atlantic Magmatic Province (CAMP) in Brazil: petrology, geochemistry, 40Ar/39Ar ages, paleomagnetism and geodynamic implications, *The central Atlantic magmatic province: insights from fragments of Pangea*, 91-128.

Deckart, K., H. Bertrand, and J.-P. Liégeois (2005), Geochemistry and Sr, Nd, Pb isotopic composition of the Central Atlantic Magmatic Province (CAMP) in Guyana and Guinea, *Lithos*, *82*(3), 289-314.

DePaolo, D. J. (1981), Trace element and isotopic effects of combined wallrock assimilation and fractional crystallization, *Earth and planetary science letters*, *53*(2), 189- 202.

Dorais, M. J., M. Harper, S. Larson, H. Nugroho, P. Richardson, and N. Roosmawati (2005), A comparison of Eastern North America and Coastal New England magma suites: implications for subcontinental mantle evolution and the broad-terrane hypothesis, *Canadian Journal of Earth Sciences*, *42*(9), 1571-1587.

Dorais, M. J., and M. Tubrett (2008), Identification of a subduction zone component in the Higganum dike, Central Atlantic Magmatic Province: A LA-ICPMS study of clinopyroxene with implications for flood basalt petrogenesis, *Geochemistry, Geophysics, Geosystems*, *9*(10).

Dostal, J., and M. Durning (1998), Geochemical constraints on the origin and evolution of early Mesozoic dikes in Atlantic Canada, *European Journal of Mineralogy*, *10*(1), 79-93.

Ernst, R. E., and K. L. Buchan (2002), Maximum size and distribution in time and space of mantle plumes: evidence from large igneous provinces, *Journal of Geodynamics*, *34*(2), 309-342.

Elkins-Tanton, L. T. (2005), Continental magmatism caused by lithospheric delamination, *Geological Society of America Special Papers*, *388*, 12.

Faill, R. T. (2003), The early Mesozoic Birdsboro central Atlantic margin basin in the Mid-Atlantic region, eastern United States, *Geological Society of America Bulletin*, *115*(4), 406-421.

Foley, S. F., D. Prelevic, T. Rehfeldt, and D. E. Jacob (2013), Minor and trace elements in olivines as probes into early igneous and mantle melting processes, *Earth and Planetary Science Letters*, *363*, 181-191.

Fokin, M. A. (2003), Space-time analysis of magmatism: the igneous record for an early Cryogenian plume track in central Appalachian orogen, Virginia Polytechnic Institute and State University.

Frizon de Lamotte, D., B. Fourdan, S. Leleu, F. Leparmentier, and P. Clarens (2015), Style of rifting and the stages of Pangea breakup, *Tectonics*.

Gale, A., C. A. Dalton, C. H. Langmuir, Y. Su, and J. G. Schilling (2013), The mean composition of ocean ridge basalts, *Geochemistry, Geophysics, Geosystems*, *14*(3), 489-518.

Gazel, E., K. Hoernle, M. J. Carr, C. Herzberg, I. Saginor, P. v. den Bogaard, F. Hauff, M. Feigenson, and C. Swisher III (2011), Plume–subduction interaction in southern Central America: Mantle upwelling and slab melting, *Lithos*, *121*(1), 117-134.

Gazel, E., Hayes, J., Hoernle, K., Everson, E., Holbrooke, W. S., Kelemen, P., Hauff, F., van den Bogaard, P., Vance, E., Chu, S., Yogodzinski, G. (2015), Generation of continental crust in oceanic arcs, Nature Geoscience 8, 321-327**.**

Greenough, J. D., A. Hayatsu, and V. S. Papezik (1988), Mineralogy, petrology and geochemistry of the alkaline Malpeque Bay sill, Prince Edward Island, *Canadian Mineralogist*, *26*, 97-108.

Hall, J., F. Marillier, and S. Dehler (1998), Geophysical studies of the structure of the Appalachian orogen in the Atlantic borderlands of Canada, *Canadian Journal of Earth Sciences*, *35*(11), 1205-1221.

Harris, P., A. Reay, and I. White (1967), Chemical composition of the upper mantle, *Journal of Geophysical Research*, *72*(24), 6359-6369.

Hatcher, R. D. (2002), Alleghanian (Appalachian) orogeny, a product of zipper tectonics: Rotational transpressive continent-continent collision and closing of ancient oceans along irregular margins, *Special paper-Geological Society of America*(364), 199-208.

Hatcher, R. D. (2010), The Appalachian orogen: A brief summary, *Geological Society of America Memoirs*, *206*, 1-19.

Hawkesworth, C., K. Gallagher, J. Hergt, and F. McDermott (1993), Mantle and slab contribution in arc magmas, *Annual Review of Earth and Planetary Sciences*, *21*, 175-204.

Hawkesworth, C., S. Turner, F. McDermott, D. Peate, and P. Van Calsteren (1997), U-Th isotopes in arc magmas: Implications for element transfer from the subducted crust, *Science*, *276*(5312), 551-555.

Hawman, R. B. (2008), Crustal thickness variations across the Blue Ridge Mountains, southern Appalachians: An alternative procedure for migrating wide-angle reflection data, *Bulletin of the Seismological Society of America*, *98*(1), 469-475.

Herzberg, C. (2011), Identification of source lithology in the Hawaiian and Canary Islands: Implications for origins, *Journal of Petrology*, *52*(1), 113-146.

Herzberg, C., and M. O'hara (2002), Plume-associated ultramafic magmas of Phanerozoic age, *Journal of Petrology*, *43*(10), 1857-1883.

Herzberg, C., and P. D. Asimow (2008), Petrology of some oceanic island basalts: PRIMELT2.XLS software for primary magma calculation, *Geochemistry, Geophysics, Geosystems*, *9*(9) Q09001, doi:10.1029/2008GC002057.

Herzberg, C., and E. Gazel (2009), Petrological evidence for secular cooling in mantle plumes, *Nature*, *458*(7238), 619-622.

Herzberg, C., W. Fyfe, and M. Carr (1983), Density constraints on the formation of the continental Moho and crust, *Contributions to Mineralogy and Petrology*, *84*(1), 1-5.

Herzberg, C., R. Cabral, M. Jackson, C. Vidito, J. Day, and E. Hauri (2014), Phantom Archean crust in Mangaia hotspot lavas and the meaning of heterogeneous mantle, *Earth and Planetary Science Letters*, *396*, 97-106.

Herzberg, C., P. D. Asimow, D. A. Ionov, C. Vidito, M. G. Jackson, and D. Geist (2013), Nickel and helium evidence for melt above the core-mantle boundary, *Nature*, *493*(7432), 393-397.

Hibbard, J. P., C. R. Van Staal, and D. W. Rankin (2007), A comparative analysis of pre-Silurian crustal building blocks of the northern and the southern Appalachian orogen, *American Journal of Science*, *307*(1), 23-45.

Hibbard, J. P., C. R. van Staal, and D. W. Rankin (2010), Comparative analysis of the geological evolution of the northern and southern Appalachian orogen: Late Ordovician-Permian, *Geological Society of America Memoirs*, *206*, 51-69.

Hill, R. I. (1991), Starting plumes and continental break-up, *Earth and Planetary Science Letters*, *104*(2), 398-416.

Hirschmann, M., P. D. Asimow, M. Ghiorso, and E. Stolper (1999), Calculation of peridotite partial melting from thermodynamic models of minerals and melts. III. Controls on isobaric melt production and the effect of water on melt production, *Journal of Petrology*, *40*(5), 831-851.

Hodych, J., and A. Hayatsu (1980), K-Ar isochron age and paleomagnetism of diabase along the trans-Avalon aeromagnetic lineament-evidence of Late Triassic rifting in Newfoundland, *Canadian Journal of Earth Sciences*, *17*(4), 491-499.

Hofmann, A., K. Jochum, M. Seufert, and W. White (1986), Nb and Pb in oceanic basalts: new constraints on mantle evolution, *Earth and Planetary Science Letters*, *79*(1), 33-45.

Hofmann, A. W. (2007), 2.03 - Sampling Mantle Heterogeneity through Oceanic Basalts: Isotopes and Trace Elements, in *Treatise on Geochemistry*, edited by H. D. Holland and K. K. Turekian, pp. 1-44, Pergamon, Oxford.

Hole, M. J. (2015), The generation of continental flood basalts by decompression melting of internally heated mantle, *Geology*, 43, 311-314.

Holm, P. M., J. R. Wilson, B. P. Christensen, L. Hansen, S. L. Hansen, K. M. Hein, A. K. Mortensen, R. Pedersen, S. Plesner, and M. K. Runge (2005), Sampling the Cape Verde mantle plume: evolution of melt compositions on Santo Antão, Cape Verde Islands, *Journal of Petrology*, 47, 145-189.

Houseman, G. A., and P. Molnar (1997), Gravitational (Rayleigh–Taylor) instability of a layer with non-linear viscosity and convective thinning of continental lithosphere, *Geophysical Journal International*, *128*(1), 125-150.

Houseman, G. A., D. McKenzie, and P. Molnar (1981), Convective instability of a thickened boundary layer and its relevance for the thermal evolution of continental convergent belts, *Journal of Geophysical Research: Solid Earth (1978–2012)*, *86*(B7), 6115-6132.

Janney, P. E., and P. R. Castillo (2001), Geochemistry of the oldest Atlantic oceanic crust suggests mantle plume involvement in the early history of the central Atlantic Ocean, *Earth and Planetary Science Letters*, *192*(3), 291-302.

Johnson, D., P. Hooper, and R. Conrey (1999), XRF analysis of rocks and minerals for major and trace elements on a single low dilution Li-tetraborate fused bead, *Advances in X-ray Analysis*, *41*, 843-867.

Jourdan, F., A. Marzoli, H. Bertrand, M. Cosca, and D. Fontignie (2003), The Northernmost CAMP: 40Ar/39Ar Age, Petrology and Sr-Nd-Pb Isotope Geochemistry of the Kerforne Dike, Brittany, France, *The Central Atlantic Magmatic Province: Insights from Fragments of Pangea*, 209-226.

Jull, M., and P. Kelemen (2001), On the conditions for lower crustal convective instability, *Journal of Geophysical Research: Solid Earth (1978–2012)*, *106*(B4), 6423-6446.

Kay, R. W., and S. Kay (1993), Delamination and delamination magmatism, *Tectonophysics*, *219*(1), 177-189.

Kelemen, P. B., G. M. Yogodzinski, and D. W. Scholl (2003), Along-strike variation in the Aleutian island arc: Genesis of high Mg# andesite and implications for continental crust, *Inside the Subduction Factory, Geophys. Monogr. Ser*, *138*, 223-276.

Keppie, D. F., C. A. Currie, and C. Warren (2009), Subduction erosion modes: comparing finite element numerical models with the geological record, *Earth and Planetary Science Letters*, *287*(1), 241-254.

Khanna, T. C., M. Bizimis, G. M. Yogodzinski, and S. Mallick (2014), Hafnium–neodymium isotope systematics of the 2.7 Ga Gadwal greenstone terrane, Eastern Dharwar craton, India: implications for the evolution of the Archean depleted mantle, *Geochimica et Cosmochimica Acta*, *127*, 10-24.

King, S. D., and D. L. Anderson (1995), An alternative mechanism of flood basalt formation, *Earth and Planetary Science Letters*, *136*(3–4), 269-279.

Kogiso, T., M. Hirschmann, and M. Pertermann (2004), High-pressure partial melting of mafic lithologies in the mantle, *Journal of Petrology*, *45*(12), 2407-2422.

Lefort, J.-P., and R. Van der Voo (1981), A kinematic model for the collision and complete suturing between Gondwanaland and Laurussia in the Carboniferous, *The Journal of Geology*, 537-550.

Lenoir, X., C. J. Garrido, J.-L. Bodinier, and J.-M. Dautria (2000), Contrasting lithospheric mantle domains beneath the Massif Central (France) revealed by geochemistry of peridotite xenoliths, *Earth and Planetary Science Letters*, *181*(3), 359-375.

Levin, V., J. Park, M. T. Brandon, and W. Menke (2000), Thinning of the upper mantle during late Paleozoic Appalachian orogenesis, *Geology*, *28*(3), 239-242.

Li, C., and E. M. Ripley (2010), The relative effects of composition and temperature on olivine-liquid Ni partitioning: Statistical deconvolution and implications for petrologic modeling, *Chemical Geology*, *275*(1), 99-104.

Lustrino, M. (2005), How the delamination and detachment of lower crust can influence basaltic magmatism, *Earth-Science Reviews*, *72*(1–2), 21-38.

Mahmoudi, A., and H. Bertrand (2007), Geochemical identification of the central Atlantic magmatic province in folded domain, exemplified by the Moroccan Middle Atlas, *Comptes Rendus Géosciences*, *339*, 545-552.

Manhes, G., C. Allègre, and A. Provost (1984), U-Th-Pb systematics of the eucrite "Juvinas": precise age determination and evidence for exotic lead, *Geochimica et Cosmochimica Acta*, *48*(11), 2247-2264.

Martins, L., J. Madeira, N. Youbi, J. Munhá, J. Mata, and R. Kerrich (2008), Rift-related magmatism of the Central Atlantic magmatic province in Algarve, Southern Portugal, *Lithos*, *101*(1), 102-124.

Marzoli, A., P. R. Renne, E. M. Piccirillo, M. Ernesto, G. Bellieni, and A. D. Min (1999), Extensive 200-Million-Year-Old Continental Flood Basalts of the Central Atlantic Magmatic Province, *Science*, *284*(5414), 616-618.

Marzoli, A., H. Bertrand, K. B. Knight, S. Cirilli, N. Buratti, C. Vérati, S. Nomade, P. R. Renne, N. Youbi, and R. Martini (2004), Synchrony of the Central Atlantic magmatic province and the Triassic-Jurassic boundary climatic and biotic crisis, *Geology*, *32*(11), 973-976.

Marzoli, A., F. Jourdan, J. H. Puffer, T. Cuppone, L. H. Tanner, R. E. Weems, H. Bertrand, S. Cirilli, G. Bellieni, and A. De Min (2011), Timing and duration of the Central Atlantic magmatic province in the Newark and Culpeper basins, eastern USA, *Lithos*, *122*(3), 175-188.

Matzen, A. K., M. B. Baker, J. R. Beckett, and E. M. Stolper (2013), The temperature and pressure dependence of nickel partitioning between olivine and silicate melt, *Journal of Petrology*, *54*(12), 2521-2545.

May, P. R. (1971), Pattern of Triassic-Jurassic diabase dikes around the North Atlantic in the context of predrift position of the continents, *Geological Society of America Bulletin*, *82*(5), 1285-1292.

Mazza, S. E., E. Gazel, E. A. Johnson, M. J. Kunk, R. McAleer, J. A. Spotila, M. Bizimis, and D. S. Coleman (2014), Volcanoes of the passive margin: The youngest magmatic event in eastern North America, *Geology*, *42*(6), 483-486.

McClellan, E., and E. Gazel (2014), The Cryogenian intra-continental rifting of Rodinia: Evidence from the Laurentian margin in eastern North America, *Lithos*, *206–207*(0), 321-337.

McCulloch, M. T., and J. Gamble (1991), Geochemical and geodynamical constraints on subduction zone magmatism, *Earth and Planetary Science Letters*, *102*(3), 358-374.

McDonough, W. F., and S.-S. Sun (1995), The composition of the Earth, *Chemical geology*, *120*(3), 223-253.

McHone, J. G. (1992), Mafic dike suites within Mesozoic igneous provinces of New England and Atlantic Canada, *Geological Society of America Special Papers*, *268*, 1-12.

McHone, J. G. (2000), Non-plume magmatism and rifting during the opening of the central Atlantic Ocean, *Tectonophysics*, *316*(3-4), 9.

McHone, J. G. (2003), Volatile emissions from Central Atlantic Magmatic Province Basalts: Mass assumptions and environmental consequences, *136*, 241-254.

McHone, J. G., and J. R. Butler (1984), Mesozoic igneous provinces of New England and the opening of the North Atlantic Ocean, *Geological Society of America Bulletin*, *95*(7), 757-765.

Merle, R., A. Marzoli, H. Bertrand, L. Reisberg, C. Verati, C. Zimmermann, M. Chiaradia, G. Bellieni, and M. Ernesto (2011), ^{40}Ar/^{39}Ar ages and Sr–Nd–Pb–Os geochemistry of CAMP tholeiites from Western Maranhão basin (NE Brazil), *Lithos*, *122*(3), 137-151.

Merle, R., A. Marzoli, L. Reisberg, H. Bertrand, A. Nemchin, M. Chiaradia, S. Callegaro, F. Jourdan, G. Bellieni, and D. Kontak (2013), Sr, Nd, Pb and Os isotope systematics of CAMP tholeiites from Eastern North America (ENA): Evidence of a subduction-enriched mantle source, *Journal of Petrology*, 55, 133-180.

Millet, M.-A., R. Doucelance, P. Schiano, K. David, and C. Bosq (2008), Mantle plume heterogeneity versus shallow-level interactions: a case study, the São Nicolau Island, Cape Verde archipelago, *Journal of Volcanology and Geothermal Research*, *176*(2), 265-

276.

Missenard, Y., and A. Cadoux (2012), Can Moroccan Atlas lithospheric thinning and volcanism be induced by Edge-Driven Convection?, *Terra Nova*, *24*(1), 27-33.

Morgan, W. J. (1983), Hotspot tracks and the early rifting of the Atlantic, *Tectonophysics*, *94*(1), 123-139.

Moran, P. C., S. M. Barr, C. E. White, and M. A. Hamilton (2007), Petrology, age, and tectonic setting of the Seal Island Pluton, offshore southwestern Nova Scotia, *Canadian Journal of Earth Sciences*, *44*(10), 1467-1478.

Morency, C., M.-P. Doin, and C. Dumoulin (2002), Convective destabilization of a thickened continental lithosphere, *Earth and Planetary Science Letters*, *202*(2), 303-320.

Murphy, J. B., J. Dostal, G. Gutiérrez-Alonso, and J. D. Keppie (2011), Early Jurassic magmatism on the northern margin of CAMP: Derivation from a Proterozoic sub-continental lithospheric mantle, *Lithos*, *123*(1), 158-164.

Navon, O., and E. Stolper (1987), Geochemical consequences of melt percolation: the upper mantle as a chromatographic column, *The Journal of Geology*, 285-307.

Nelson, K. (1992), Are crustal thickness variations in old mountain belts like the Appalachians a consequence of lithospheric delamination?, *Geology*, *20*(6), 498-502.

Niu, Y., M. Wilson, E. R. Humphreys, and M. J. O'Hara (2011), The origin of intra-plate ocean island basalts (OIB): the lid effect and its geodynamic implications, *Journal of Petrology*, *52*(7-8), 1443-1468.

O'hara, M. (1968), The bearing of phase equilibria studies in synthetic and natural systems on the origin and evolution of basic and ultrabasic rocks, *Earth-Science Reviews*, *4*, 69-133.

Olsen, P. E. (1997), Stratigraphic record of the early Mesozoic breakup of Pangea in the Laurasia-Gondwana rift system, *Annual Review of Earth and Planetary Sciences*, *25*(1), 337-401.

Olsen, P. E., R. Schlische, and P. Gore (1989), Tectonic, depositional, and paleoecological history of early Mesozoic rift basins, eastern North America, *Int. Geol. Cong. Field Trip Guidebook*, *351*, 1989.

Ong, P. F., B. A. Van der Pluijm, and R. Van der Voo (2007), Early rotation and late folding in the Pennsylvania salient (US Appalachians): Evidence from calcite-twinning analysis of Paleozoic carbonates, *Geological Society of America Bulletin*, *119*(7-8), 796-804.

Pegram, W. J. (1990), Development of continental lithospheric mantle as reflected in the chemistry of the Mesozoic Appalachian tholeiites, USA, *Earth and Planetary Science Letters*, *97*(3), 316-331.

Pe-Piper, G., and L. F. Jansa (1986), Triassic olivine-normative diabase from Northumberland Strait, eastern Canada: implications for continental rifting, *Canadian Journal of Earth Sciences*, *23*(7), 1013-1021.

Pe-Piper, G., and D. J. Piper (1998), Geochemical evolution of Devonian-Carboniferous igneous rocks of the Magdalen basin, eastern Canada: Pb-and Nd-isotope evidence for mantle and lower crustal sources, *Canadian Journal of Earth Sciences*, *35*(3), 201-221.

Pe-Piper, G., and P. H. Reynolds (2000), Early Mesozoic alkaline mafic dykes, southwestern Nova Scotia, Canada, and their bearing on Triassic–Jurassic magmatism, *The Canadian Mineralogist*, *38*(1), 217-232.

Pe-Piper, G., L. F. Jansa, and R. S. J. Lambert (1992), Early Mesozoic magmatism on the eastern Canadian margin: Petrogenetic and tectonic significance, *Geological Society of America Special Papers*, *268*, 13-36.

Pearce, J., and D. Peate (1995), Tectonic implications of the composition of volcanic arc magmas, *Annual Review of Earth and Planetary Sciences*, *23*, 251-286.

Pearce, J. A. (2008), Geochemical fingerprinting of oceanic basalts with applications to ophiolite classification and the search for Archean oceanic crust, *Lithos*, *100*(1), 14-48.

Pettingill, H. S., A. Sinha, and M. Tatsumoto (1984), Age and origin of anorthosites, charnockites, and granulites in the central Virginia Blue Ridge: Nd and Sr isotopic evidence, *Contributions to Mineralogy and Petrology*, *85*(3), 279-291.

Plank, T. (2005), Constraints from thorium/lanthanum on sediment recycling at subduction zones and the evolution of the continents, *Journal of Petrology*, *46*(5), 921-944.

Plank, T., K. A. Kelley, M. M. Zimmer, E. H. Hauri, and P. J. Wallace (2013), Why do mafic arc magmas contain~ 4wt% water on average?, *Earth and Planetary Science Letters*, *364*, 168-179.

Plank, T. (2014), 4.17 - The Chemical Composition of Subducting Sediments, in *Treatise on Geochemistry (Second Edition)*, edited by H. D. H. K. Turekian, pp. 607-629, Elsevier, Oxford.

Puffer, J. H. (2001), Contrasting high field strength element contents of continental flood basalts from plume versus reactivated-arc sources, *Geology*, *29*(8), 675-678.

Puffer, J. H. (2003), A Reactivated Backield strength element cgma, *The Central Atlantic Magmatic Province: Insights from Fragments of Pangea*, 151-162.

Puffer, J. H., and R. A. Volkert (2001), Pegmatoid and gabbroid layers in Jurassic Preakness and Hook Mountain basalts, Newark Basin, New Jersey, *The Journal of Geology*, *109*(5), 585-601.

Qin, L., and M. Humayun (2008), The Fe/Mn ratio in MORB and OIB determined by ICP-MS, *Geochimica et Cosmochimica Acta*, *72*(6), 1660-1677.

Renne, P. R., C. C. Swisher, A. L. Deino, D. B. Karner, T. L. Owens, and D. J. DePaolo (1998), Intercalibration of standards, absolute ages and uncertainties in 40Ar/39Ar dating, *Chemical Geology*, *145*(1–2), 117-152.

Reynolds, P., P. Elias, G. Muecke, and A. Grist (1987), Thermal history of the southwestern Meguma zone, Nova Scotia, from an 40Ar/39Ar and fission track dating study of intrusive rocks, *Canadian Journal of Earth Sciences*, *24*(10), 1952-1965.

Roeder, P., and R. Emslie (1970), Olivine-liquid equilibrium, *Contributions to mineralogy and petrology*, *29*(4), 275-289.

Ross, M. E. (1992), Petrology and tectonic significance of Mesozoic mafic dikes of the coastal New England igneous province, Massachusetts, *Geological Society of America Special Papers*, *268*, 63-74.

Ross, M. E. (2010), An Early Triassic 40Ar/39Ar age for a camptonite dyke in Cambridge, Massachusetts, *Atlantic Geology*, *46*, 127-135.

Rudnick, R., and S. Gao (2003), Composition of the continental crust, *Treatise on geochemistry*, *3*, 1-64.

Ruiz-Martínez, V. C., T. H. Torsvik, D. J. van Hinsbergen, and C. Gaina (2012), Earth at 200Ma: Global palaeogeography refined from CAMP palaeomagnetic data, *Earth and Planetary Science Letters*, *331*, 67-79.

Sacks, P. E., and D. T. Secor (1990), Delamination in collisional orogens, *Geology*, *18*(10), 999-1002.

Salters, V. J., and A. Stracke (2004), Composition of the depleted mantle, *Geochemistry, Geophysics, Geosystems*, *5*(5).

Samson, S. D., D. G. Coler, and J. A. Speer (1995), Geochemical and NdSrPb isotopic composition of Alleghanian granites of the southern Appalachians: Origin, tectonic setting, and source characterization, *Earth and Planetary Science Letters*, *134*(3), 359-376.

Schlische, R. W., and P. E. Olsen (1990), Quantitative filling model for continental extensional basins with applications to early Mesozoic rifts of eastern North America, *The Journal of Geology*, 135-155.

Schlische, R. W., M. O. Withjack, and P. E. Olsen (2003), Relative timing of CAMP, rifting, continental breakup, and basin inversion: tectonic significance, *The Central Atlantic Magmatic Province: Insights from Fragments of Pangea*, 33-59.

Schott, B., and H. Schmeling (1998), Delamination and detachment of a lithospheric root, *Tectonophysics*, *296*(3), 225-247.

Schott, B., D. A. Yuen, and H. Schmeling (2000), The significance of shear heating in continental delamination, *Physics of the Earth and Planetary Interiors*, *118*(3), 273-290.

Sinha, A., J. Hogan, and J. Parks (1996), Lead isotope mapping of crustal reservoirs within the Grenville Superterrane: I. Central and Southern Appalachians, *Earth Processes: Reading the Isotopic Code*, 293-305.

Sobolev, A. V., A. W. Hofmann, S. V. Sobolev, and I. K. Nikogosian (2005), An olivine-free mantle source of Hawaiian shield basalts, *Nature*, *434*(7033), 590-597.

Sobolev, A. V., et al. (2007), The Amount of Recycled Crust in Sources of Mantle-Derived Melts, *Science*, *316*(5823), 412-417.

Steiger, R. H., and E. Jäger (1977), Subcommission on geochronology: convention on the use of decay constants in geo-and cosmochronology, *Earth and planetary science letters*, *36*(3), 359-362.

Stern, C. R. (2011), Subduction erosion: rates, mechanisms, and its role in arc magmatism and the evolution of the continental crust and mantle, *Gondwana Research*, *20*(2), 284-308.

Storey, B. C. (1995), The role of mantle plumes in continental breakup: case histories from Gondwanaland, *Nature*, *377*(6547), 301-308.

Sun, S.-S., and W. McDonough (1989), Chemical and isotopic systematics of oceanic basalts: implications for mantle composition and processes, *Geological Society, London, Special Publications*, *42*(1), 313-345.

Sundeen, D. A., and M. C. Huff (1992), Petrography, petrology, and K-Ar geochronology of hypabyssal mafic and silicic Mesozoic igneous rocks in southeastern New Hampshire, *Geological Society of America Special Papers*, *268*, 75-94

Swanson, M. T. (1992), Structural sequence and tectonic significance of Mesozoic dikes in southern coastal Maine, *Geological Society of America Special Papers*, *268*, 37-62.

Tanton, L. T. E., and B. H. Hager (2000), Melt intrusion as a trigger for lithospheric foundering and the eruption of the Siberian flood basalts, *Geophysical research letters*, *27*(23), 3937-3940.

Tarduno, J., H. Mayer, E. Winterer, W. Sliter, L. Kroenke, J. Mahoney, M. Leckie, R. Musgrave, and M. Storey (1991), Rapid formation of Ontong Java Plateau by Aptian mantle plume volcanism, *Science*, *254*(5030), 399-403.

Toplis, M. (2005), The thermodynamics of iron and magnesium partitioning between olivine and liquid: criteria for assessing and predicting equilibrium in natural and experimental systems, *Contributions to Mineralogy and Petrology*, *149*(1), 22-39.

van Staal, C. R., J. B. Whalen, P. Valverde-Vaquero, A. Zagorevski, and N. Rogers (2009), Pre-Carboniferous, episodic accretion-related, orogenesis along the Laurentian margin of the northern Appalachians, *Geological Society, London, Special Publications*, *327*(1), 271-316.

Verati, C., H. Bertrand, and G. Féraud (2005), The farthest record of the Central Atlantic Magmatic Province into West Africa craton: Precise 40 Ar/39 Ar dating and geochemistry of Taoudenni basin intrusives (northern Mali), *Earth and Planetary Science Letters*, *235*(1), 391-407.

Wagner, L. S., K. Stewart, and K. Metcalf (2012), Crustal-scale shortening structures beneath the Blue Ridge Mountains, North Carolina, USA, *Lithosphere*, *4*(3), 242-256.

Walter, M. J. (1998), Melting of garnet peridotite and the origin of komatiite and depleted lithosphere, *Journal of Petrology*, *39*(1), 29-60.

Wang, Z., and G. A. Gaetani (2008), Partitioning of Ni between olivine and siliceous eclogite partial melt: experimental constraints on the mantle source of Hawaiian basalts, *Contributions to Mineralogy and Petrology*, *156*(5), 661-678.

Weigand, P. W., and P. C. Ragland (1970), Geochemistry of Mesozoic dolerite dikes from eastern North America, *Contributions to Mineralogy and Petrology*, *29*(3), 195-214.

White, W. M., F. Albarède, and P. Télouk (2000), High-precision analysis of Pb isotope ratios by multi-collector ICP-MS, *Chemical Geology*, *167*(3), 257-270.

White, R., and D. McKenzie (1989), Magmatism at Rift Zones: The Generation of Volcanic Continental Margins and Flood Basalts, *Journal of Geophysical Research*, *94*(B6), 44.

White, W. M., and B. Dupré (1986), Sediment subduction and magma genesis in the Lesser Antilles: isotopic and trace element constraints, *Journal of Geophysical Research: Solid Earth (1978–2012)*, *91*(B6), 5927-5941.

Wilson, J. T. (1965), A New Class of Faults and their Bearing on Continental Drift, *Nature*, *207*(4995), 343-347.

Wilson, J. T. (1966), Did the Atlantic Close and then Re-Open?, *Nature*, *211*(5050), 676-681.

Wilson, M. (1997), Thermal evolution of the Central Atlantic passive margins: continental break-up above a Mesozoic super-plume, *Journal of the Geological Society*, *154*(3), 491-495.

Wise, D. U. (2004), Pennsylvania salient of the Appalachians: A two-azimuth transport model based on new compilations of Piedmont data, *Geology*, *32*(9), 777-780.

Withjack, M. O., P. E. Olsen, and R. W. Schlische (1995), Tectonic evolution of the Fundy rift basin, Canada: evidence of extension and shortening during passive margin development, *Tectonics*, *14*(2), 390-405.

Woodcock, N., N. Soper, and R. Strachan (2007), A Rheic cause for the Acadian deformation in Europe, *Journal of the Geological Society*, *164*(5), 1023-1036.

Woodhead, J., J. Hergt, J. Davidson, and S. Eggins (2001), Hafnium isotope evidence for 'conservative'element mobility during subduction zone processes, *Earth and Planetary Science Letters*, *192*(3), 331-346.

Wortel, M., and W. Spakman (2000), Subduction and slab detachment in the Mediterranean-Carpathian region, *Science*, *290*(5498), 1910-1917.

Zhang, H.-F., Y.-L. Sun, Y.-J. Tang, Y. Xiao, W.-H. Zhang, X.-M. Zhao, M. Santosh, and M. A. Menzies (2012), Melt-peridotite interaction in the Pre-Cambrian mantle beneath the western North China Craton: Petrology, geochemistry and Sr, Nd and Re isotopes, *Lithos*, *149*, 100-114.

Figures

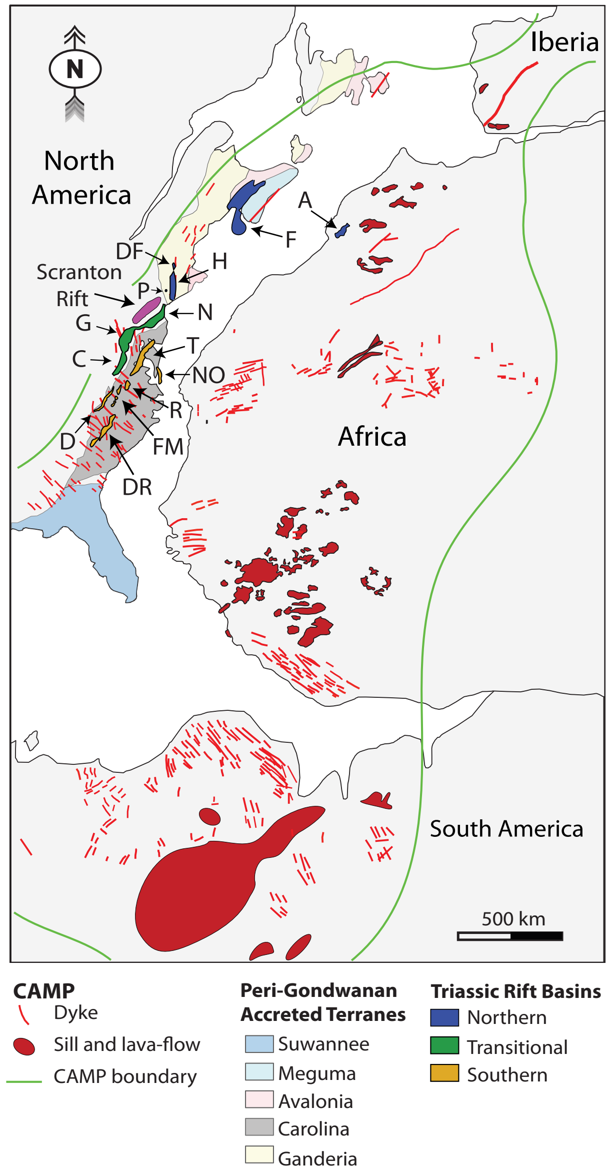

Figure 1. Map of CAMP modified from Deckart et al. [2005]. Continents are in the prerift configuration of Pangea after Bullard et al. [1965]. CAMP exposures and boundary after McHone [2003]. Mesozoic rift basin loca- tions: F, Fundy; A, Argana; DF, Deerfield; H, Hartford; P, Pomperaug; N, Newark; G, Gettysburg; C, Culpepper; T,

Taylorsville; NO, Norfolk; R, Richmond; FM, Farmville; D, Danville; DR, Deep River from Schlische et al. [2003] and Olsen [1997]. Accreted terrane boundaries from Hibbard et al. [2010] and Hatcher [2010]. It should be noted that the extension of the Carolina terrane to the North and East beneath the coastal plain is based on subsurface data and is much less certain [Hatcher, 2010]. Alternatively the more northern portion of Carolina could be part of Avalonia [Hatcher, 2010]. The Scranton Rift location is from Benoit et al. [2014].

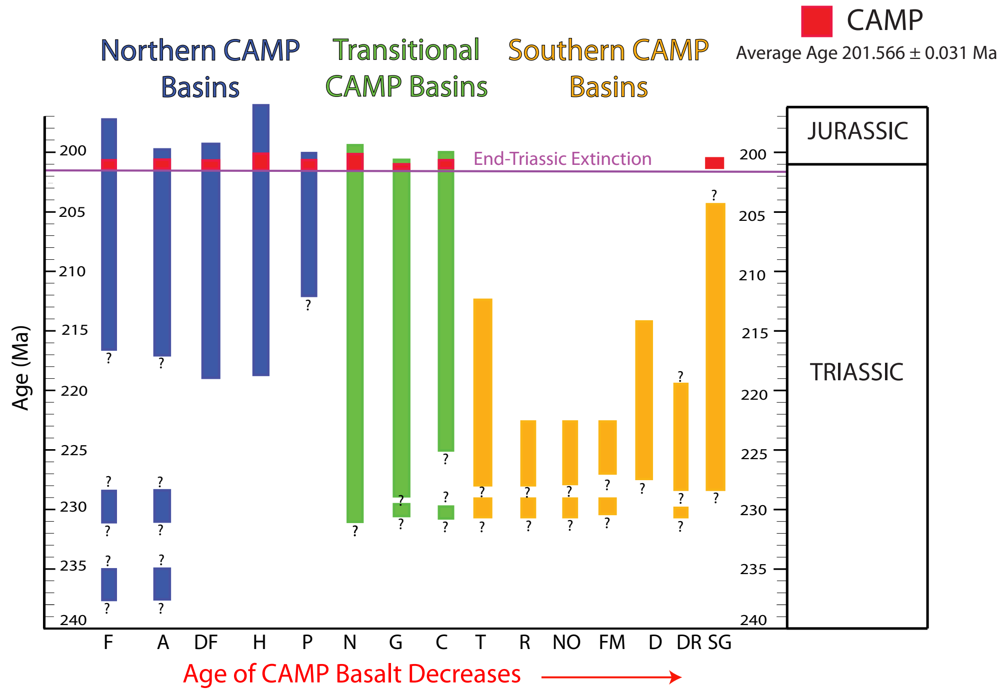

Figure 2. Rifting and sediment depositional history of Mesozoic rift basins after Olsen [1997]. Rift basins from left to right: northern basins: F, Fundy; A, Argana; DF, Deerfield; H, Hartford; P, Pomperaug; transitional basins: N, Newark; G, Gettysburg; C, Culpepper; southern basins: T, Taylorsville; R, Richmond; N, Norfolk; FM, Farmville; D, Danville/Deep River; DR, Deep River; SG, South Georgia. The average age of CAMP and timing of the End-Triassic Extinction (ETE) are from Blackburn et al. [2013]. Rifting and deposition begins and ends earlier in the southern than in the northern basins. Additionally, synrift CAMP flows are absent from the southern rift basins. Deposition in the Newark, Gettysburg, and Culpepper basins begins in the Late Triassic, as in the case with the southern basins, but continues into the Jurassic like the northern basins. Age constraints for basin fill rely on biostratigraphy, paleomagnetic data and Milankovitch cyclicity and are poorly constrained [Olsen, 1997]. Shown here are the best estimates of maximum ages based on the available information.

A)

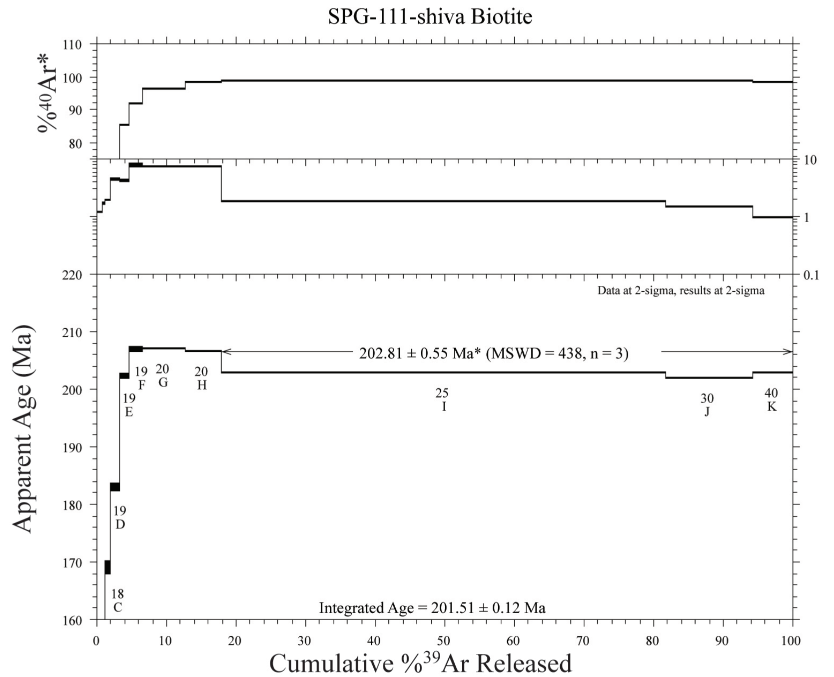

B)

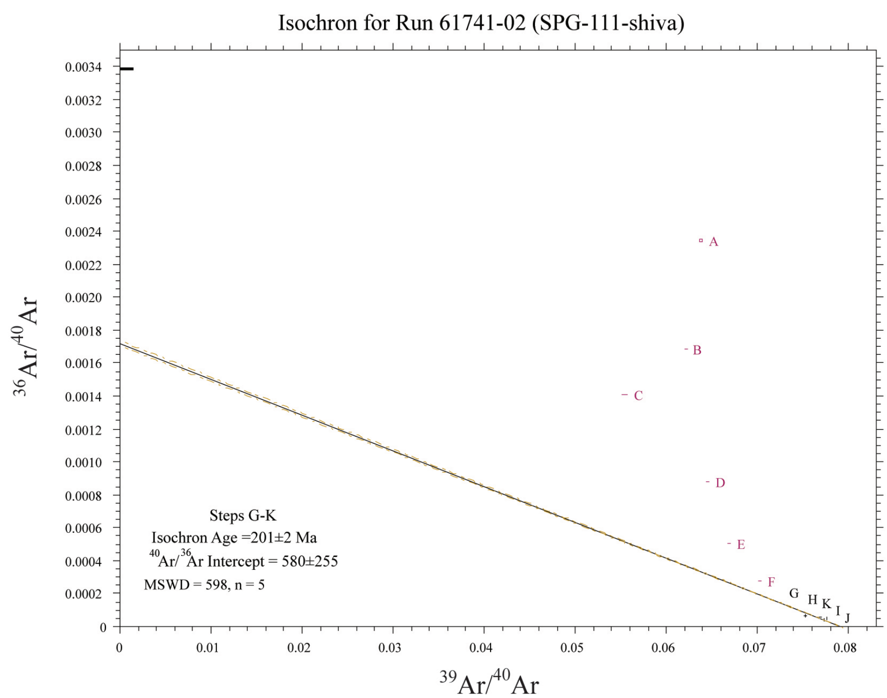

Figure 3. $^{40}Ar/^{39}Ar$ age dating results. A) Age spectra was produced for sample

SPG-111. After 82% of the ^{39}Ar was released a weighted mean average of 202±0.55Ma was obtained. B) Evaluation with the inverse isochron technique yielded a large MSWD for the calculated age, resulting in a large error.

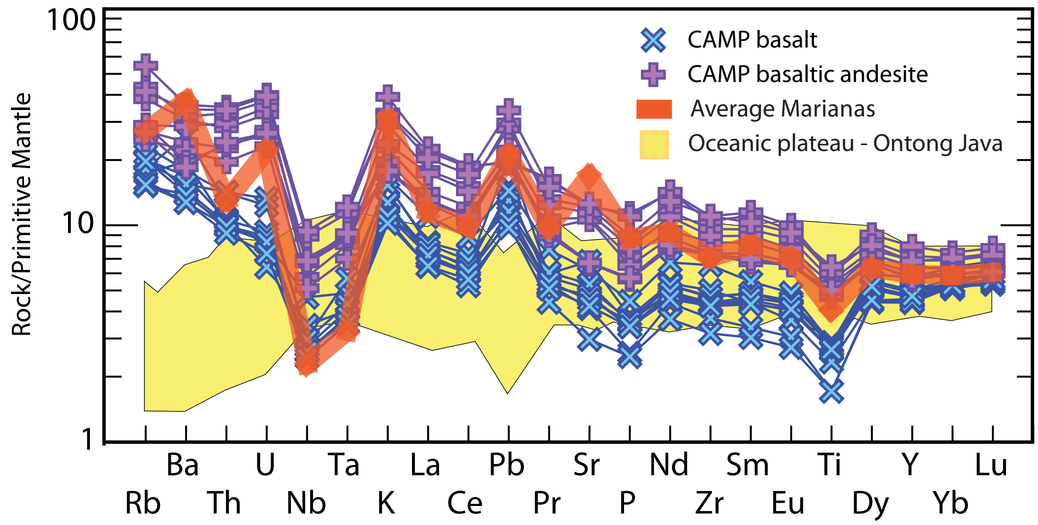

Figure 4. Multi-element diagram normalized to primitive mantle after McDonough and Sun [1995]. This diagram compares CAMP to a Marianas Arc average from Gazel et al. [2015] and representative samples from the Ontong Java oceanic plateau (data from the GEOROC database http://georoc.mpch-mainz.gwdg.de/georoc/). CAMP samples have both Nb and Ta depletions as well as LILE enrichments similar to the Marianas Arc average, but differing from the Ontong Java Plateau, which is plume-derived [e.g., Tarduno et al., 1991].

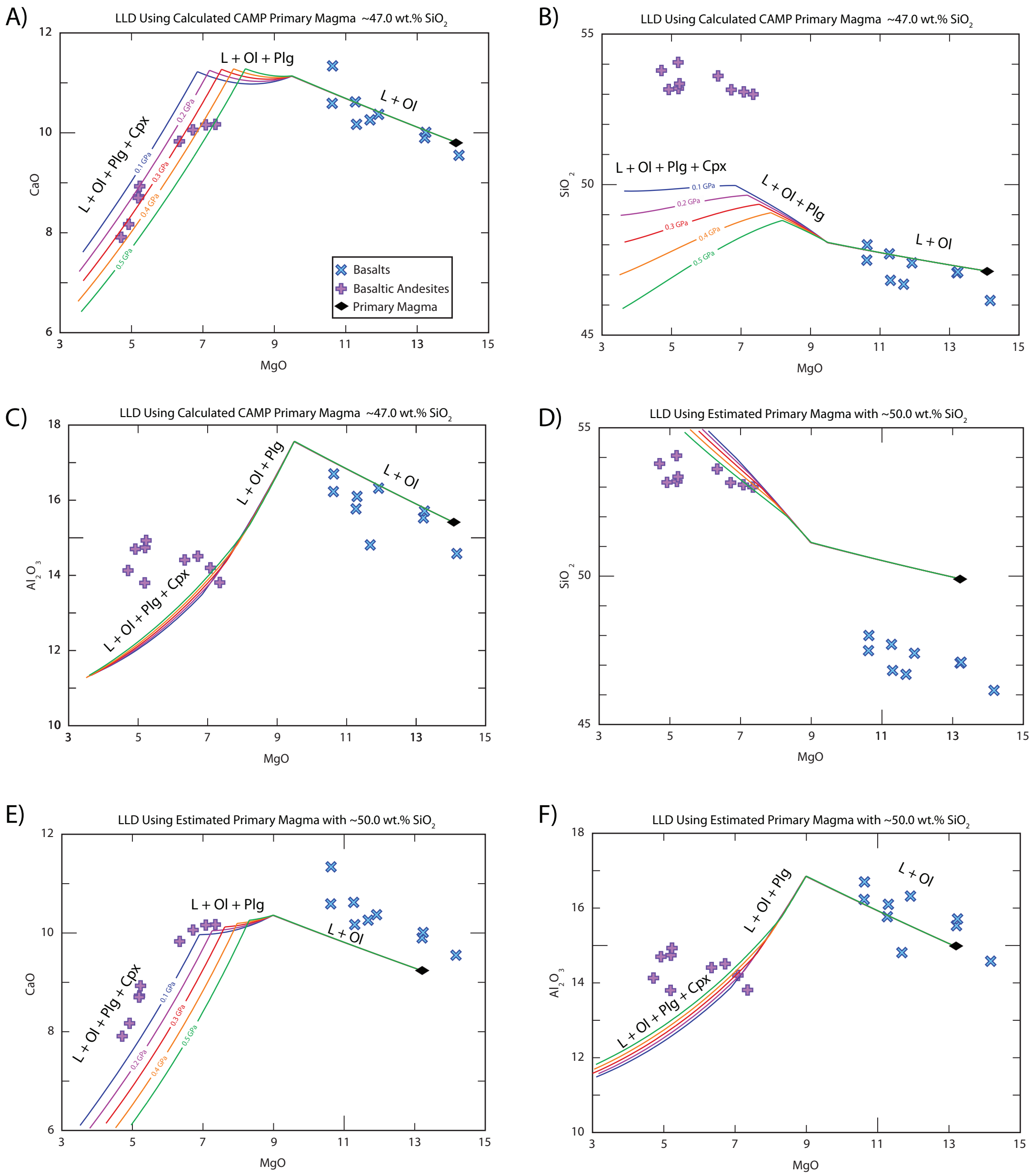
A)
LLD Using Calculated CAMP Primary Magma ~47.0 wt.% SiO2
L + Ol + Plg
L + Ol + Plg + Cpx
L + Ol
0.1 GPa
0.2 GPa
0.3 GPa
0.4 GPa
0.5 GPa
Basalts
Basaltic Andesites
Primary Magma
CaO
MgO
B)
LLD Using Calculated CAMP Primary Magma ~47.0 wt.% SiO2
L + Ol + Plg + Cpx
L + Ol + Plg
L + Ol
SiO2
MgO
C)
LLD Using Calculated CAMP Primary Magma ~47.0 wt.% SiO2
L + Ol + Plg
L + Ol
L + Ol + Plg + Cpx
Al2O3
MgO
D)
LLD Using Estimated Primary Magma with ~50.0 wt.% SiO2
SiO2
MgO
E)
LLD Using Estimated Primary Magma with ~50.0 wt.% SiO2
L + Ol + Plg
L + Ol
L + Ol + Plg + Cpx
CaO
MgO
F)
LLD Using Estimated Primary Magma with ~50.0 wt.% SiO2
L + Ol
L + Ol + Plg
L + Ol + Plg + Cpx
Al2O3
MgO

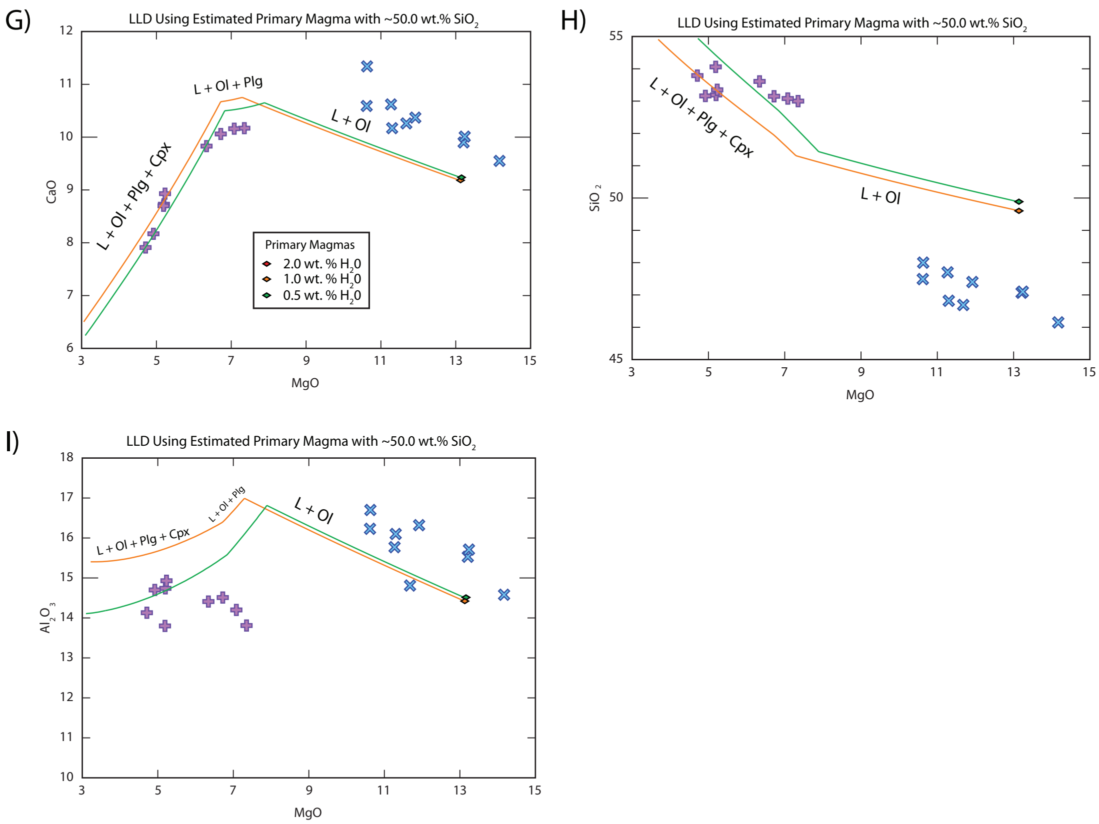

Figure 5. Major Element variation diagrams. This diagram shows liquid lines of descent (LLD) for samples analyzed in this study. LLDs calculated with Petrolog3 software [Danyushevsky and Plechov, 2011].

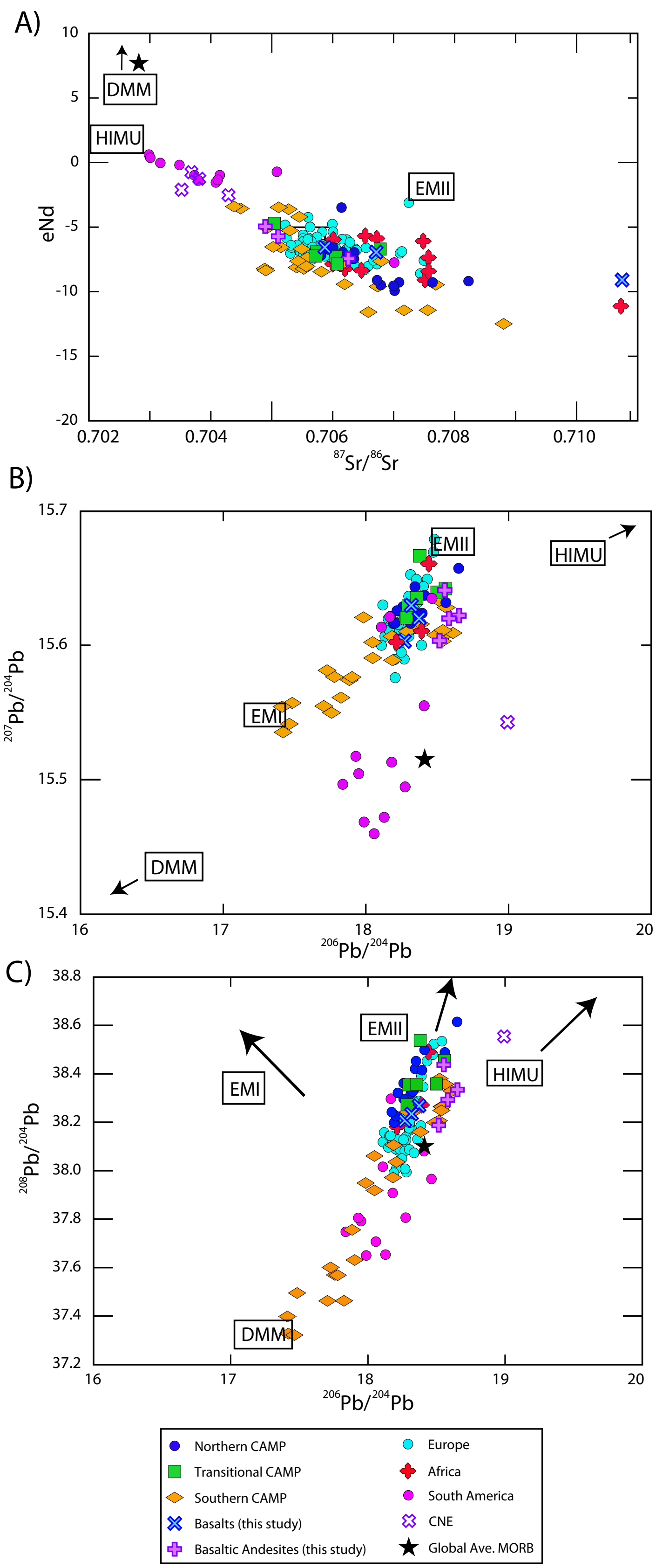
A)
DMM
HIMU
EMII
eNd
87Sr/86Sr
B)
EMII
HIMU
EMI
DMM
207Pb/204Pb
206Pb/204Pb
C)
EMII
EMI
HIMU
DMM
208Pb/204Pb
206Pb/204Pb
Northern CAMP
Transitional CAMP
Southern CAMP
Basalts (this study)
Basaltic Andesites (this study)
Europe
Africa
South America
CNE
Global Ave. MORB

Figure 6. Age corrected (200 Ma) Sr-Nd-Pb radiogenic isotopes. Samples are from Africa [Bertrand, 1991; Marzoli et al., 2004; Deckart et al., 2005; Verati et al., 2005; Mahmoudi and Bertrand, 2007] and Europe [Cebria et al., 2003; Jourdan et al., 2003; Martins et al., 2008; Callegaro et al., 2014] plot alongside northern and transitional CAMP [Dostal and Durning, 1998; Marzoli et al., 2011; Merle et al., 2013]. South Ameri- can CAMP [Deckart et al., 2005; Merle et al., 2011] lavas plot with northern and transitional CAMP or depleted MORB mantle (DMM) and Global Average MORB [Gale et al., 2013] indicative of the transition to oceanic crust [Deckart et al., 2005]. Coastal New England Province lavas are from Pe-Piper and Reynolds [2000] and Dorais et al. [2005]. Global average MORB from Gale et al. [2013]. Location of mantle reservoirs HIMU (high l 5 $^{238}U/^{204}Pb$), depleted MORB mantle (DMM), enriched mantle I (EMI) and enriched mantle II (EMII) after Hofmann [2007]. Additional southern CAMP data from Callegaro et al. [2013] and Mazza et al. [2014]. Radiogenic isotope ratios were age corrected to initial eruptive values at 200 Ma assuming parent/daughter values reported in Table 4 using decay constants from Steiger and Jäger [1977].

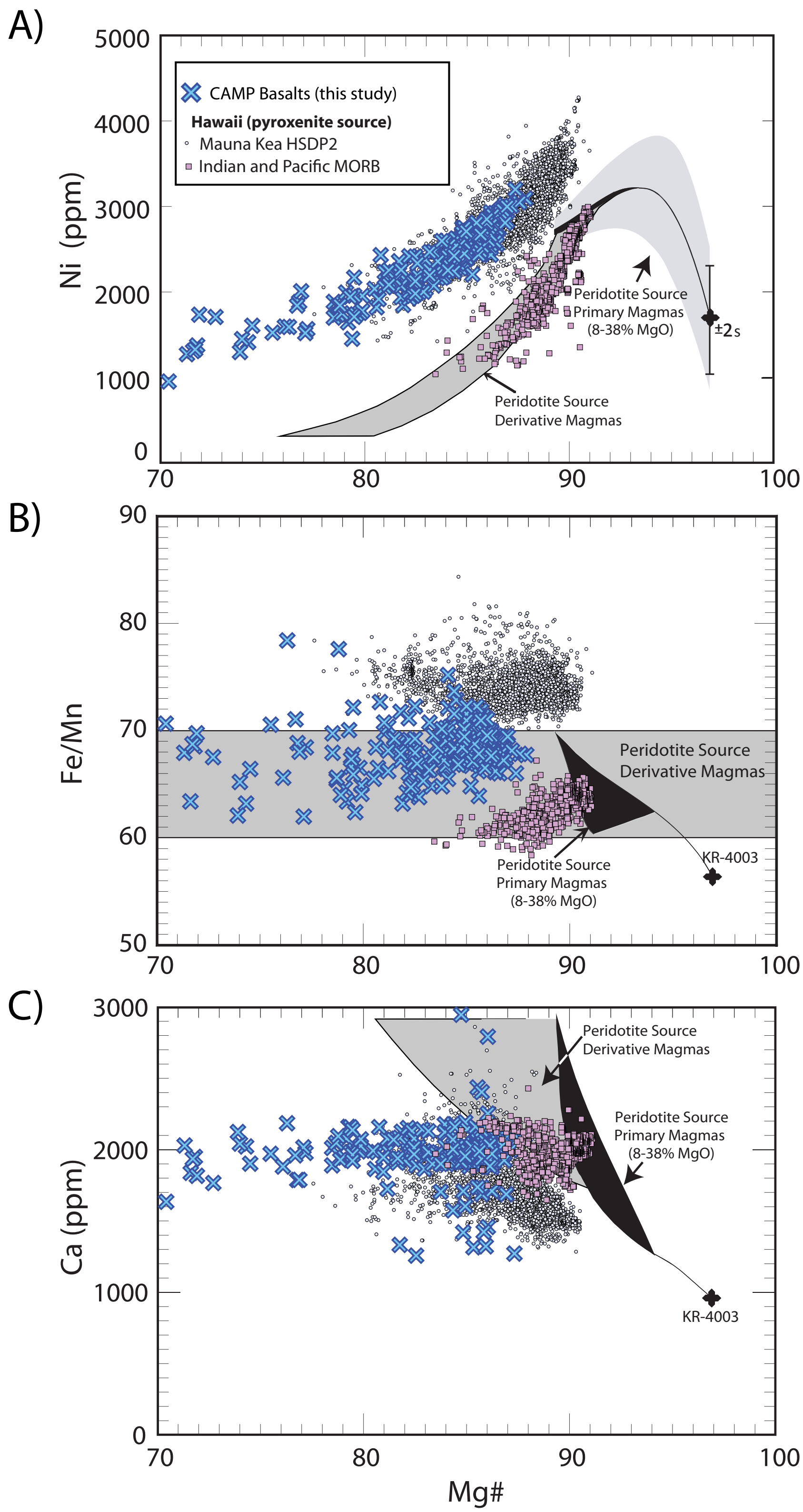

A)
CAMP Basalts (this study)
Hawaii (pyroxenite source)
Mauna Kea HSDP2
Indian and Pacific MORB
Ni (ppm)
Peridotite Source
Primary Magmas
(8-38% MgO)
±2s
Peridotite Source
Derivative Magmas
B)
Fe/Mn
Peridotite Source
Derivative Magmas
Peridotite Source
Primary Magmas
(8-38% MgO)
KR-4003
C)
Peridotite Source
Derivative Magmas
Peridotite Source
Primary Magmas
(8-38% MgO)
Ca (ppm)
KR-4003
Mg#

Figure 7. Trace element data from CAMP olivine phenocrysts. Diagram shows trace element data versus Mg# ([molar MgO/FeO1MgO]*100%). (a) CAMP samples plot alongside data from Mauna Kea and above Indian and Pacific MORB samples [Sobolev et al., 2007] suggesting a pyroxenite component. (b) CAMP data plots within the peridotite-derived field, but also at elevated Fe/Mn values indicating a pyroxenite component. (c) CAMP data plots at lower Ca values than expected for peridotite-derived melts further supporting a pyroxenite component in the source. Diagrams modified from Herzberg [2011].

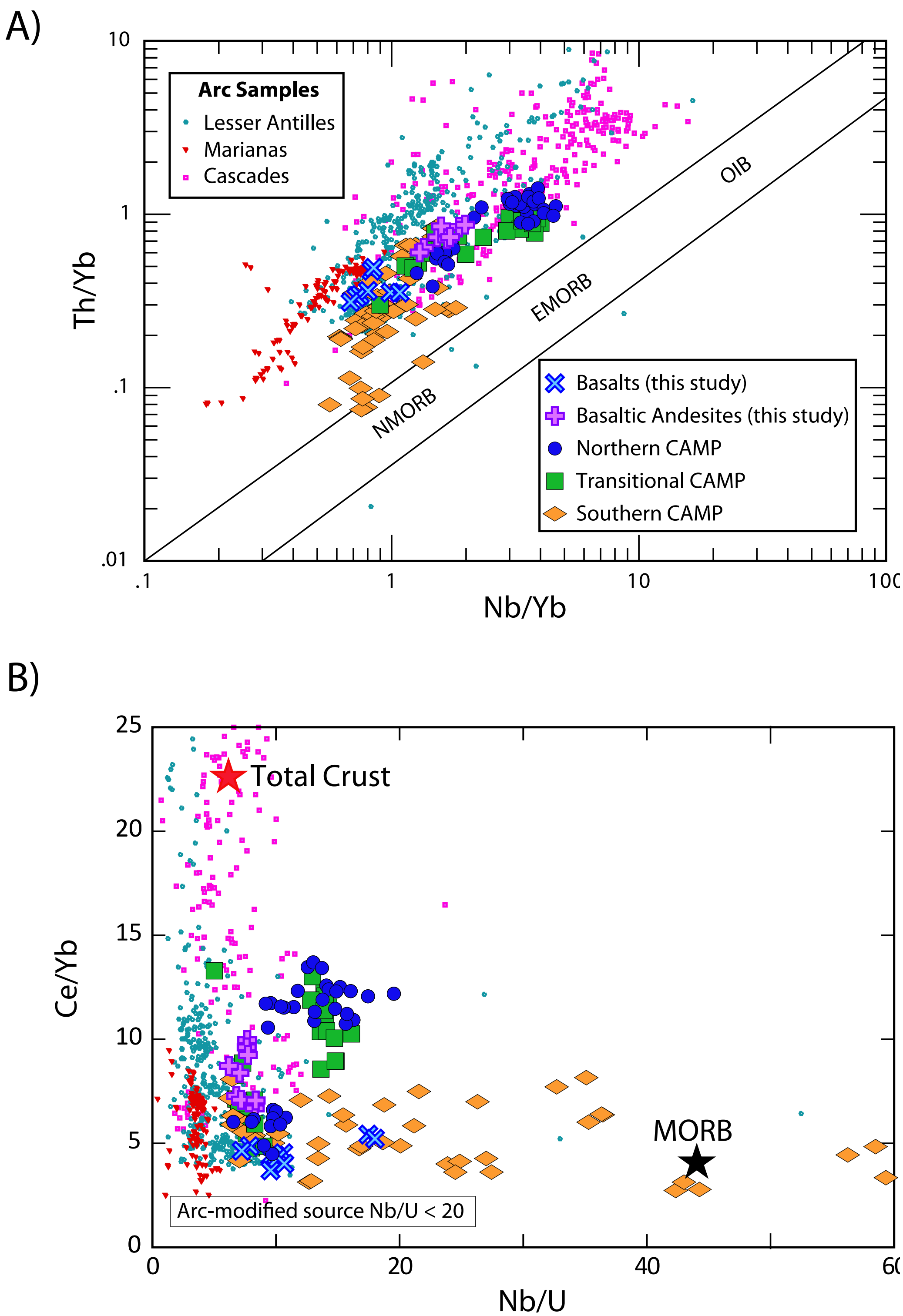
A)
Arc Samples
Lesser Antilles
Marianas
Cascades
Basalts (this study)
Basaltic Andesites (this study)
Northern CAMP
Transitional CAMP
Southern CAMP
OIB
EMORB
NMORB
Th/Yb
Nb/Yb
10
1
.1
.01
.1
1
10
100
B)
Total Crust
MORB
Arc-modified source Nb/U < 20
Ce/Yb
Nb/U
25
20
15
10
5
0
0
20
40
60

Figure 8. Trace element comparison of northern, southern and transitional CAMP. The Lesser Antilles and Marianas arcs were selected for comparison as the terranes accreted to the Laurentian margin were most likely island arcs [Hatcher, 2010]. The Cascades Arc was included because it developed on previously accreted terranes [e.g., Coney et al., 1980] making it similar to the arcs that may have developed on the Laurentian margin. (a) Th/Yb-Nb/Yb diagram after Pearce [2008] showing CAMP lavas plotting above the mantle array along with arc samples. (b) Nb/U - Ce/Yb plot for northern, transitional and southern CAMP. The small group of northern and transitional CAMP samples with lower Ce/Yb, Th/Yb, and Nb/U ratios are younger pulses of CAMP [Blackburn et al., 2013]. Additional CAMP data from Bertrand [1991]; Dostal and Durning [1998]; Puffer and Volkert [2001]; Cebria et al. [2003]; Jourdan et al. [2003]; Marzoli et al. [2004]; Deckart et al. [2005]; Verati et al. [2005]; Mahmoudi and Bertrand [2007]; Martins et al. [2008]; Marzoli et al. [2011]; Merle et al. [2011]; Callegaro et al. [2013]; Merle et al. [2013]; Callegaro et al. [2014]; Mazza et al. [2014] and arc data from the GEOROC database (http:// georoc.mpch-mainz.gwdg.de/georoc/).

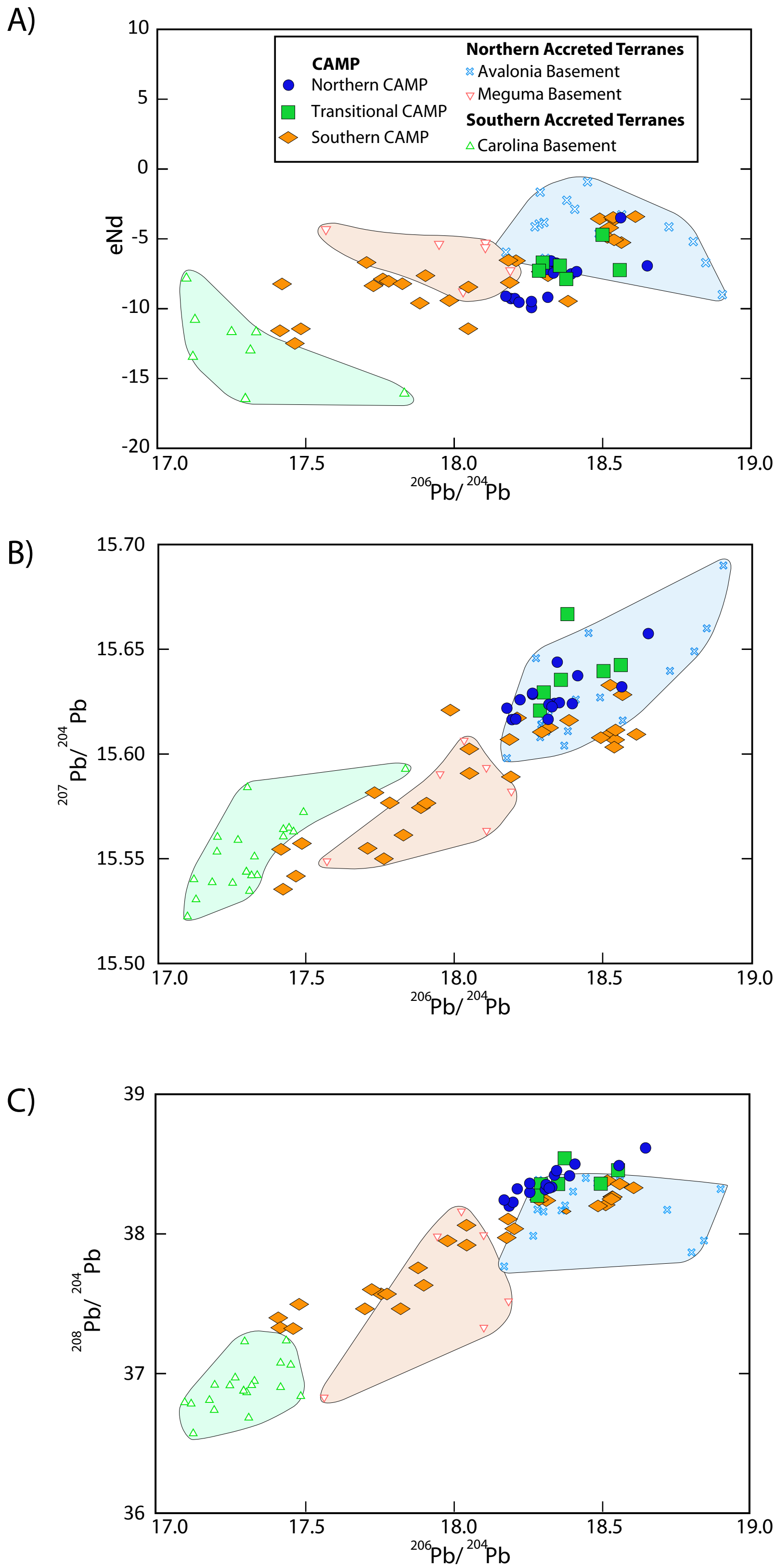
A)
CAMP
Northern CAMP
Transitional CAMP
Southern CAMP
Northern Accreted Terranes
Avalonia Basement
Meguma Basement
Southern Accreted Terranes
Carolina Basement
eNd
206Pb/204Pb
B)
207Pb/204Pb
206Pb/204Pb
C)
208Pb/204Pb
206Pb/204Pb

Figure 9. Age corrected (200 Ma) Nd-Pb radiogenic isotope comparison between northern, southern and transitional CAMP. CAMP is compared with data from Paleozoic accreted terranes: Avalonia [Pe-Piper and Piper, 1998], Meguma [Currie et al., 1998] and Carolina [Pettingill et al., 1984; Sinha et al., 1996]. For A-C northern and transitional CAMP plot with the northern accreted terranes, Avalonia and Meguma, while southern CAMP spans all three. Previous workers have shown that crustal contamination cannot account for the isotopic signature of CAMP lavas [Puffer, 2001; Merle et al., 2011; Callegaro et al., 2013, 2014]. Additional CAMP data: [Dostal and Durning, 1998; Marzoli et al., 2011; Callegaro et al., 2013; Merle et al., 2013; Mazza et al., 2014]. Radiogenic isotope ratios were age corrected to initial eruptive values at 200 Ma assuming parent/daughter values reported in Table 4 using decay constants from Steiger and Jäger
[1977].

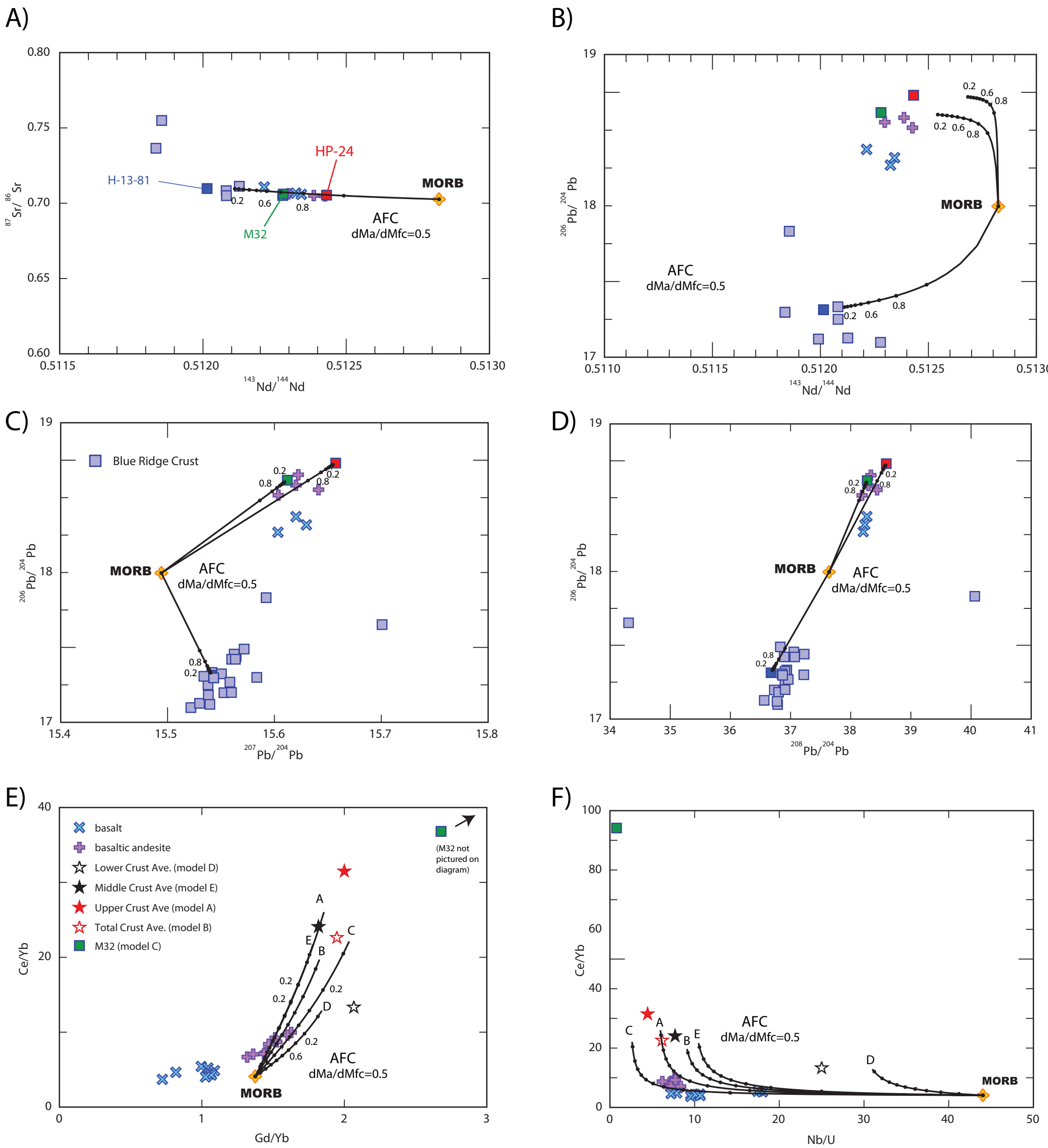

A)
0.80
0.75
0.70
0.65
0.60
0.5115
0.5120
0.5125
0.5130
87Sr/86Sr
143Nd/144Nd
H-13-81
HP-24
MORB
M32
AFC
dMa/dMfc=0.5
0.2
0.6
0.8
B)
19
18
17
0.5110
0.5115
0.5120
0.5125
0.5130
206Pb/204Pb
143Nd/144Nd
MORB
AFC
dMa/dMfc=0.5
0.2
0.6
0.8
C)
Blue Ridge Crust
MORB
AFC
dMa/dMfc=0.5
15.4
15.5
15.6
15.7
15.8
206Pb/204Pb
207Pb/204Pb
0.2
0.8
D)
MORB
AFC
dMa/dMfc=0.5
34
35
36
37
38
39
40
41
206Pb/204Pb
208Pb/204Pb
0.2
0.8
E)
40
20
0
0
1
2
3
basalt
basaltic andesite
Lower Crust Ave. (model D)
Middle Crust Ave (model E)
Upper Crust Ave (model A)
Total Crust Ave. (model B)
M32 (model C)
(M32 not pictured on diagram)
A
B
C
D
E
0.2
0.6
AFC
dMa/dMfc=0.5
MORB
Ce/Yb
Gd/Yb
F)
100
80
60
40
20
0
0
10
20
30
40
50
A
B
C
D
E
AFC
dMa/dMfc=0.5
MORB
Ce/Yb
Nb/U

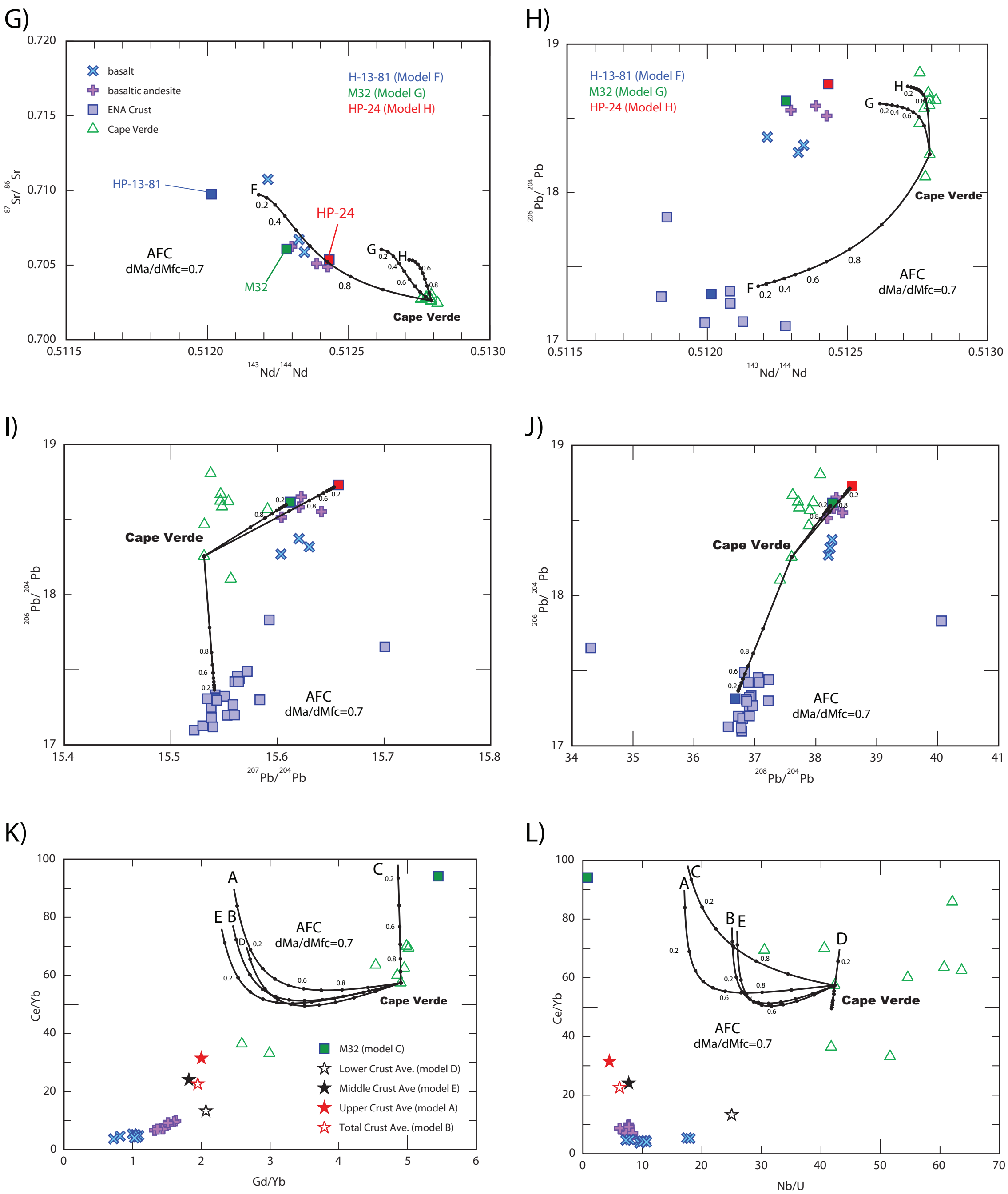

Figure 10. Assimilation Fractional crystallization models. A-F shows models using MORB starting composition from Gale et al. [2013]. G-L shows models using a basanite from Cape Verde as an Atlantic plume starting composition [*Holm et al.,* 2005; *Millet et al.,* 2008].

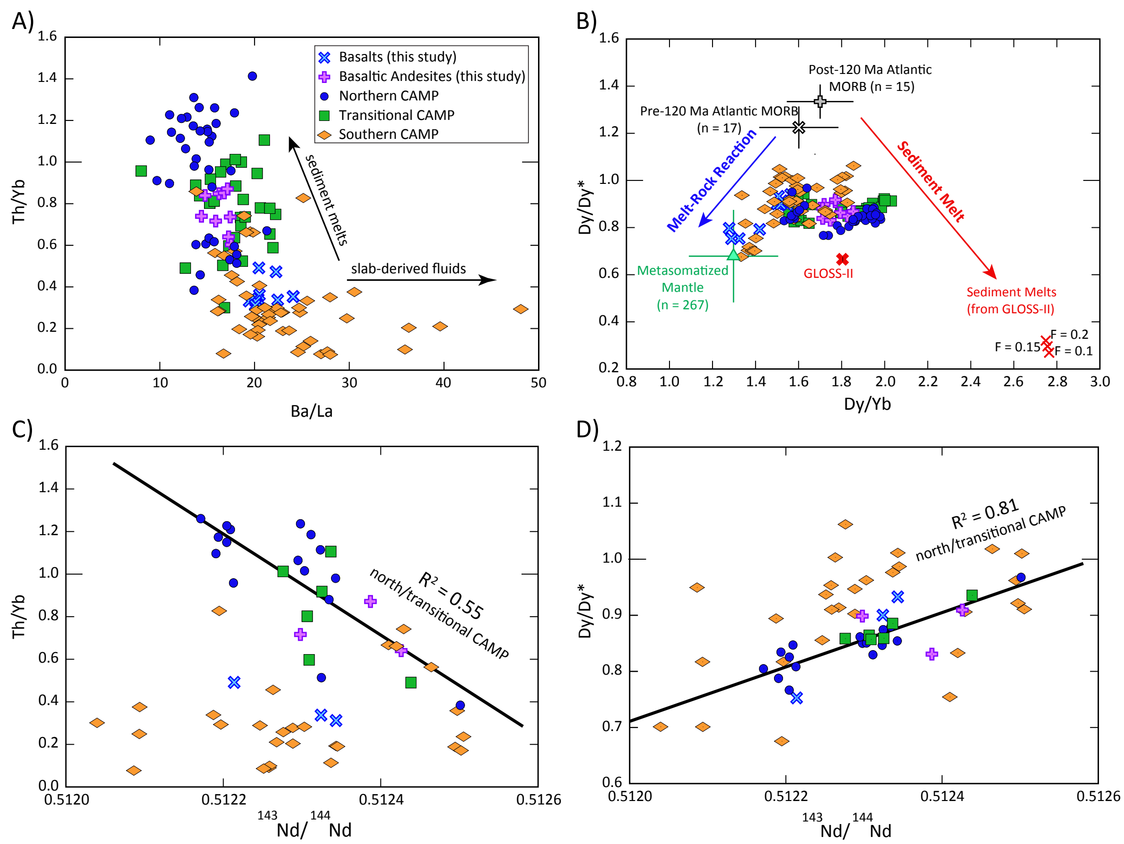

Figure 11. Discriminating between metasomatism by fluids or sediment-melt components in CAMP magmas. (a) Ba/La-Th/Yb diagram [after Woodhead et al., 2001] shows a high Th/Yb trend indicating a sediment melt component, and a high Ba/La trend indicating a fluid component. Northern and transitional CAMP follow the high Th/Yb trend, while southern CAMP follows the high Ba/La trend. (a) CAMP plots similarly to arc magmas on a Dy/Dy*-Dy/Yb diagram (modified from Davidson et al. [2013] with REE used in the Dy/Dy* calculation normalized to values from Sun and McDonough [1989]). Northern and transitional CAMP have higher middle rare earth element contents relative to heavy rare earth element contents than southern CAMP as indicated by higher Dy/Yb. Northern and transitional CAMP show positive trends between Dy/Dy* and Dy/Yb (Figure 11b). A subset of mostly southern CAMP (including the Virginia basalt

samples analyzed for this study) and one northern CAMP sample from the Caraquet dike from New Brunswick [Dostal and Durning, 1998] plot in the lower left- hand corner of the diagram (Dy/Dy* < 1.0, Dy/Yb < 1.55). Atlantic MORB averages calculated from Janney and Castillo [2001]. Mantle xenolith data from the GEOROC database (http://georoc.mpch-mainz.gwdg.de/georoc/). Composition of subducting sediment (GLOSS-II) from Plank [2014]. As an example of possible sediment melt composition we calculated equilibrium melting (at melt fractions 0.05, 0.1, 0.20) starting from GLOSS-II in eclogite facies using the partition coefficients in Kelemen et al. [2003].

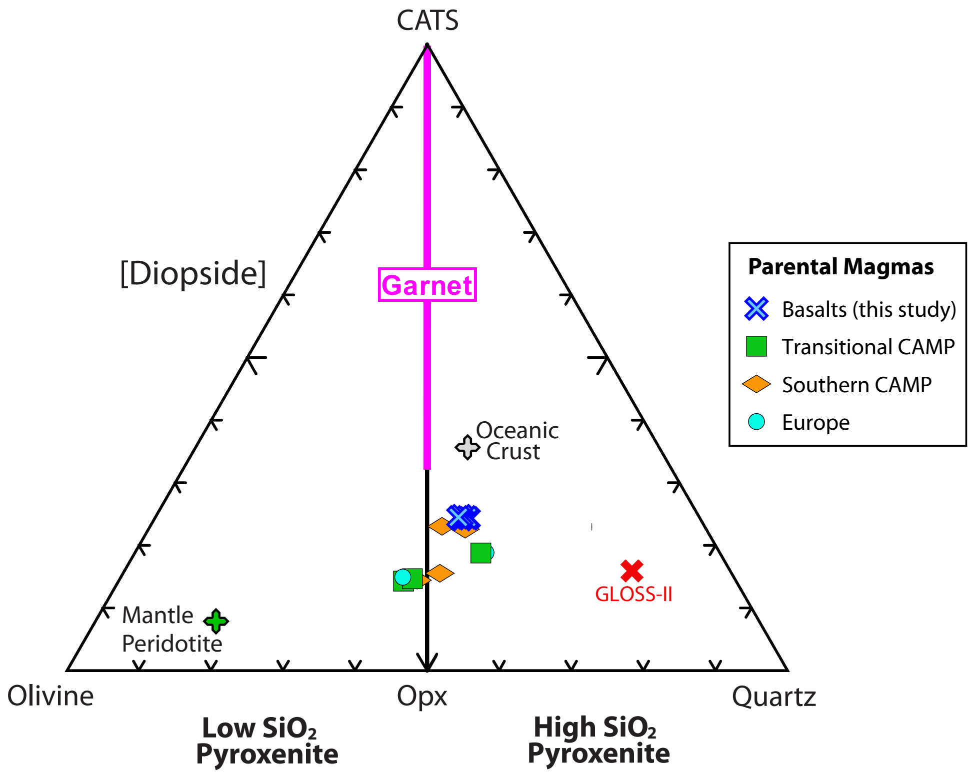

Figure 12. CAMP primary magma compositions (Table 9) on a mole% projection toward diopside into the olivine-quartz-calcium Tschermak's plane after O'hara [1968]. Reference values: mantle peridotite (KR-4003) [Walter, 1998], oceanic crust (Siqueiros Fracture Zone) [Herzberg and Asimow, 2008], and the composition of subducting sediment (GLOSS-II) from Plank [2014]. Most of the CAMP primary magmas plot on the high SiO_2 side of the diagram, possibly indicating a significant silica-rich, olivine-free pyroxenite component in the source. Northern CAMP could not be compared as samples are too evolved to be in olivine control.

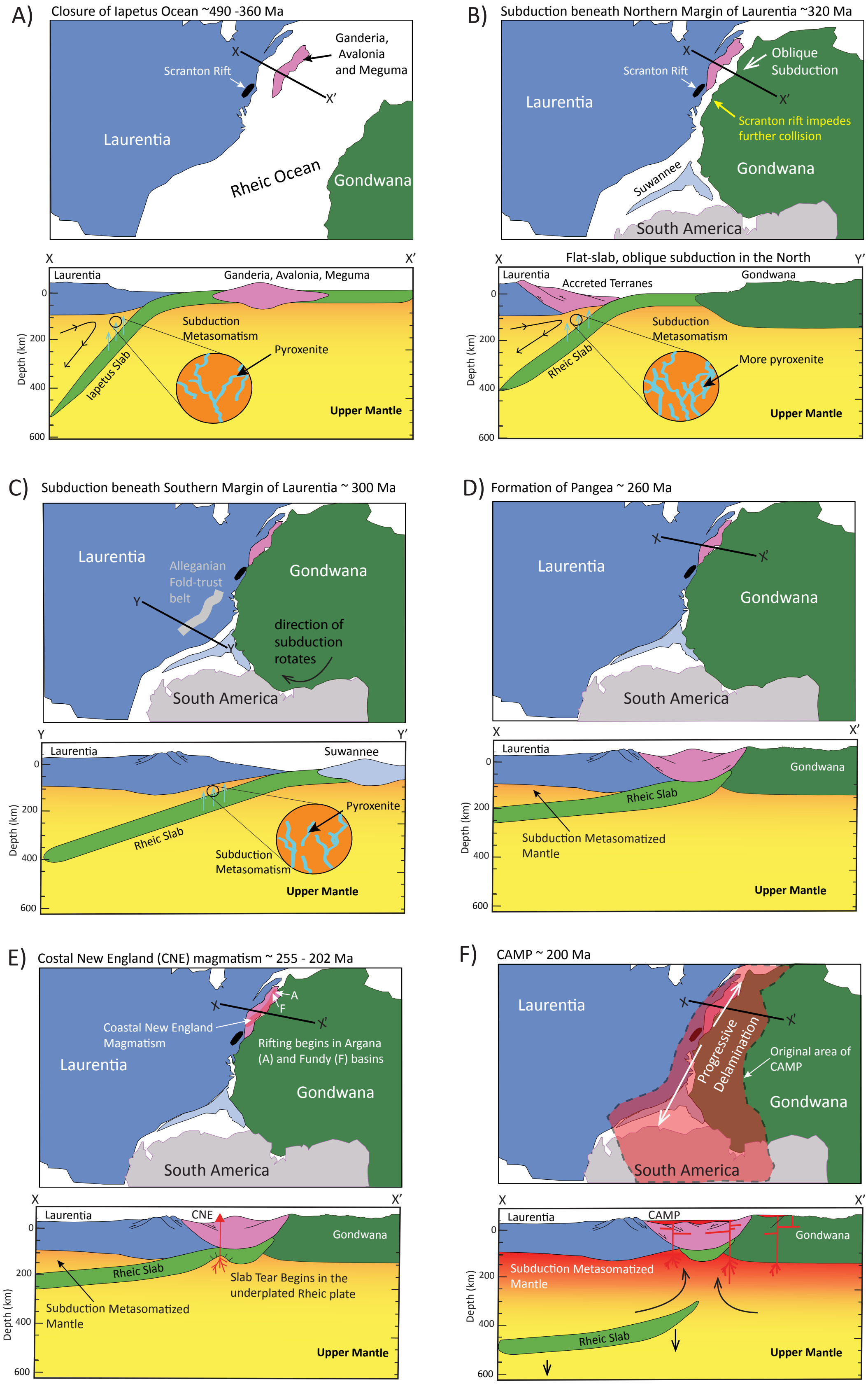
A) Closure of Iapetus Ocean ~490 -360 Ma
Ganderia, Avalonia and Meguma
Scranton Rift
X
X'
Laurentia
Rheic Ocean
Gondwana
X
X'
Laurentia
Ganderia, Avalonia, Meguma
Subduction Metasomatism
Pyroxenite
Iapetus Slab
Upper Mantle
Depth (km)
0
200
400
600
B) Subduction beneath Northern Margin of Laurentia ~320 Ma
Scranton Rift
Oblique Subduction
Laurentia
Scranton rift impedes further collision
Gondwana
Suwannee
South America
X
X'
Flat-slab, oblique subduction in the North
Y'
Laurentia
Accreted Terranes
Gondwana
Subduction Metasomatism
More pyroxenite
Rheic Slab
Upper Mantle
Depth (km)
0
200
400
600
C) Subduction beneath Southern Margin of Laurentia ~ 300 Ma
Laurentia
Alleganian Fold-trust belt
Gondwana
Y
Y'
direction of subduction rotates
South America
Y
Y'
Laurentia
Suwannee
Pyroxenite
Rheic Slab
Subduction Metasomatism
Upper Mantle
Depth (km)
0
200
400
600
D) Formation of Pangea ~ 260 Ma
X
X'
Laurentia
Gondwana
South America
X
X'
Laurentia
Gondwana
Rheic Slab
Subduction Metasomatized Mantle
Upper Mantle
Depth (km)
0
200
400
600
E) Costal New England (CNE) magmatism ~ 255 - 202 Ma
X
X'
A
F
Coastal New England Magmatism
Rifting begins in Argana (A) and Fundy (F) basins
Laurentia
Gondwana
South America
X
X'
Laurentia
CNE
Gondwana
Rheic Slab
Slab Tear Begins in the underplated Rheic plate
Subduction Metasomatized Mantle
Upper Mantle
Depth (km)
0
200
400
600
F) CAMP ~ 200 Ma
Laurentia
X
X'
Progressive Delamination
Original area of CAMP
Gondwana
South America
X
X'
Laurentia
CAMP
Gondwana
Subduction Metasomatized Mantle
Rheic Slab
Upper Mantle
Depth (km)
0
200
400
600

Figure 13. Schematic model for CAMP formation (not to scale). (a) Accretion of Ganderia, Avalonia and Meguma (shown here as one landmass for simplicity) resulted in metasomatization of the upper mantle beneath Laurentia as well as the formation of pyroxenite through the reaction of sediment melts with the overlying peridotite. (b) The Alleghanian collisional event begins with oblique collision and flat subduction of the Rheic plate in the North leading to more metasomatism of the mantle wedge and the production of more pyroxenite. The Scranton Rift may have been an indenter to the advancing Gondwanan plate, blocking the advancing thrust sheets [Benoit et al., 2014]. This blockage may have in turn stalled the subduction of the Rheic plate beneath Laurentia. (c) The clogging of subduction in the North leads to a rotation of the subduction zone producing head-on collision in the South. This results in metasomatism of the mantle wedge as well as the production of pyroxenite in the South. (d) Pangea is formed with the closure of the Rheic ocean. The low angle and stalling of subduction in the North results in the Rheic plate underplating the lithosphere. (e) P/T conditions cause the Rheic plate to eclogitize and begin to tear. The plate may have also been weakened by the jamming of the subduction zone. This tear initially leads to small amounts of mantle melting, which form the Coastal New England dike swarm. (f) The slab tear propagates in both directions (first toward the North, then later toward the South) due to slab pull, eventually resulting in a catastrophic delamination event. This delamination produces mantle upwelling (increasing the mantle potential temperature indicated by red in the figure), uplift and significant melting of the mantle (CAMP), which had been meta-somatized by previous episodes of subduction. Accreted terrane boundaries from Hibbard et al. [2010] and Hatcher [2010]. CAMP boundary after McHone [2003]. Scranton Rift

location from Benoit et al. [2014]. Final closure of Pangea after Hatcher [2002].

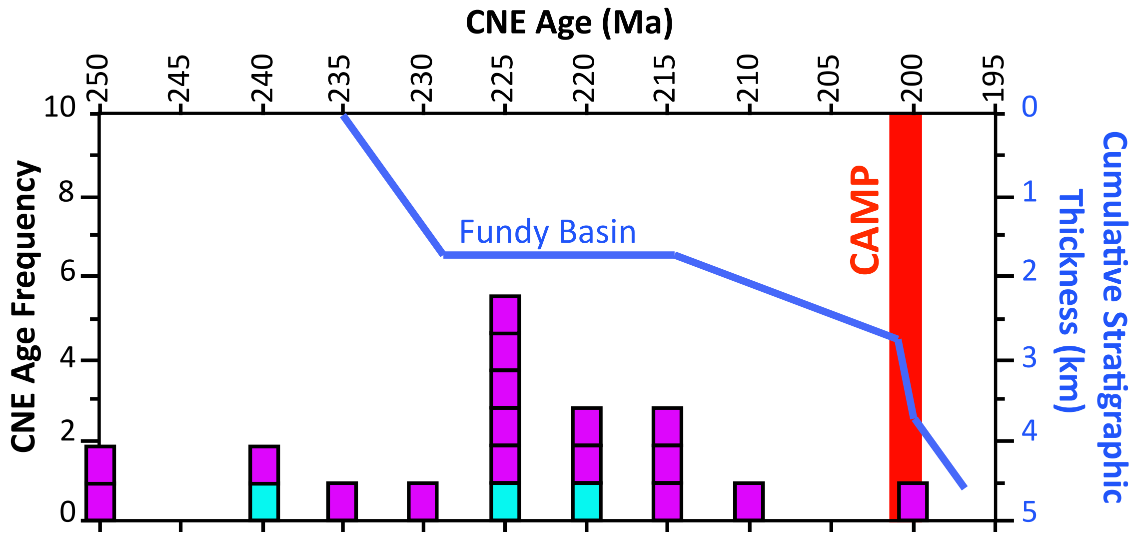

Figure 14. Histogram of ages of Late Triassic Coastal New England (CNE) dikes (purple) and plutons (light blue). Modified from McHone and Butler [1984] and updated with ages from [Pe-Piper and Jansa, 1986; Reynolds et al., 1987; Greenough et al., 1988; McHone, 1992; Pe-Piper et al., 1992; Sundeen and Huff, 1992; Pe-Piper and Reynolds, 2000; Ross, 2010]. The cumulative stratigraphic thickness for the Fundy Basin over time [Schlische et al., 2003] is shown as the blue line, which increases rapidly at the time of CAMP emplacement (indicated by red bar). CNE overlaps with CAMP magmatism in time and uplift may have occurred at the time of CNE emplacement as the majority of CNE coincides with a hiatus in sedimentation in the Fundy Basin.

Tables

Sample	ROCK TYPE	$^{40}Ar/^{39}Ar$ Age (Ma)	LATITUDE	LONGITUDE	SiO_2	TiO_2	Al_2O_3	Cr_2O_3	FeOT	CaO	MgO	MnO	NiO	K_2O	Na_2O	P_2O_5
AXT971/150812-5	basaltic andesite		36.97	-79.66	53.19	1.12	14.74	0.00	12.30	8.73	5.20	0.23	0.00	0.84	2.71	0.17
BLR531A/030812-5A	basaltic andesite		36.70	-79.30	53.16	1.20	14.70	0.00	11.71	8.17	4.92	0.21	0.00	0.96	3.10	0.23
BLR531B/030812-5B	basaltic andesite		36.70	-79.30	53.79	1.21	14.13	0.00	11.58	7.91	4.71	0.22	0.00	1.13	3.17	0.23
NVW-551	basaltic andesite		36.70	-79.93	53.61	1.00	14.41	0.00	11.44	9.83	6.34	0.21	0.00	0.65	2.53	0.15
PRC251/150812-2	basaltic andesite		36.60	-79.94	53.15	0.94	14.51	0.00	11.22	10.06	6.72	0.21	0.01	0.57	2.40	0.13
PRC631/150812-3	basaltic andesite		36.58	-79.89	53.35	1.06	14.93	0.00	11.51	8.93	5.23	0.21	0.00	0.69	2.78	0.16
SPG111/030812-3	basaltic andesite	201±2	36.87	-79.34	54.06	1.29	13.80	0.00	12.26	8.70	5.19	0.23	0.00	0.94	2.76	0.18
STS971/030812-1	basaltic andesite		37.00	-79.17	53.00	0.95	13.81	0.02	11.68	10.17	7.35	0.21	0.01	0.51	2.18	0.12
STS972/030812-2	basaltic andesite		37.00	-79.16	53.08	1.00	14.20	0.02	11.58	10.16	7.08	0.21	0.01	0.52	2.23	0.12
GCY342	basalt		37.22	-79.92	47.49	0.58	16.23	0.08	10.34	10.59	10.62	0.18	0.04	0.36	1.91	0.07
GDH-271	basalt		36.96	-79.82	46.82	0.55	16.10	0.09	10.18	10.17	11.30	0.18	0.04	0.44	1.82	0.07
GDH-831	basalt		36.91	-79.81	47.07	0.53	15.53	0.11	10.52	9.90	13.21	0.18	0.06	0.37	1.72	0.07
PHT911	basalt		36.79	-80.04	47.70	0.34	15.77	0.11	9.77	10.62	11.27	0.18	0.04	0.33	1.67	0.05
PRC771/150812-1	basalt		36.59	-79.99	48.00	0.34	16.70	0.09	10.02	11.34	10.63	0.18	0.04	0.31	1.75	0.05
R-4693	basalt		36.60	-79.79	47.40	0.56	16.32	0.10	10.60	10.37	11.92	0.18	0.05	0.32	1.88	0.07
SPY681/150812-4	basalt		36.55	-79.78	47.10	0.54	15.71	0.11	10.68	10.01	13.24	0.18	0.06	0.29	1.79	0.07
042 SINGERS GLEN*	basalt		38.56	-78.91	46.15	0.47	14.58	0.15	9.64	9.55	14.17	0.18	0.06	0.44	1.68	0.08
12DJ Mosque 1*	basalt		38.44	-78.85	46.69	0.57	14.81	0.11	9.91	10.26	11.68	0.18	0.04	0.48	1.90	0.09

* from Mazza et al. (2014)

Table 1 New dataset – major elements

Sample	Sc	V	Cr	Co	Ni	Cu	Zn	Rb	Sr	Y	Zr	Nb	Ba	Hf	Ta	Pb	Th	U
AXT971/150812-5	46.68		13.10		18.30			22.93	241.49	29.59	100.99	4.65	202.87	2.68	0.33	4.19	2.23	0.66
BLR531A/030812-5A	43.18		19.10		17.20			26.16	242.71	31.05	109.69	5.83	209.76	2.91	0.42	2.97	2.61	0.76
BLR531B/030812-5B	42.83		19.10		16.30			32.69	247.84	34.37	115.51	6.18	237.44	3.01	0.45	2.90	2.79	0.81
NVW-551	46.36		21.50		38.60			16.36	214.40	27.40	87.39	3.80	159.63	2.37	0.30	3.35	1.80	0.56
PRC251/150812-2	46.06		26.70		41.50			14.90	211.22	25.98	77.86	3.37	145.84	2.10	0.26	3.00	1.56	0.47
PRC631/150812-3	44.41		9.80		18.20			17.39	226.75	27.74	93.41	4.39	188.83	2.52	0.32	4.47	2.35	0.71
SPG111/030812-3	47.15		19.00		17.00			24.87	250.03	29.30	115.59	6.18	225.78	3.03	0.45	5.08	2.71	0.80
STS971/030812-1	48.41		109.91		57.64			17.43	132.94	24.19	76.47	4.39	129.24	2.09	0.33	3.07	1.87	0.53
STS972/030812-2	47.09		102.87		54.36			16.05	133.64	24.62	77.24	4.51	122.48	2.11	0.34	3.15	1.93	0.54
GCY342	42.71		558.30		308.70			12.08	100.91	21.57	48.85	1.81	111.09	1.36	0.15	3.05	0.84	0.19
GDH-271	40.99		618.70		353.10			13.92	106.39	20.95	49.23	1.97	117.78	1.32	0.21	1.95	1.12	0.25
GDH-831	39.43		772.60		469.00			11.99	93.02	19.77	44.56	1.70	92.30	1.25	0.14	1.57	0.78	0.17
PHT911	43.18		718.60		338.60			11.83	82.00	18.89	39.02	1.95	102.08	1.02	0.16	2.16	1.13	0.27
PRC771/150812-1	45.02		643.70		281.10			9.60	59.17	19.16	33.22	1.72	83.92	0.90	0.14	1.50	0.79	0.18
R-4693	40.94		649.86		403.35			9.12	89.71	21.42	46.22	1.72	91.36	1.30	0.14	1.57	0.79	0.17
SPY681/150812-4	39.79		749.00		477.20			9.21	84.35	20.24	44.47	1.60	84.30	1.26	0.13	1.46	0.73	0.15
042 SINGERS GLEN*	33.35	173.16	1017.25	72.07	481.57	116.57	76.01	10.38	135.56	19.61	52.59	2.27	130.13	1.29	0.15	1.77	0.81	0.13
12DJ Mosque 1*	32.95	191.70	731.39	60.70	341.12	112.15	84.76	10.93	123.08	24.61	68.63	3.06	170.85	1.89	0.18	2.25	1.00	0.17

* from Mazza et al. (2014)

Table 2 New dataset – trace elements

Sample	La	Ce	Pr	Nd	Sm	Eu	Gd	Tb	Dy	Ho	Er	Tm	Yb	Lu
AXT971/150812-5	11.64	25.42	3.35	14.47	3.88	1.33	4.45	0.80	5.18	1.16	3.21	0.48	3.03	0.49
BLR531A/030812-5A	14.19	30.98	4.15	17.61	4.50	1.46	5.06	0.89	5.68	1.23	3.39	0.50	3.11	0.50
BLR531B/030812-5B	14.62	31.62	4.15	17.84	4.66	1.54	5.27	0.93	6.10	1.32	3.67	0.54	3.29	0.53
NVW-551	9.25	20.44	2.73	11.86	3.37	1.13	4.06	0.75	4.97	1.08	2.99	0.44	2.81	0.44
PRC251/150812-2	8.32	18.37	2.46	10.98	3.01	1.04	3.72	0.68	4.60	1.00	2.83	0.42	2.59	0.42
PRC631/150812-3	11.24	24.06	3.14	13.67	3.63	1.20	4.21	0.76	4.95	1.08	3.00	0.44	2.76	0.44
SPG111/030812-3	13.17	28.76	3.80	16.12	4.18	1.42	4.71	0.84	5.43	1.17	3.31	0.48	3.11	0.49
STS971/030812-1	8.13	17.43	2.27	9.80	2.74	1.01	3.44	0.64	4.49	0.96	2.76	0.42	2.61	0.42
STS972/030812-2	8.51	18.42	2.36	10.14	2.84	1.01	3.55	0.65	4.47	0.99	2.81	0.41	2.61	0.41
GCY342	4.95	10.87	1.46	6.57	1.97	0.69	2.61	0.53	3.73	0.86	2.51	0.39	2.49	0.40
GDH-271	5.29	11.52	1.54	6.61	1.97	0.67	2.58	0.51	3.66	0.82	2.36	0.36	2.37	0.37
GDH-831	4.53	10.04	1.34	5.91	1.78	0.62	2.39	0.47	3.47	0.78	2.33	0.35	2.28	0.38
PHT911	4.99	10.67	1.35	5.46	1.37	0.47	1.88	0.40	2.97	0.71	2.27	0.36	2.30	0.38
PRC771/150812-1	4.17	8.80	1.12	4.61	1.23	0.42	1.72	0.38	3.04	0.75	2.32	0.37	2.38	0.40
R-4693	4.70	10.19	1.39	6.15	1.88	0.67	2.54	0.51	3.73	0.85	2.48	0.37	2.38	0.40
SPY681/150812-4	4.20	9.41	1.29	5.70	1.75	0.63	2.40	0.49	3.52	0.81	2.38	0.36	2.34	0.38
042 SINGERS GLEN*	5.40	12.41	1.52	6.73	1.78	0.56	2.28	0.48	3.03	0.71	2.12	0.32	2.29	0.36
12DJ Mosque 1*	7.10	14.78	1.96	8.42	2.23	0.75	2.95	0.58	4.01	0.92	2.58	0.38	2.83	0.46

* from Mazza et al. (2014)

Table 3 New dataset – rare earth elements

Sample	$^{143}Nd/^{144}Nd$ measured	error	$^{143}Nd/^{144}Nd$ 200 Ma	$^{87}Sr/^{86}Sr$ measured	error	$^{87}Sr/^{86}Sr$ 200 Ma	$^{206}Pb/^{204}Pb$ measured	error	$^{206}Pb/^{204}Pb$ 200 Ma	$^{207}Pb/^{204}Pb$ measured	error	$^{207}Pb/^{204}Pb$ 200 Ma	$^{208}Pb/^{204}Pb$ measured	error	$^{208}Pb/^{204}Pb$ 200 Ma
BLR531B/030812-5B				0.706241	0.000009	0.705156	19.219	0.000	18.653	15.651	0.00	15.622	38.974	0.001	38.335
NVW-551	0.512650	0.000013	0.512426	0.705521	0.000151	0.704893	18.853	0.000	18.516	15.621	0.00	15.604	38.541	0.001	38.189
SPG111/030812-3	0.512591	0.000008	0.512387	0.705924	0.000014	0.705105	18.898	0.000	18.582	15.636	0.00	15.620	38.646	0.001	38.294
STS971/030812-1	0.512518	0.000008	0.512298	0.707331	0.000007	0.706252	18.903	0.000	18.553	15.659	0.00	15.641	38.840	0.002	38.438
GCY342	0.512561	0.000012	0.512324	0.707696	0.000010	0.706711	18.391	0.000	18.269	15.609	0.00	15.603	38.387	0.001	38.208
PHT911	0.512411	0.000005	0.512214	0.711932	0.000016	0.710745	18.629	0.000	18.373	15.633	0.00	15.620	38.614	0.001	38.269
SPY681/150812-4	0.512585	0.000015	0.512343	0.706768	0.000007	0.705869	18.530	0.001	18.318	15.641	0.00	15.630	38.563	0.005	38.235

Table 4 New dataset - radiogenic isotopes

Sample	SiO_2 (wt. %)	MgO (wt. %)	FeO (wt. %)	NiO (wt. %)	MnO (wt. %)	CaO (wt. %)	Fo#	Fe (ppm)	Mn (ppm)	Ni (ppm)	Ca (ppm)	Fe/Mn
12DJ Mosque 1*_Olivine1	40.14	45.56	13.52	0.32	0.19	0.27	85.73	105086	1462	2529	1914	72
12DJ Mosque 1*_Olivine1	39.85	44.40	15.00	0.29	0.20	0.27	84.07	116585	1551	2250	1894	75
12DJ Mosque 1*_Olivine1	38.72	38.81	21.67	0.20	0.33	0.26	76.14	168480	2566	1601	1877	66
12DJ Mosque 1*_Olivine1	38.46	37.25	23.44	0.17	0.38	0.30	73.91	182238	2931	1303	2118	62
12DJ Mosque 1*_Olivine2	40.33	46.06	12.82	0.33	0.19	0.27	86.49	99676	1442	2565	1947	69
12DJ Mosque 1*_Olivine2	40.26	45.85	13.12	0.31	0.19	0.27	86.17	101959	1472	2439	1943	69
12DJ Mosque 1*_Olivine2	40.00	44.37	14.85	0.29	0.21	0.27	84.19	115429	1640	2307	1924	70
12DJ Mosque 1*_Olivine2	40.11	45.24	13.89	0.28	0.21	0.28	85.31	107946	1606	2211	2017	67
12DJ Mosque 1*_Olivine3	39.94	44.59	14.69	0.29	0.22	0.29	84.40	114159	1669	2255	2065	68
12DJ Mosque 1*_Olivine3	39.63	43.12	16.46	0.27	0.25	0.28	82.36	127926	1904	2114	1985	67
12DJ Mosque 1*_Olivine3	39.68	43.23	16.31	0.25	0.24	0.28	82.53	126804	1864	1987	2010	68
12DJ Mosque 1*_Olivine3	39.29	40.96	18.98	0.19	0.28	0.30	79.37	147510	2188	1458	2151	67
12DJ Mosque 1*_Olivine5	40.18	45.51	13.52	0.31	0.20	0.28	85.71	105091	1541	2455	2013	68
12DJ Mosque 1*_Olivine5	39.98	44.57	14.68	0.29	0.21	0.28	84.40	114122	1595	2244	1997	72
12DJ Mosque 1*_Olivine5	38.66	38.36	22.19	0.19	0.32	0.28	75.50	172506	2445	1530	1966	71
12DJ Mosque 1*_Olivine6	40.23	45.66	13.32	0.32	0.19	0.28	85.94	103522	1486	2553	1974	70
12DJ Mosque 1*_Olivine6	40.27	45.84	13.11	0.32	0.19	0.28	86.18	101873	1457	2520	2017	70
12DJ Mosque 1*_Olivine6	40.28	45.87	13.05	0.33	0.19	0.28	86.24	101447	1450	2557	2026	70
12DJ Mosque 1*_Olivine6	39.80	43.67	15.71	0.28	0.24	0.30	83.21	122136	1840	2199	2124	66
12DJ Mosque 1*_Olivine7	40.19	45.50	13.52	0.32	0.20	0.28	85.71	105083	1534	2484	1976	68
12DJ Mosque 1*_Olivine7	40.16	45.44	13.62	0.31	0.20	0.28	85.61	105850	1515	2442	1967	70
12DJ Mosque 1*_Olivine7	39.42	42.21	17.59	0.26	0.25	0.27	81.05	136757	1932	2060	1942	71
12DJ Mosque 1*_Olivine7	38.47	37.73	22.98	0.20	0.35	0.27	74.53	178641	2686	1611	1897	67
12DJ Mosque 1*_Olivine8	40.27	46.06	12.88	0.33	0.19	0.27	86.44	100098	1461	2595	1936	69
12DJ Mosque 1*_Olivine8	40.14	45.62	13.45	0.32	0.19	0.27	85.81	104563	1498	2538	1929	70
12DJ Mosque 1*_Olivine8	39.91	44.37	14.95	0.29	0.21	0.27	84.10	116209	1663	2259	1915	70
12DJ Mosque 1*_Olivine8	39.35	41.05	18.83	0.22	0.29	0.27	79.53	146365	2218	1715	1916	66
12DJ Mosque 1*_Olivine9	40.25	45.81	13.15	0.33	0.19	0.27	86.13	102208	1458	2607	1938	70
12DJ Mosque 1*_Olivine9	40.38	46.37	12.44	0.36	0.18	0.27	86.92	96708	1389	2813	1920	70
12DJ Mosque 1*_Olivine9	40.25	45.90	13.05	0.34	0.19	0.27	86.24	101438	1458	2668	1928	70
12DJ Mosque 1*_Olivine9	39.66	43.21	16.35	0.27	0.24	0.27	82.49	127063	1832	2131	1963	69
GDH-831_Olivine1	40.40	45.74	13.03	0.37	0.19	0.28	86.22	101289	1489	2875	1969	68
GDH-831_Olivine1	40.29	45.49	13.40	0.35	0.20	0.28	85.82	104122	1517	2749	2023	69
GDH-831_Olivine1	39.99	44.23	14.99	0.31	0.21	0.27	84.03	116494	1658	2424	1934	70
GDH-831_Olivine1	39.22	40.46	19.52	0.22	0.30	0.28	78.70	151697	2315	1740	2037	66
GDH-831_Olivine10	40.19	45.60	13.38	0.36	0.19	0.27	85.87	103998	1500	2820	1938	69
GDH-831_Olivine10	40.09	45.34	13.76	0.34	0.20	0.27	85.45	106961	1547	2662	1936	69
GDH-831_Olivine10	39.93	44.71	14.56	0.32	0.21	0.27	84.55	113214	1652	2499	1909	69
GDH-831_Olivine10	39.62	43.22	16.36	0.27	0.25	0.28	82.48	127190	1908	2140	1974	67
GDH-831_Olivine2	40.35	46.35	12.43	0.38	0.18	0.29	86.92	96636	1433	3024	2081	67
GDH-831_Olivine2	40.35	46.25	12.55	0.38	0.18	0.29	86.79	97535	1413	2991	2059	69

GDH-831_Olivine2	40.10	45.81	13.26	0.36	0.20	0.28	86.03	103067	1521	2797	2013	68
GDH-831_Olivine2	39.13	40.39	19.68	0.24	0.28	0.28	78.53	152953	2191	1890	2007	70
GDH-831_Olivine3	40.29	45.84	13.03	0.37	0.19	0.27	86.24	101304	1485	2904	1960	68
GDH-831_Olivine3	40.24	45.60	13.33	0.36	0.20	0.27	85.91	103650	1533	2802	1957	68
GDH-831_Olivine3	40.10	44.75	14.35	0.31	0.21	0.27	84.75	111577	1646	2452	1928	68
GDH-831_Olivine3	38.19	35.88	25.11	0.18	0.37	0.27	71.80	195206	2845	1380	1944	69
GDH-831_Olivine4	40.33	45.83	13.01	0.36	0.19	0.28	86.26	101144	1500	2832	1996	67
GDH-831_Olivine4	40.31	45.53	13.33	0.35	0.20	0.29	85.90	103593	1529	2732	2045	68
GDH-831_Olivine4	40.15	45.01	14.01	0.33	0.21	0.28	85.13	108923	1614	2599	2006	68
GDH-831_Olivine4	38.09	35.54	25.55	0.16	0.38	0.28	71.26	198573	2918	1278	2024	68
GDH-831_Olivine5	40.20	45.05	13.94	0.35	0.21	0.26	85.21	108336	1621	2723	1878	67
GDH-831_Olivine5	40.49	45.15	13.54	0.34	0.21	0.26	85.60	105219	1645	2696	1873	64
GDH-831_Olivine7	40.29	46.02	12.84	0.37	0.19	0.28	86.47	99815	1466	2925	2027	68
GDH-831_Olivine7	40.29	46.00	12.87	0.37	0.19	0.28	86.44	100021	1450	2925	2002	69
GDH-831_Olivine7	40.30	45.85	13.02	0.36	0.19	0.28	86.26	101229	1463	2829	1974	69
GDH-831_Olivine7	39.29	41.39	18.50	0.25	0.29	0.28	79.95	143834	2213	1959	2020	65
GDH-831_Olivine8	40.50	46.00	12.67	0.37	0.19	0.28	86.61	98494	1458	2888	1980	68
GDH-831_Olivine8	40.46	46.00	12.71	0.37	0.19	0.28	86.58	98771	1462	2878	1973	68
GDH-831_Olivine8	40.28	44.97	13.92	0.34	0.22	0.27	85.21	108181	1666	2707	1924	65
GDH-831_Olivine9	40.36	45.94	12.85	0.37	0.19	0.28	86.43	99902	1471	2928	2009	68
GDH-831_Olivine9	40.41	46.06	12.69	0.38	0.19	0.28	86.61	98637	1449	2948	1987	68
GDH-831_Olivine9	40.23	45.26	13.69	0.34	0.20	0.28	85.49	106417	1580	2672	1984	67
GDH-831_Olivine9	39.28	40.75	19.14	0.25	0.30	0.27	79.14	148812	2301	1999	1940	65
R-4693_Olivine10	40.13	45.86	13.27	0.36	0.19	0.18	86.03	103183	1482	2855	1320	70
R-4693_Olivine10	40.16	45.31	13.69	0.36	0.19	0.30	85.51	106379	1470	2815	2155	72
R-4693_Olivine10	40.10	45.53	13.56	0.34	0.19	0.28	85.68	105405	1485	2677	1985	71
R-4693_Olivine10	39.94	45.06	14.19	0.35	0.20	0.27	84.99	110286	1526	2713	1949	72
R-4693_Olivine11	40.26	46.54	12.41	0.38	0.18	0.24	86.99	96467	1387	3003	1684	70
R-4693_Olivine11	40.67	46.60	11.96	0.41	0.18	0.18	87.41	92962	1406	3204	1269	66
R-4693_Olivine16	40.18	45.73	13.15	0.36	0.19	0.39	86.11	102246	1503	2797	2784	68
R-4693_Olivine16	40.04	45.72	13.45	0.35	0.20	0.24	85.83	104542	1520	2776	1731	69
R-4693_Olivine16	39.70	43.53	15.66	0.31	0.22	0.57	83.21	121735	1719	2473	4094	71
R-4693_Olivine16	39.71	43.28	16.29	0.30	0.24	0.18	82.57	126631	1890	2341	1255	67
R-4693_Olivine17	40.07	44.98	14.23	0.33	0.20	0.20	84.93	110594	1575	2580	1417	70
R-4693_Olivine17	40.24	45.84	13.18	0.35	0.19	0.20	86.11	102414	1501	2756	1455	68
R-4693_Olivine17	40.08	44.98	14.17	0.33	0.21	0.22	84.98	110145	1607	2628	1600	69
R-4693_Olivine17	39.71	42.64	16.93	0.29	0.25	0.19	81.78	131582	1939	2264	1330	68
R-4693_Olivine18	40.08	45.37	13.82	0.34	0.20	0.18	85.40	107458	1563	2671	1313	69
R-4693_Olivine18	40.14	46.04	13.03	0.37	0.19	0.24	86.30	101252	1484	2902	1706	68
R-4693_Olivine18	40.09	45.75	13.41	0.36	0.20	0.20	85.88	104238	1542	2790	1421	68
R-4693_Olivine18	39.37	42.35	17.52	0.27	0.26	0.24	81.16	136167	1996	2090	1721	68
R-4693_Olivine19	40.15	45.33	13.64	0.34	0.20	0.34	85.56	106011	1562	2664	2429	68

R-4693_Olivine19	40.23	44.54	14.24	0.34	0.21	0.44	84.79	110712	1617	2684	3112	68
R-4693_Olivine19	40.18	44.62	14.24	0.34	0.21	0.41	84.81	110697	1599	2694	2937	69
R-4693_Olivine19	40.04	44.94	14.22	0.35	0.21	0.24	84.92	110558	1591	2755	1705	69
R-4693_Olivine20	40.38	45.81	13.00	0.36	0.19	0.26	86.27	101033	1486	2841	1872	68
R-4693_Olivine20	40.43	45.75	13.00	0.36	0.19	0.28	86.25	101027	1488	2796	1966	68
R-4693_Olivine20	40.42	45.72	13.05	0.35	0.19	0.26	86.19	101463	1498	2787	1880	68
R-4693_Olivine20	40.01	43.97	15.20	0.33	0.22	0.27	83.75	118184	1685	2601	1895	70
R-4693_Olivine8	39.96	45.70	13.46	0.35	0.19	0.34	85.82	104609	1491	2718	2397	70
R-4693_Olivine8	39.91	45.80	13.51	0.35	0.19	0.24	85.80	105030	1471	2752	1685	71
R-4693_Olivine8	39.78	44.77	14.72	0.31	0.20	0.22	84.43	114396	1551	2427	1571	74
R-4693_Olivine8	39.30	42.00	17.84	0.31	0.25	0.30	80.76	138648	1908	2436	2152	73
R-4693_Olivine9	40.19	45.60	13.20	0.36	0.19	0.46	86.03	102586	1443	2811	3297	71
R-4693_Olivine9	40.02	45.52	13.68	0.34	0.19	0.24	85.57	106362	1489	2688	1733	71
PRC771/150812-1_Olivine1	39.46	42.25	17.47	0.29	0.25	0.29	81.17	135789	1929	2258	2071	70
PRC771/150812-1_Olivine1	39.58	42.72	16.91	0.26	0.24	0.29	81.83	131463	1831	2078	2078	72
PRC771/150812-1_Olivine1	39.91	44.34	14.94	0.31	0.21	0.30	84.10	116132	1608	2421	2112	72
PRC771/150812-1_Olivine1	39.16	40.95	19.07	0.25	0.27	0.30	79.29	148234	2116	1948	2154	70
PRC771/150812-1_Olivine10	38.65	40.91	19.66	0.24	0.25	0.29	78.77	152802	1970	1848	2089	78
PRC771/150812-1_Olivine10	36.93	33.20	29.14	0.11	0.39	0.22	67.01	226531	3043	848	1586	74
PRC771/150812-1_Olivine3	40.34	46.13	12.70	0.35	0.18	0.30	86.62	98725	1421	2744	2117	69
PRC771/150812-1_Olivine3	40.35	46.48	12.34	0.36	0.18	0.29	87.04	95904	1394	2835	2083	69
PRC771/150812-1_Olivine3	40.00	44.97	14.20	0.34	0.20	0.28	84.95	110381	1542	2702	2031	72
PRC771/150812-1_Olivine3	38.07	36.02	25.08	0.22	0.36	0.25	71.91	194955	2795	1740	1812	70
PRC771/150812-1_Olivine4	39.65	42.95	16.56	0.31	0.23	0.30	82.22	128698	1807	2424	2146	71
PRC771/150812-1_Olivine4	38.80	39.16	21.23	0.23	0.30	0.27	76.68	165018	2320	1846	1955	71
PRC771/150812-1_Olivine4	37.69	34.24	27.23	0.19	0.40	0.25	69.15	211653	3083	1502	1800	69
PRC771/150812-1_Olivine4	36.83	30.42	31.88	0.12	0.49	0.26	62.98	247810	3810	943	1840	65
PRC771/150812-1_Olivine5	39.93	44.25	14.98	0.33	0.22	0.30	84.04	116408	1686	2605	2117	69
PRC771/150812-1_Olivine5	40.07	44.91	14.18	0.33	0.20	0.31	84.95	110232	1552	2608	2186	71
PRC771/150812-1_Olivine5	39.91	44.56	14.69	0.32	0.21	0.30	84.39	114221	1640	2484	2173	70
PRC771/150812-1_Olivine5	39.64	43.15	16.42	0.25	0.24	0.30	82.40	127672	1872	1961	2125	68
PRC771/150812-1_Olivine6	39.46	42.54	17.19	0.27	0.25	0.29	81.52	133586	1928	2155	2064	69
PRC771/150812-1_Olivine6	39.59	43.23	16.35	0.31	0.23	0.29	82.49	127120	1759	2420	2072	72
PRC771/150812-1_Olivine6	37.49	33.89	27.79	0.18	0.40	0.25	68.50	215993	3134	1384	1804	69
PRC771/150812-1_Olivine7	40.09	45.02	14.06	0.33	0.20	0.30	85.09	109285	1574	2622	2138	69
PRC771/150812-1_Olivine7	40.16	45.40	13.61	0.33	0.20	0.30	85.60	105793	1540	2621	2127	69
PRC771/150812-1_Olivine7	40.06	44.55	14.56	0.32	0.20	0.29	84.50	113211	1577	2546	2089	72
PRC771/150812-1_Olivine7	39.16	40.47	19.55	0.23	0.30	0.29	78.68	151955	2312	1844	2042	66
PRC771/150812-1_Olivine8b	39.15	41.15	18.86	0.28	0.26	0.30	79.54	146626	2030	2174	2132	72
PRC771/150812-1_Olivine8b	38.45	39.13	21.63	0.20	0.28	0.30	76.33	168161	2145	1596	2179	78
PRC771/150812-1_Olivine8b	37.65	35.25	26.37	0.12	0.37	0.23	70.44	204961	2901	959	1631	71
PRC771/150812-1_Olivine9	39.99	44.60	14.57	0.33	0.20	0.30	84.51	113250	1553	2631	2154	73

PRC771/150812-1_Olivine9	40.19	45.77	13.20	0.34	0.19	0.31	86.08	102568	1486	2692	2247	69
PRC771/150812-1_Olivine9	40.33	45.95	12.88	0.36	0.19	0.29	86.41	100098	1459	2836	2087	69
GCY342_Olivine1	39.55	42.64	17.02	0.28	0.25	0.27	81.70	132294	1919	2222	1904	69
GCY342_Olivine1	39.46	42.53	17.22	0.28	0.25	0.27	81.49	133817	1954	2168	1936	68
GCY342_Olivine1	39.44	42.14	17.63	0.28	0.25	0.26	80.99	137029	1960	2238	1840	70
GCY342_Olivine1	38.83	39.28	21.10	0.24	0.31	0.25	76.85	163980	2381	1888	1783	69
GCY342_Olivine10	39.78	44.00	15.42	0.30	0.23	0.28	83.57	119879	1749	2363	1965	69
GCY342_Olivine10	39.16	40.69	19.36	0.22	0.30	0.27	78.93	150503	2347	1756	1923	64
GCY342_Olivine10	39.26	41.35	18.58	0.23	0.29	0.29	79.87	144424	2251	1784	2067	64
GCY342_Olivine10	37.70	34.43	27.02	0.15	0.41	0.28	69.43	210034	3190	1202	1994	66
GCY342_Olivine2	39.80	43.16	16.26	0.28	0.24	0.26	82.55	126374	1891	2201	1885	67
GCY342_Olivine2	39.82	43.54	15.85	0.30	0.24	0.26	83.04	123175	1828	2382	1860	67
GCY342_Olivine2	38.84	39.29	21.06	0.26	0.31	0.25	76.89	163664	2403	2014	1784	68
GCY342_Olivine2	38.19	36.52	24.47	0.22	0.36	0.25	72.68	190175	2812	1713	1762	68
GCY342_Olivine3	39.90	44.23	15.07	0.31	0.22	0.27	83.95	117170	1718	2397	1920	68
GCY342_Olivine3	39.84	44.25	15.11	0.30	0.23	0.27	83.92	117477	1745	2346	1917	67
GCY342_Olivine3	37.99	35.92	25.28	0.17	0.37	0.27	71.70	196487	2854	1333	1931	69
GCY342_Olivine3	37.34	33.06	28.75	0.13	0.45	0.28	67.21	223448	3463	1036	1966	65
GCY342_Olivine4	40.09	45.14	13.96	0.34	0.20	0.27	85.21	108533	1571	2658	1931	69
GCY342_Olivine4	39.87	44.18	15.17	0.29	0.22	0.27	83.85	117911	1734	2287	1902	68
GCY342_Olivine4	40.03	44.88	14.29	0.32	0.21	0.27	84.85	111046	1644	2536	1904	68
GCY342_Olivine4	39.58	42.22	17.39	0.27	0.26	0.28	81.23	135146	2039	2134	1986	66
GCY342_Olivine5	39.96	44.69	14.54	0.33	0.22	0.27	84.56	113046	1681	2566	1925	67
GCY342_Olivine5	39.95	44.69	14.54	0.33	0.21	0.27	84.56	113034	1656	2568	1926	68
GCY342_Olivine5	39.64	43.81	15.75	0.29	0.23	0.28	83.22	122439	1800	2265	1977	68
GCY342_Olivine5	38.24	37.44	23.48	0.19	0.36	0.29	73.97	182549	2797	1455	2037	65
GCY342_Olivine6	39.84	44.36	14.98	0.32	0.23	0.27	84.08	116414	1774	2535	1939	66
GCY342_Olivine6	39.74	44.27	15.23	0.29	0.24	0.24	83.82	118361	1825	2317	1701	65
GCY342_Olivine6	39.67	43.91	15.61	0.31	0.23	0.27	83.37	121347	1796	2474	1895	68
GCY342_Olivine6	38.96	40.50	19.76	0.22	0.29	0.26	78.51	153628	2258	1705	1885	68
GCY342_Olivine7	39.93	45.38	13.87	0.35	0.20	0.27	85.36	107802	1576	2711	1938	68
GCY342_Olivine7	39.92	45.16	14.11	0.34	0.20	0.27	85.09	109647	1568	2641	1954	70
GCY342_Olivine7	39.84	44.89	14.45	0.33	0.22	0.27	84.71	112322	1668	2631	1915	67
GCY342_Olivine7	39.15	41.11	18.94	0.25	0.28	0.27	79.46	147235	2172	1962	1960	68
GCY342_Olivine8	40.04	45.35	13.79	0.35	0.20	0.27	85.43	107201	1558	2777	1907	69
GCY342_Olivine8	39.94	44.91	14.32	0.35	0.21	0.27	84.82	111341	1615	2753	1910	69
GCY342_Olivine8	39.76	44.47	14.97	0.32	0.22	0.27	84.11	116377	1683	2520	1895	69
GCY342_Olivine8	39.28	41.86	18.04	0.26	0.28	0.28	80.53	140257	2140	2042	1988	66
GCY342_Olivine9	40.26	46.03	12.88	0.37	0.19	0.27	86.43	100106	1485	2882	1954	67
GCY342_Olivine9	40.17	45.89	13.10	0.37	0.20	0.27	86.20	101795	1514	2936	1951	67
GCY342_Olivine9	40.09	45.39	13.69	0.35	0.21	0.27	85.53	106425	1588	2787	1938	67
GCY342_Olivine9	39.42	42.68	17.08	0.30	0.25	0.27	81.66	132772	1950	2365	1934	68

042 SINGERS GLEN*_Olivine1	39.57	44.42	15.22	0.28	0.23	0.27	83.88	118303	1772	2187	1962	67
43 SINGERS GLEN*_Olivine1	39.42	43.80	16.00	0.26	0.24	0.28	82.99	124365	1870	2043	1985	67
44 SINGERS GLEN*_Olivine1	39.36	43.60	16.25	0.26	0.26	0.28	82.70	126344	1977	2006	2013	64
45 SINGERS GLEN*_Olivine1	39.26	43.00	16.94	0.24	0.27	0.30	81.90	131655	2079	1853	2120	63
042 SINGERS GLEN*_Olivine10	40.21	45.38	13.59	0.33	0.21	0.28	85.62	105633	1593	2595	2036	66
43 SINGERS GLEN*_Olivine10	39.94	44.21	15.02	0.29	0.23	0.30	83.99	116783	1749	2310	2172	67
44 SINGERS GLEN*_Olivine10	39.93	44.59	14.67	0.31	0.21	0.28	84.42	114051	1661	2398	2025	69
45 SINGERS GLEN*_Olivine10	39.66	43.06	16.47	0.27	0.26	0.29	82.34	127988	1976	2113	2038	65
042 SINGERS GLEN*_Olivine2	40.02	46.17	13.01	0.34	0.19	0.27	86.35	101122	1486	2672	1911	68
43 SINGERS GLEN*_Olivine2	39.93	45.62	13.64	0.33	0.20	0.27	85.63	106063	1548	2614	1900	69
44 SINGERS GLEN*_Olivine2	39.85	45.36	13.98	0.32	0.21	0.28	85.26	108691	1596	2520	2001	68
45 SINGERS GLEN*_Olivine2	39.43	43.18	16.59	0.26	0.26	0.28	82.27	128943	2012	2050	2006	64
042 SINGERS GLEN*_Olivine3	39.40	43.34	16.46	0.26	0.25	0.28	82.44	127935	1968	2067	2021	65
43 SINGERS GLEN*_Olivine3	39.51	44.22	15.48	0.28	0.23	0.28	83.58	120346	1793	2165	1968	67
44 SINGERS GLEN*_Olivine3	39.59	44.33	15.31	0.28	0.23	0.27	83.77	118975	1744	2172	1947	68
45 SINGERS GLEN*_Olivine3	38.53	39.72	20.96	0.20	0.31	0.28	77.16	162918	2378	1571	1972	69
042 SINGERS GLEN*_Olivine4	38.96	41.03	19.21	0.21	0.30	0.29	79.20	149307	2351	1650	2071	64
43 SINGERS GLEN*_Olivine4	39.00	41.28	18.92	0.22	0.30	0.28	79.55	147045	2354	1744	1991	62
44 SINGERS GLEN*_Olivine4	39.35	42.84	17.04	0.25	0.25	0.27	81.76	132447	1969	1945	1929	67
45 SINGERS GLEN*_Olivine4	38.25	37.71	23.21	0.18	0.37	0.28	74.33	180422	2848	1418	2017	63
042 SINGERS GLEN*_Olivine5	39.70	43.95	15.58	0.26	0.22	0.27	83.41	121122	1741	2080	1921	70
43 SINGERS GLEN*_Olivine5	39.51	43.13	16.60	0.25	0.24	0.28	82.24	129039	1863	1931	1967	69
44 SINGERS GLEN*_Olivine5	39.48	43.33	16.42	0.25	0.24	0.28	82.47	127653	1883	1978	1972	68
45 SINGERS GLEN*_Olivine5	39.18	42.03	18.03	0.23	0.26	0.26	80.60	140181	2046	1826	1860	69
042 SINGERS GLEN*_Olivine6	39.82	44.55	14.85	0.29	0.22	0.27	84.25	115418	1711	2298	1924	67
43 SINGERS GLEN*_Olivine6	39.94	44.62	14.65	0.30	0.22	0.27	84.45	113875	1703	2327	1958	67
44 SINGERS GLEN*_Olivine6	39.20	41.40	18.62	0.22	0.28	0.28	79.85	144755	2173	1761	1983	67
45 SINGERS GLEN*_Olivine6	38.77	39.49	20.93	0.19	0.34	0.28	77.08	162663	2618	1525	2011	62
042 SINGERS GLEN*_Olivine7	39.96	44.26	14.99	0.29	0.23	0.28	84.03	116511	1752	2253	2018	67
43 SINGERS GLEN*_Olivine7	39.74	43.60	15.86	0.28	0.24	0.28	83.05	123305	1858	2191	1973	66
44 SINGERS GLEN*_Olivine7	39.73	43.76	15.69	0.29	0.24	0.28	83.25	121997	1879	2271	1970	65
45 SINGERS GLEN*_Olivine7	39.63	42.92	16.66	0.27	0.26	0.27	82.12	129473	2014	2094	1912	64
042 SINGERS GLEN*_Olivine8	40.00	44.55	14.65	0.31	0.22	0.27	84.42	113901	1692	2448	1925	67
43 SINGERS GLEN*_Olivine8	39.62	42.97	16.63	0.26	0.25	0.28	82.16	129236	1955	2009	1989	66
44 SINGERS GLEN*_Olivine8	39.21	41.05	18.96	0.22	0.29	0.28	79.42	147375	2210	1733	1976	67
45 SINGERS GLEN*_Olivine8	38.06	35.79	25.33	0.17	0.40	0.26	71.58	196874	3102	1315	1833	63
042 SINGERS GLEN*_Olivine9	40.28	45.39	13.55	0.32	0.20	0.27	85.65	105332	1513	2518	1942	70
43 SINGERS GLEN*_Olivine9	40.09	44.91	14.23	0.29	0.20	0.27	84.90	110636	1572	2271	1934	70
44 SINGERS GLEN*_Olivine9	40.12	44.68	14.42	0.29	0.21	0.27	84.67	112079	1652	2282	1926	68
45 SINGERS GLEN*_Olivine9	39.50	41.86	17.85	0.24	0.27	0.28	80.70	138752	2084	1921	1978	67
R_4694_Olivine1	40.20	46.05	12.91	0.36	0.20	0.28	86.41	100333	1516	2860	2009	66
R_4694_Olivine1	40.25	46.15	12.76	0.37	0.19	0.28	86.57	99175	1501	2868	1993	66

R_4694_Olivine1	40.19	45.90	13.09	0.35	0.20	0.28	86.21	101731	1515	2749	1971	67
R_4694_Olivine1	39.58	43.62	16.00	0.26	0.25	0.30	82.93	124400	1902	2007	2136	65
R_4694_Olivine10	40.22	46.50	12.44	0.38	0.18	0.28	86.95	96711	1427	2963	1968	68
R_4694_Olivine10	40.13	46.33	12.70	0.37	0.19	0.28	86.67	98751	1453	2928	1988	68
R_4694_Olivine10	40.20	46.76	12.20	0.38	0.18	0.28	87.23	94842	1391	3010	1992	68
R_4694_Olivine10	40.20	46.41	12.54	0.38	0.19	0.28	86.84	97475	1449	2961	2023	67
R_4694_Olivine2	40.20	46.04	12.93	0.36	0.19	0.28	86.39	100542	1470	2804	1994	68
R_4694_Olivine2	40.25	46.03	12.89	0.36	0.20	0.28	86.42	100206	1511	2811	1994	66
R_4694_Olivine2	40.27	45.97	12.93	0.36	0.19	0.28	86.37	100540	1492	2791	1976	67
R_4694_Olivine2	40.15	45.68	13.33	0.36	0.20	0.28	85.93	103652	1550	2807	1986	67
R_4694_Olivine3	40.39	46.19	12.58	0.38	0.18	0.28	86.74	97798	1428	2970	1974	68
R_4694_Olivine3	40.28	46.16	12.73	0.37	0.19	0.27	86.60	98986	1446	2888	1953	68
R_4694_Olivine3	40.27	46.01	12.89	0.36	0.19	0.27	86.42	100210	1453	2835	1955	69
R_4694_Olivine3	39.93	44.61	14.67	0.30	0.22	0.28	84.42	114034	1672	2341	2023	68
R_4694_Olivine4	40.25	45.38	13.55	0.33	0.20	0.29	85.65	105343	1567	2561	2060	67
R_4694_Olivine4	40.28	45.47	13.44	0.33	0.20	0.29	85.78	104438	1554	2561	2045	67
R_4694_Olivine4	40.24	45.15	13.80	0.32	0.20	0.29	85.36	107262	1562	2488	2040	69
R_4694_Olivine4	40.17	44.85	14.17	0.31	0.21	0.28	84.94	110165	1633	2406	2035	67
R_4694_Olivine5	40.27	45.95	12.95	0.35	0.19	0.28	86.35	100683	1494	2757	2005	67
R_4694_Olivine5	40.30	46.04	12.84	0.35	0.19	0.28	86.47	99823	1480	2747	2002	67
R_4694_Olivine5	40.14	45.44	13.61	0.33	0.20	0.28	85.62	105767	1563	2625	1982	68
R_4694_Olivine5	40.09	44.94	14.18	0.30	0.21	0.28	84.96	110220	1614	2390	1994	68
R_4694_Olivine6	40.34	45.86	12.99	0.34	0.19	0.28	86.29	100976	1502	2687	2000	67
R_4694_Olivine6	40.30	45.73	13.14	0.35	0.19	0.28	86.12	102167	1499	2740	1986	68
R_4694_Olivine6	40.12	45.23	13.84	0.32	0.20	0.28	85.34	107612	1574	2549	1973	68
R_4694_Olivine6	40.07	44.97	14.17	0.31	0.21	0.28	84.98	110110	1599	2401	2013	69
R_4694_Olivine7	40.54	47.05	11.56	0.39	0.17	0.29	87.89	89825	1324	3098	2093	68
R_4694_Olivine7	40.49	46.81	11.85	0.39	0.18	0.29	87.56	92101	1357	3053	2073	68
R_4694_Olivine7	40.29	46.16	12.71	0.37	0.19	0.29	86.62	98770	1466	2869	2050	67
R_4694_Olivine7	40.14	45.65	13.36	0.36	0.20	0.29	85.90	103845	1560	2791	2066	67
R_4694_Olivine8	40.00	45.38	13.81	0.33	0.20	0.28	85.42	107361	1563	2619	1968	69
R_4694_Olivine8	39.93	45.30	13.96	0.32	0.21	0.27	85.26	108543	1594	2543	1958	68
R_4694_Olivine8	39.94	45.10	14.16	0.31	0.21	0.28	85.03	110067	1613	2462	2000	68
R_4694_Olivine8	39.94	44.75	14.51	0.30	0.22	0.28	84.61	112798	1686	2336	2015	67
R_4694_Olivine9	40.04	45.44	13.72	0.33	0.20	0.28	85.52	106623	1555	2571	1973	69
R_4694_Olivine9	40.03	45.69	13.46	0.34	0.20	0.28	85.81	104657	1546	2681	2013	68
R_4694_Olivine9	39.96	45.67	13.53	0.35	0.20	0.30	85.75	105135	1531	2747	2130	69
R_4694_Olivine9	39.90	45.02	14.29	0.31	0.21	0.28	84.89	111055	1606	2453	1978	69

* from Mazza et al. (2014)

Table 5 Olivine phenocryst analyses

Sample	Si Detection	Mg Detectio	Fe Detection	Ca Detection	Mn Detectio	Ni Detection	Si % Errors	Mg % Errors	Fe % Errors	Ca % Errors	Mn % Errors	Ni % Errors	Si 2σ Errors
SCOL	0.0045	0.0037	0.0028	0.0023	0.0022	0.0010	0.0685	0.0679	0.1185	0.5580	1.3504	1.1726	0.056
SCOL	0.0045	0.0036	0.0029	0.0023	0.0022	0.0010	0.0684	0.0677	0.1187	0.5638	1.3373	1.1794	0.056
SCOL	0.0045	0.0037	0.0028	0.0023	0.0022	0.0010	0.0684	0.0678	0.1187	0.5648	1.3238	1.1858	0.056
3LV_002_Olivine1	0.0045	0.0038	0.0029	0.0023	0.0022	0.0010	0.0691	0.0717	0.1027	0.5617	1.0076	0.3748	0.056
3LV_002_Olivine1	0.0045	0.0038	0.0029	0.0023	0.0022	0.0010	0.0690	0.0718	0.1010	0.5782	0.9893	0.3666	0.056
3LV_002_Olivine1	0.0045	0.0039	0.0029	0.0024	0.0023	0.0010	0.0693	0.0735	0.0955	0.6408	0.9296	0.3801	0.055
3LV_002_Olivine1	0.0046	0.0040	0.0029	0.0024	0.0023	0.0010	0.0699	0.0785	0.0834	0.8375	0.7356	0.3689	0.055
3LV_002_Olivine2	0.0045	0.0038	0.0029	0.0023	0.0022	0.0010	0.0690	0.0708	0.1051	0.5396	1.0275	0.3615	0.056
3LV_002_Olivine2	0.0045	0.0038	0.0028	0.0023	0.0022	0.0010	0.0690	0.0709	0.1047	0.5448	1.0416	0.3647	0.056
3LV_002_Olivine2	0.0045	0.0038	0.0029	0.0023	0.0023	0.0010	0.0692	0.0715	0.1018	0.5724	0.9874	0.3715	0.055
3LV_002_Olivine2	0.0046	0.0040	0.0030	0.0024	0.0023	0.0010	0.0701	0.0788	0.0834	0.7902	0.7695	0.3762	0.055
3LV_002_Olivine3	0.0045	0.0038	0.0029	0.0023	0.0022	0.0010	0.0690	0.0714	0.1029	0.5573	1.0048	0.3799	0.056
3LV_002_Olivine3	0.0045	0.0038	0.0029	0.0024	0.0023	0.0010	0.0691	0.0717	0.1018	0.5733	0.9843	0.3806	0.056
3LV_002_Olivine3	0.0046	0.0038	0.0029	0.0024	0.0023	0.0010	0.0692	0.0727	0.0980	0.6363	0.9314	0.3854	0.055
3LV_002_Olivine3	0.0047	0.0042	0.0030	0.0025	0.0023	0.0010	0.0706	0.0855	0.0734	1.0297	0.6397	0.3857	0.054
3LV_002_Olivine4	0.0045	0.0038	0.0029	0.0023	0.0022	0.0010	0.0690	0.0714	0.1032	0.5691	0.9977	0.3764	0.056
3LV_002_Olivine4	0.0046	0.0038	0.0029	0.0024	0.0023	0.0010	0.0690	0.0718	0.1021	0.5867	0.9856	0.3708	0.056
3LV_002_Olivine4	0.0046	0.0039	0.0029	0.0024	0.0022	0.0010	0.0691	0.0724	0.0994	0.6081	0.9445	0.3755	0.055
3LV_002_Olivine4	0.0047	0.0042	0.0031	0.0025	0.0024	0.0010	0.0708	0.0861	0.0730	1.1067	0.6314	0.3776	0.054
3LV_002_Olivine5	0.0045	0.0038	0.0029	0.0024	0.0023	0.0010	0.0689	0.0722	0.0996	0.5860	0.9446	0.3934	0.055
3LV_002_Olivine5	0.0045	0.0038	0.0029	0.0023	0.0022	0.0010	0.0686	0.0720	0.1011	0.5893	0.9290	0.3945	0.056
SCOL	0.0045	0.0037	0.0028	0.0023	0.0022	0.0010	0.0683	0.0678	0.1204	0.5667	1.3279	1.2217	0.056
SCOL	0.0045	0.0037	0.0028	0.0023	0.0022	0.0010	0.0683	0.0677	0.1205	0.5673	1.3737	1.2114	0.056
SCOL	0.0045	0.0037	0.0028	0.0023	0.0022	0.0010	0.0682	0.0677	0.1203	0.5684	1.3407	1.2397	0.056
3LV_002_Olivine7	0.0046	0.0038	0.0029	0.0024	0.0022	0.0010	0.0689	0.0711	0.1042	0.5585	1.0103	0.3740	0.056
3LV_002_Olivine7	0.0046	0.0038	0.0028	0.0023	0.0022	0.0010	0.0689	0.0711	0.1042	0.5576	1.0246	0.3779	0.056
3LV_002_Olivine7	0.0045	0.0038	0.0029	0.0023	0.0023	0.0010	0.0688	0.0713	0.1035	0.5706	1.0219	0.3813	0.055
3LV_002_Olivine7	0.0046	0.0040	0.0029	0.0024	0.0023	0.0010	0.0697	0.0771	0.0865	0.7687	0.7617	0.3781	0.055
3LV_002_Olivine8	0.0045	0.0038	0.0028	0.0023	0.0023	0.0010	0.0687	0.0711	0.1050	0.5630	1.0278	0.3808	0.056
3LV_002_Olivine8	0.0045	0.0037	0.0029	0.0023	0.0023	0.0010	0.0687	0.0711	0.1049	0.5657	1.0229	0.3825	0.056
3LV_002_Olivine8	0.0045	0.0038	0.0029	0.0024	0.0022	0.0010	0.0688	0.0722	0.1001	0.5925	0.9265	0.3894	0.055
3LV_002_Olivine9	0.0045	0.0037	0.0029	0.0023	0.0022	0.0010	0.0688	0.0712	0.1044	0.5590	1.0152	0.3778	0.056
3LV_002_Olivine9	0.0046	0.0038	0.0029	0.0023	0.0022	0.0010	0.0685	0.0708	0.1048	0.5535	1.0242	0.3787	0.055
3LV_002_Olivine9	0.0046	0.0038	0.0028	0.0024	0.0022	0.0010	0.0688	0.0719	0.1009	0.5995	0.9636	0.3798	0.055
3LV_002_Olivine9	0.0046	0.0040	0.0030	0.0024	0.0023	0.0010	0.0696	0.0779	0.0850	0.7619	0.7437	0.3884	0.055
3LV_002_Olivine10	0.0046	0.0038	0.0029	0.0023	0.0023	0.0010	0.0689	0.0715	0.1022	0.5765	1.0067	0.3873	0.055
3LV_002_Olivine10	0.0045	0.0038	0.0029	0.0024	0.0022	0.0010	0.0690	0.0719	0.1008	0.6061	0.9822	0.3873	0.055
3LV_002_Olivine10	0.0046	0.0038	0.0029	0.0024	0.0022	0.0010	0.0691	0.0727	0.0978	0.6335	0.9344	0.3909	0.055
3LV_002_Olivine10	0.0046	0.0039	0.0029	0.0024	0.0022	0.0010	0.0694	0.0746	0.0922	0.7184	0.8429	0.3833	0.055
3LV_009_Olivine1	0.0046	0.0039	0.0029	0.0024	0.0023	0.0010	0.0694	0.0758	0.0890	0.6916	0.8431	0.3695	0.055
3LV_009_Olivine1	0.0046	0.0039	0.0029	0.0024	0.0023	0.0010	0.0693	0.0752	0.0906	0.7366	0.8731	0.3692	0.055
3LV_009_Olivine1	0.0045	0.0037	0.0029	0.0024	0.0022	0.0010	0.0690	0.0731	0.0966	0.6529	0.9568	0.3638	0.055

3LV_009_Olivine1	0.0046	0.0039	0.0030	0.0024	0.0023	0.0010	0.0696	0.0776	0.0851	0.7808	0.7906	0.3601	0.055
SCOL	0.0045	0.0036	0.0028	0.0023	0.0022	0.0010	0.0681	0.0677	0.1206	0.5753	1.3640	1.2516	0.056
SCOL	0.0045	0.0036	0.0028	0.0023	0.0022	0.0010	0.0682	0.0677	0.1208	0.5767	1.3728	1.2697	0.056
SCOL	0.0045	0.0036	0.0028	0.0023	0.0022	0.0010	0.0682	0.0678	0.1207	0.5782	1.3307	1.2201	0.056
3LV_009_Olivine3	0.0045	0.0037	0.0029	0.0023	0.0022	0.0010	0.0688	0.0710	0.1052	0.5940	1.0554	0.3632	0.056
3LV_009_Olivine3	0.0046	0.0038	0.0029	0.0023	0.0022	0.0010	0.0687	0.0705	0.1066	0.5762	1.0650	0.3665	0.055
3LV_009_Olivine3	0.0046	0.0038	0.0029	0.0024	0.0023	0.0010	0.0689	0.0722	0.0990	0.6002	0.9925	0.3723	0.055
3LV_009_Olivine3	0.0046	0.0042	0.0030	0.0025	0.0024	0.0010	0.0707	0.0853	0.0741	0.8723	0.6612	0.4091	0.054
3LV_009_Olivine4	0.0046	0.0039	0.0029	0.0024	0.0023	0.0010	0.0693	0.0750	0.0917	0.6598	0.8933	0.3598	0.055
3LV_009_Olivine4	0.0046	0.0040	0.0030	0.0024	0.0023	0.0010	0.0700	0.0802	0.0806	0.8235	0.7512	0.3856	0.054
3LV_009_Olivine4	0.0047	0.0043	0.0031	0.0025	0.0024	0.0010	0.0709	0.0883	0.0709	0.9935	0.6196	0.4109	0.053
3LV_009_Olivine4	0.0048	0.0044	0.0031	0.0025	0.0024	0.0010	0.0717	0.0957	0.0653	1.4968	0.5387	0.4054	0.053
3LV_009_Olivine5	0.0046	0.0038	0.0029	0.0024	0.0023	0.0010	0.0692	0.0734	0.0967	0.6244	0.9383	0.3629	0.055
3LV_009_Olivine5	0.0045	0.0038	0.0029	0.0024	0.0022	0.0010	0.0690	0.0725	0.0994	0.6223	0.9938	0.3534	0.055
3LV_009_Olivine5	0.0045	0.0038	0.0028	0.0024	0.0023	0.0010	0.0691	0.0729	0.0976	0.6465	0.9565	0.3556	0.055
3LV_009_Olivine5	0.0045	0.0038	0.0029	0.0024	0.0023	0.0010	0.0693	0.0748	0.0922	0.7847	0.8721	0.3615	0.055
3LV_009_Olivine6	0.0045	0.0039	0.0029	0.0024	0.0023	0.0010	0.0695	0.0756	0.0901	0.7286	0.8552	0.3693	0.055
3LV_009_Olivine6	0.0046	0.0038	0.0029	0.0024	0.0023	0.0010	0.0694	0.0747	0.0925	0.6650	0.9153	0.3677	0.055
3LV_009_Olivine6	0.0047	0.0043	0.0031	0.0025	0.0024	0.0010	0.0712	0.0891	0.0703	1.0697	0.6149	0.4097	0.053
3LV_009_Olivine7	0.0045	0.0038	0.0029	0.0024	0.0022	0.0010	0.0689	0.0723	0.0998	0.6213	0.9864	0.3583	0.055
3LV_009_Olivine7	0.0045	0.0038	0.0029	0.0024	0.0022	0.0010	0.0688	0.0718	0.1014	0.6222	0.9963	0.3590	0.055
3LV_009_Olivine7	0.0045	0.0038	0.0029	0.0024	0.0023	0.0010	0.0688	0.0728	0.0979	0.6359	0.9887	0.3632	0.055
3LV_009_Olivine7	0.0046	0.0039	0.0030	0.0024	0.0023	0.0010	0.0696	0.0783	0.0842	0.8294	0.7518	0.3708	0.054
SCOL	0.0045	0.0036	0.0028	0.0023	0.0022	0.0010	0.0682	0.0678	0.1210	0.5837	1.3420	1.2452	0.056
SCOL	0.0045	0.0036	0.0028	0.0023	0.0022	0.0010	0.0682	0.0678	0.1206	0.5871	1.3300	1.2231	0.056
SCOL	0.0045	0.0036	0.0028	0.0023	0.0022	0.0010	0.0682	0.0678	0.1210	0.5838	1.3639	1.2444	0.056
3LV_009_Olivine9	0.0046	0.0038	0.0029	0.0024	0.0023	0.0010	0.0690	0.0728	0.0980	0.6250	1.0093	0.3559	0.055
3LV_009_Olivine9	0.0046	0.0037	0.0029	0.0024	0.0022	0.0010	0.0689	0.0714	0.1031	0.6151	1.0362	0.3449	0.055
3LV_009_Olivine9	0.0046	0.0038	0.0028	0.0023	0.0023	0.0010	0.0688	0.0713	0.1045	0.5923	1.0589	0.3643	0.056
3LV_009_Olivine10	0.0045	0.0039	0.0029	0.0024	0.0023	0.0010	0.0703	0.0779	0.0840	0.8439	0.8556	0.3651	0.054
3LV_009_Olivine10	0.0046	0.0042	0.0031	0.0025	0.0024	0.0010	0.0716	0.0903	0.0684	1.6847	0.6355	0.4485	0.053
3LV_0016_Olivine1	0.0045	0.0038	0.0029	0.0024	0.0022	0.0010	0.0685	0.0712	0.1011	0.6503	1.0515	0.3839	0.055
3LV_0016_Olivine1	0.0046	0.0038	0.0029	0.0024	0.0023	0.0010	0.0685	0.0724	0.0956	0.7099	1.0078	0.3851	0.055
3LV_0016_Olivine1	0.0046	0.0040	0.0030	0.0024	0.0023	0.0010	0.0695	0.0801	0.0792	0.9534	0.7062	0.3902	0.054
3LV_0016_Olivine1	0.0047	0.0041	0.0030	0.0025	0.0023	0.0010	0.0703	0.0831	0.0766	1.1510	0.6518	0.3624	0.054
3LV_0016_Olivine2	0.0046	0.0038	0.0029	0.0023	0.0023	0.0010	0.0684	0.0706	0.1039	0.6423	1.0647	0.3788	0.055
3LV_0016_Olivine2	0.0046	0.0038	0.0029	0.0024	0.0022	0.0010	0.0685	0.0709	0.1028	0.6734	1.0484	0.3805	0.055
3LV_0016_Olivine2	0.0046	0.0039	0.0029	0.0024	0.0023	0.0010	0.0687	0.0727	0.0965	0.7081	0.9768	0.3835	0.055
3LV_0016_Olivine2	0.0046	0.0038	0.0029	0.0024	0.0022	0.0010	0.0685	0.0715	0.0996	0.7302	0.9818	0.3698	0.055
3LV_0016_Olivine3	0.0046	0.0038	0.0029	0.0024	0.0023	0.0010	0.0688	0.0725	0.0970	0.7267	0.9636	0.3657	0.055
3LV_0016_Olivine3	0.0046	0.0039	0.0029	0.0024	0.0023	0.0010	0.0689	0.0742	0.0913	0.7654	0.8773	0.3757	0.055
3LV_0016_Olivine3	0.0046	0.0039	0.0030	0.0024	0.0023	0.0010	0.0689	0.0740	0.0917	0.8070	0.8905	0.3723	0.055
3LV_0016_Olivine3	0.0047	0.0040	0.0030	0.0024	0.0023	0.0010	0.0692	0.0770	0.0848	1.0500	0.8008	0.3561	0.054

SCOL	0.0045	0.0037	0.0028	0.0023	0.0022	0.0010	0.0677	0.0672	0.1197	0.6125	1.4358	1.1875	0.056
SCOL	0.0045	0.0037	0.0028	0.0023	0.0022	0.0010	0.0678	0.0671	0.1197	0.6140	1.4315	1.1962	0.055
SCOL	0.0045	0.0037	0.0028	0.0023	0.0022	0.0010	0.0677	0.0671	0.1195	0.6034	1.4216	1.2024	0.055
3LV_0016_Olivine5	0.0046	0.0038	0.0029	0.0024	0.0022	0.0010	0.0684	0.0711	0.1008	0.6847	1.0254	0.3714	0.055
3LV_0016_Olivine5	0.0046	0.0039	0.0029	0.0024	0.0023	0.0010	0.0684	0.0720	0.0964	0.7358	0.9985	0.3728	0.055
3LV_0016_Olivine5	0.0047	0.0041	0.0030	0.0025	0.0023	0.0010	0.0696	0.0806	0.0780	1.0265	0.7445	0.3795	0.054
3LV_0016_Olivine6	0.0045	0.0038	0.0029	0.0024	0.0023	0.0010	0.0682	0.0707	0.1014	0.6646	1.0573	0.3763	0.055
3LV_0016_Olivine6	0.0045	0.0038	0.0029	0.0024	0.0022	0.0010	0.0682	0.0705	0.1022	0.6727	1.0684	0.3702	0.055
3LV_0016_Olivine6	0.0046	0.0038	0.0029	0.0023	0.0022	0.0010	0.0682	0.0704	0.1024	0.6626	1.0741	0.3686	0.055
3LV_0016_Olivine6	0.0046	0.0039	0.0029	0.0024	0.0023	0.0010	0.0686	0.0732	0.0931	0.7522	0.9052	0.3576	0.055
3LV_0016_Olivine7	0.0046	0.0038	0.0029	0.0024	0.0023	0.0010	0.0682	0.0708	0.1004	0.6792	1.0342	0.3743	0.055
3LV_0016_Olivine7	0.0046	0.0038	0.0029	0.0024	0.0023	0.0010	0.0683	0.0710	0.1002	0.6924	1.0481	0.3773	0.055
3LV_0016_Olivine7	0.0046	0.0040	0.0029	0.0024	0.0023	0.0010	0.0688	0.0750	0.0877	0.7969	0.8753	0.3798	0.054
3LV_0016_Olivine7	0.0047	0.0041	0.0030	0.0025	0.0023	0.0010	0.0697	0.0815	0.0764	0.9888	0.6974	0.3892	0.054
3LV_0016_Olivine8	0.0046	0.0038	0.0029	0.0023	0.0023	0.0010	0.0682	0.0702	0.1031	0.6571	1.0762	0.3803	0.055
3LV_0016_Olivine8	0.0045	0.0038	0.0029	0.0024	0.0023	0.0010	0.0685	0.0709	0.1010	0.6718	1.0593	0.3834	0.055
3LV_0016_Olivine8	0.0046	0.0038	0.0029	0.0024	0.0023	0.0010	0.0686	0.0723	0.0955	0.7373	0.9819	0.3843	0.055
3LV_0016_Olivine8	0.0046	0.0039	0.0029	0.0024	0.0023	0.0010	0.0691	0.0768	0.0850	0.9302	0.7998	0.3857	0.054
3LV_0016_Olivine9	0.0046	0.0038	0.0029	0.0024	0.0022	0.0010	0.0682	0.0705	0.1019	0.6562	1.0718	0.3800	0.055
3LV_0016_Olivine9	0.0046	0.0037	0.0029	0.0024	0.0023	0.0010	0.0680	0.0697	0.1047	0.6179	1.1177	0.3817	0.055
3LV_0016_Olivine9	0.0046	0.0038	0.0029	0.0024	0.0023	0.0010	0.0682	0.0703	0.1022	0.6411	1.0798	0.3804	0.055
3LV_0016_Olivine9	0.0046	0.0039	0.0029	0.0024	0.0023	0.0010	0.0687	0.0738	0.0911	0.7724	0.9168	0.3764	0.055
SCOL	0.0045	0.0037	0.0028	0.0023	0.0022	0.0010	0.0676	0.0669	0.1194	0.6099	1.4323	1.1900	0.055
SCOL	0.0045	0.0037	0.0028	0.0023	0.0022	0.0010	0.0676	0.0670	0.1193	0.6086	1.4634	1.2146	0.055
SCOL	0.0045	0.0037	0.0028	0.0023	0.0022	0.0010	0.0677	0.0670	0.1191	0.6142	1.4215	1.2166	0.055
SCOL	0.0045	0.0037	0.0028	0.0023	0.0022	0.0010	0.0675	0.0670	0.1195	0.6064	1.4114	1.1814	0.055
SCOL	0.0044	0.0036	0.0028	0.0023	0.0022	0.0010	0.0676	0.0670	0.1197	0.6024	1.4170	1.2032	0.055
SCOL	0.0044	0.0036	0.0028	0.0023	0.0022	0.0010	0.0676	0.0670	0.1197	0.6090	1.4523	1.2202	0.055
3LV_004_Olivine8	0.0044	0.0037	0.0029	0.0024	0.0022	0.0010	0.0686	0.0709	0.1014	0.6358	1.0670	0.3268	0.055
3LV_004_Olivine8	0.0044	0.0037	0.0029	0.0024	0.0022	0.0010	0.0685	0.0706	0.1009	0.6242	1.0802	0.4176	0.055
3LV_004_Olivine8	0.0045	0.0038	0.0029	0.0024	0.0023	0.0010	0.0687	0.0719	0.0966	0.6889	1.0414	0.4412	0.055
3LV_004_Olivine8	0.0045	0.0039	0.0029	0.0024	0.0023	0.0010	0.0692	0.0756	0.0877	0.6962	0.9025	0.3537	0.054
3LV_004_Olivine9	0.0044	0.0037	0.0029	0.0023	0.0022	0.0010	0.0683	0.0708	0.1022	0.6156	1.0996	0.2638	0.055
3LV_004_Olivine9	0.0044	0.0037	0.0029	0.0024	0.0023	0.0010	0.0686	0.0711	0.1004	0.6406	1.0780	0.4108	0.055
3LV_004_Olivine10	0.0045	0.0038	0.0029	0.0024	0.0022	0.0010	0.0683	0.0704	0.1016	0.6103	1.0738	0.5004	0.055
3LV_004_Olivine10	0.0045	0.0038	0.0029	0.0024	0.0023	0.0010	0.0682	0.0709	0.1000	0.6163	1.0816	0.3501	0.055
3LV_004_Olivine10	0.0045	0.0038	0.0029	0.0024	0.0023	0.0010	0.0682	0.0707	0.1004	0.6413	1.0772	0.3705	0.055
3LV_004_Olivine10	0.0045	0.0037	0.0029	0.0024	0.0023	0.0010	0.0683	0.0712	0.0980	0.6346	1.0537	0.3757	0.055
3LV_009_Olivine8b	0.0045	0.0039	0.0030	0.0024	0.0023	0.0010	0.0690	0.0763	0.0847	0.7644	0.8568	0.3544	0.054
3LV_009_Olivine8b	0.0045	0.0040	0.0030	0.0024	0.0024	0.0010	0.0699	0.0795	0.0792	0.9957	0.8393	0.3515	0.054
3LV_009_Olivine8b	0.0046	0.0041	0.0031	0.0025	0.0024	0.0010	0.0708	0.0860	0.0718	1.5668	0.6831	0.4376	0.053
SCOL	0.0045	0.0037	0.0028	0.0023	0.0022	0.0010	0.0676	0.0669	0.1194	0.6166	1.4471	1.1963	0.055
SCOL	0.0045	0.0037	0.0028	0.0023	0.0022	0.0010	0.0677	0.0669	0.1192	0.6201	1.4405	1.2017	0.055

SCOL	0.0045	0.0037	0.0029	0.0023	0.0022	0.0010	0.0675	0.0667	0.1194	0.6120	1.4465	1.2117	0.055
SCOL	0.0043	0.0036	0.0028	0.0023	0.0022	0.0009	0.0673	0.0668	0.1183	0.5615	1.3219	1.1406	0.055
SCOL	0.0043	0.0036	0.0028	0.0023	0.0022	0.0009	0.0675	0.0668	0.1183	0.5642	1.3203	1.1323	0.055
SCOL	0.0043	0.0035	0.0028	0.0023	0.0022	0.0010	0.0675	0.0668	0.1184	0.5647	1.3254	1.1496	0.055
3LV-015_Olivine1	0.0044	0.0037	0.0029	0.0024	0.0022	0.0010	0.0684	0.0723	0.0942	0.6913	0.8802	0.3608	0.054
3LV-015_Olivine1	0.0044	0.0038	0.0029	0.0024	0.0022	0.0010	0.0686	0.0731	0.0919	0.7319	0.8502	0.3581	0.054
3LV-015_Olivine1	0.0044	0.0038	0.0029	0.0024	0.0022	0.0010	0.0686	0.0734	0.0912	0.7387	0.8146	0.3547	0.054
3LV-015_Olivine1	0.0044	0.0038	0.0029	0.0024	0.0023	0.0010	0.0687	0.0742	0.0893	0.7910	0.7894	0.3427	0.054
3LV-015_Olivine2	0.0043	0.0037	0.0029	0.0023	0.0022	0.0010	0.0680	0.0702	0.1023	0.5922	1.0005	0.3667	0.054
3LV-015_Olivine2	0.0043	0.0037	0.0029	0.0023	0.0022	0.0010	0.0681	0.0708	0.0998	0.6020	0.9754	0.3688	0.054
3LV-015_Olivine2	0.0043	0.0037	0.0029	0.0023	0.0022	0.0010	0.0681	0.0710	0.0985	0.6196	0.9545	0.3551	0.054
3LV-015_Olivine2	0.0043	0.0037	0.0029	0.0024	0.0022	0.0010	0.0685	0.0738	0.0903	0.7310	0.8043	0.3545	0.054
3LV-015_Olivine3	0.0043	0.0038	0.0029	0.0024	0.0022	0.0010	0.0685	0.0736	0.0907	0.7259	0.8185	0.3526	0.054
3LV-015_Olivine3	0.0044	0.0038	0.0029	0.0023	0.0022	0.0010	0.0685	0.0725	0.0937	0.6990	0.8770	0.3599	0.054
3LV-015_Olivine3	0.0043	0.0038	0.0029	0.0024	0.0022	0.0010	0.0683	0.0722	0.0941	0.6973	0.8904	0.3619	0.054
3LV-015_Olivine3	0.0044	0.0039	0.0030	0.0024	0.0023	0.0010	0.0692	0.0784	0.0801	0.9180	0.7208	0.3593	0.053
3LV-015_Olivine4	0.0044	0.0039	0.0030	0.0024	0.0023	0.0010	0.0689	0.0766	0.0838	0.8797	0.7279	0.3472	0.054
3LV-015_Olivine4	0.0044	0.0039	0.0029	0.0024	0.0023	0.0010	0.0689	0.0763	0.0846	0.8424	0.7252	0.3569	0.054
3LV-015_Olivine4	0.0043	0.0038	0.0029	0.0024	0.0022	0.0010	0.0686	0.0741	0.0893	0.7695	0.8229	0.3651	0.054
3LV-015_Olivine4	0.0044	0.0040	0.0030	0.0024	0.0023	0.0010	0.0695	0.0813	0.0761	1.0088	0.6396	0.3540	0.053
3LV-015_Olivine5	0.0043	0.0038	0.0029	0.0024	0.0022	0.0010	0.0682	0.0725	0.0934	0.7259	0.8970	0.3639	0.054
3LV-015_Olivine5	0.0044	0.0038	0.0029	0.0024	0.0022	0.0010	0.0684	0.0735	0.0903	0.7724	0.8527	0.3584	0.054
3LV-015_Olivine5	0.0044	0.0038	0.0030	0.0024	0.0023	0.0010	0.0684	0.0733	0.0909	0.7592	0.8516	0.3576	0.054
3LV-015_Olivine5	0.0044	0.0038	0.0030	0.0024	0.0023	0.0010	0.0687	0.0749	0.0867	0.8139	0.8050	0.3737	0.054
SCOL	0.0043	0.0035	0.0028	0.0023	0.0022	0.0009	0.0674	0.0666	0.1191	0.5775	1.3645	1.1082	0.055
SCOL	0.0043	0.0035	0.0028	0.0023	0.0022	0.0010	0.0675	0.0666	0.1192	0.5699	1.3312	1.1647	0.055
SCOL	0.0043	0.0036	0.0028	0.0023	0.0022	0.0010	0.0675	0.0667	0.1193	0.5724	1.3467	1.1475	0.055
3LV-015_Olivine6	0.0044	0.0037	0.0029	0.0024	0.0022	0.0010	0.0682	0.0716	0.0959	0.6785	0.9116	0.3640	0.054
3LV-015_Olivine6	0.0043	0.0037	0.0029	0.0024	0.0022	0.0010	0.0681	0.0715	0.0966	0.6729	0.9173	0.3597	0.054
3LV-015_Olivine6	0.0044	0.0038	0.0030	0.0024	0.0023	0.0010	0.0687	0.0757	0.0854	0.8420	0.7715	0.3575	0.054
3LV-015_Olivine6	0.0044	0.0039	0.0030	0.0024	0.0023	0.0010	0.0691	0.0784	0.0805	0.9582	0.6819	0.3549	0.054
3LV-015_Olivine7	0.0043	0.0037	0.0029	0.0024	0.0022	0.0010	0.0680	0.0719	0.0955	0.6904	0.9017	0.3525	0.054
3LV-015_Olivine7	0.0043	0.0038	0.0029	0.0024	0.0022	0.0010	0.0682	0.0727	0.0928	0.7063	0.8637	0.3583	0.054
3LV-015_Olivine7	0.0043	0.0037	0.0029	0.0024	0.0022	0.0010	0.0682	0.0725	0.0933	0.6886	0.8533	0.3588	0.054
3LV-015_Olivine7	0.0044	0.0038	0.0029	0.0024	0.0023	0.0010	0.0682	0.0734	0.0903	0.7312	0.8175	0.3658	0.054
3LV-015_Olivine8	0.0043	0.0037	0.0029	0.0024	0.0022	0.0010	0.0678	0.0713	0.0964	0.6465	0.9226	0.3636	0.054
3LV-015_Olivine8	0.0043	0.0037	0.0029	0.0024	0.0022	0.0010	0.0682	0.0733	0.0904	0.7591	0.8332	0.3565	0.054
3LV-015_Olivine8	0.0044	0.0039	0.0030	0.0024	0.0023	0.0010	0.0685	0.0759	0.0845	0.8615	0.7657	0.3581	0.054
3LV-015_Olivine8	0.0044	0.0040	0.0030	0.0024	0.0023	0.0010	0.0693	0.0836	0.0726	1.0929	0.6089	0.3787	0.053
3LV-015_Olivine9	0.0043	0.0037	0.0029	0.0023	0.0022	0.0010	0.0675	0.0701	0.1002	0.6306	0.9989	0.3604	0.054
3LV-015_Olivine9	0.0043	0.0037	0.0028	0.0023	0.0022	0.0010	0.0677	0.0708	0.0978	0.6849	0.9757	0.3625	0.054
3LV-015_Olivine9	0.0043	0.0037	0.0029	0.0024	0.0022	0.0010	0.0676	0.0710	0.0972	0.6855	0.9408	0.3633	0.054
3LV-015_Olivine9	0.0044	0.0038	0.0029	0.0024	0.0023	0.0010	0.0681	0.0746	0.0870	0.7885	0.7990	0.3576	0.054

3LV-015_Olivine10	0.0044	0.0037	0.0029	0.0023	0.0022	0.0010	0.0674	0.0701	0.1000	0.6190	0.9623	0.3482	0.054
3LV-015_Olivine10	0.0044	0.0037	0.0029	0.0024	0.0023	0.0010	0.0682	0.0721	0.0957	0.6850	0.9157	0.3365	0.054
3LV-015_Olivine10	0.0043	0.0037	0.0029	0.0024	0.0022	0.0010	0.0681	0.0716	0.0968	0.6654	0.9457	0.3537	0.054
3LV-015_Olivine10	0.0044	0.0038	0.0029	0.0024	0.0023	0.0010	0.0684	0.0736	0.0913	0.7387	0.8364	0.3524	0.054
SCOL	0.0043	0.0036	0.0028	0.0023	0.0022	0.0010	0.0674	0.0667	0.1193	0.5799	1.3276	1.1245	0.055
SCOL	0.0043	0.0035	0.0028	0.0023	0.0022	0.0009	0.0674	0.0666	0.1192	0.5887	1.3638	1.1077	0.055
SCOL	0.0043	0.0036	0.0028	0.0023	0.0022	0.0010	0.0673	0.0665	0.1193	0.5807	1.3423	1.1445	0.055
3LV-010_Olivine1	0.0044	0.0038	0.0030	0.0024	0.0023	0.0010	0.0684	0.0741	0.0897	0.7116	0.8574	0.3701	0.054
3LV-010_Olivine1	0.0044	0.0038	0.0029	0.0024	0.0023	0.0010	0.0684	0.0742	0.0890	0.7267	0.8450	0.3649	0.054
3LV-010_Olivine1	0.0044	0.0039	0.0029	0.0024	0.0023	0.0010	0.0684	0.0747	0.0880	0.7083	0.8453	0.3786	0.054
3LV-010_Olivine1	0.0044	0.0039	0.0030	0.0024	0.0023	0.0010	0.0688	0.0786	0.0801	0.8151	0.7374	0.3874	0.053
3LV-010_Olivine2	0.0044	0.0038	0.0029	0.0024	0.0022	0.0010	0.0680	0.0732	0.0916	0.7141	0.8617	0.3719	0.054
3LV-010_Olivine2	0.0044	0.0038	0.0029	0.0024	0.0022	0.0010	0.0680	0.0728	0.0928	0.6713	0.8811	0.3756	0.054
3LV-010_Olivine2	0.0044	0.0039	0.0030	0.0024	0.0023	0.0010	0.0688	0.0786	0.0801	0.7766	0.7310	0.3880	0.053
3LV-010_Olivine2	0.0045	0.0041	0.0031	0.0024	0.0023	0.0010	0.0692	0.0827	0.0740	0.8870	0.6595	0.3913	0.053
3LV-010_Olivine3	0.0043	0.0037	0.0029	0.0024	0.0022	0.0010	0.0681	0.0721	0.0955	0.6704	0.9276	0.3681	0.054
3LV-010_Olivine3	0.0044	0.0037	0.0029	0.0024	0.0022	0.0010	0.0680	0.0719	0.0951	0.6776	0.9127	0.3670	0.054
3LV-010_Olivine3	0.0045	0.0041	0.0030	0.0024	0.0023	0.0010	0.0695	0.0838	0.0729	1.0950	0.6516	0.3677	0.053
3LV-010_Olivine3	0.0045	0.0042	0.0031	0.0025	0.0024	0.0010	0.0700	0.0888	0.0682	1.3810	0.5744	0.3639	0.052
3LV-010_Olivine4	0.0043	0.0037	0.0029	0.0024	0.0022	0.0010	0.0677	0.0708	0.0990	0.6158	0.9837	0.3646	0.054
3LV-010_Olivine4	0.0044	0.0037	0.0029	0.0024	0.0022	0.0010	0.0678	0.0718	0.0946	0.6900	0.9093	0.3676	0.054
3LV-010_Olivine4	0.0043	0.0037	0.0029	0.0024	0.0022	0.0010	0.0676	0.0710	0.0976	0.6378	0.9519	0.3677	0.054
3LV-010_Olivine4	0.0044	0.0038	0.0029	0.0024	0.0022	0.0010	0.0680	0.0744	0.0883	0.7329	0.8160	0.3583	0.054
3LV-010_Olivine5	0.0043	0.0037	0.0029	0.0023	0.0022	0.0010	0.0678	0.0714	0.0969	0.6309	0.9373	0.3652	0.054
3LV-010_Olivine5	0.0043	0.0037	0.0029	0.0023	0.0022	0.0010	0.0678	0.0714	0.0969	0.6323	0.9462	0.3657	0.054
3LV-010_Olivine5	0.0043	0.0038	0.0029	0.0024	0.0022	0.0010	0.0682	0.0726	0.0931	0.6987	0.8924	0.3601	0.054
3LV-010_Olivine5	0.0044	0.0040	0.0030	0.0024	0.0023	0.0010	0.0693	0.0815	0.0757	1.0174	0.6605	0.3536	0.053
SCOL	0.0043	0.0036	0.0028	0.0023	0.0022	0.0009	0.0671	0.0663	0.1189	0.5919	1.3602	1.1125	0.055
SCOL	0.0043	0.0036	0.0028	0.0023	0.0022	0.0010	0.0671	0.0663	0.1190	0.5920	1.3595	1.1471	0.055
SCOL	0.0043	0.0036	0.0028	0.0023	0.0022	0.0009	0.0672	0.0665	0.1190	0.5845	1.3868	1.1432	0.055
3LV-010_Olivine6	0.0043	0.0037	0.0029	0.0024	0.0022	0.0010	0.0678	0.0718	0.0953	0.6394	0.9022	0.3634	0.054
3LV-010_Olivine6	0.0044	0.0038	0.0029	0.0023	0.0022	0.0010	0.0680	0.0720	0.0947	0.6845	0.8832	0.4008	0.054
3LV-010_Olivine6	0.0044	0.0037	0.0029	0.0024	0.0022	0.0010	0.0681	0.0725	0.0935	0.6537	0.8970	0.3714	0.054
3LV-010_Olivine6	0.0044	0.0039	0.0030	0.0024	0.0023	0.0010	0.0686	0.0769	0.0827	0.8817	0.7636	0.3731	0.053
3LV-010_Olivine7	0.0044	0.0037	0.0029	0.0023	0.0022	0.0010	0.0677	0.0705	0.0991	0.6046	0.9838	0.3640	0.054
3LV-010_Olivine7	0.0043	0.0037	0.0029	0.0024	0.0022	0.0010	0.0677	0.0708	0.0982	0.6207	0.9911	0.3615	0.054
3LV-010_Olivine7	0.0044	0.0037	0.0029	0.0024	0.0022	0.0010	0.0678	0.0711	0.0970	0.6195	0.9395	0.3662	0.054
3LV-010_Olivine7	0.0044	0.0039	0.0030	0.0024	0.0023	0.0010	0.0684	0.0760	0.0844	0.7870	0.7826	0.3622	0.054
3LV-010_Olivine8	0.0044	0.0037	0.0029	0.0024	0.0022	0.0010	0.0677	0.0706	0.0994	0.5958	0.9917	0.3687	0.054
3LV-010_Olivine8	0.0043	0.0037	0.0029	0.0023	0.0022	0.0010	0.0679	0.0712	0.0977	0.5998	0.9693	0.3685	0.054
3LV-010_Olivine8	0.0043	0.0037	0.0029	0.0024	0.0022	0.0010	0.0681	0.0718	0.0955	0.6461	0.9446	0.3709	0.054
3LV-010_Olivine8	0.0044	0.0039	0.0029	0.0024	0.0023	0.0010	0.0685	0.0752	0.0868	0.7633	0.7967	0.3596	0.054
3LV-010_Olivine9	0.0043	0.0037	0.0029	0.0023	0.0022	0.0010	0.0675	0.0696	0.1029	0.5757	1.0270	0.3612	0.054

3LV-010_Olivine9	0.0043	0.0036	0.0029	0.0023	0.0022	0.0010	0.0676	0.0699	0.1021	0.5675	1.0159	0.3630	0.054
3LV-010_Olivine9	0.0043	0.0037	0.0029	0.0023	0.0022	0.0010	0.0677	0.0705	0.0998	0.5920	0.9808	0.3639	0.054
3LV-010_Olivine9	0.0044	0.0038	0.0029	0.0024	0.0023	0.0010	0.0681	0.0738	0.0889	0.6735	0.8442	0.3643	0.054
3LV-010_Olivine10	0.0044	0.0037	0.0029	0.0024	0.0022	0.0010	0.0680	0.0723	0.0940	0.6747	0.9096	0.3611	0.054
3LV-010_Olivine10	0.0044	0.0039	0.0030	0.0024	0.0023	0.0010	0.0685	0.0767	0.0836	0.8624	0.7420	0.3683	0.054
3LV-010_Olivine10	0.0044	0.0038	0.0030	0.0024	0.0023	0.0010	0.0684	0.0756	0.0853	0.8480	0.7649	0.3483	0.054
3LV-010_Olivine10	0.0045	0.0041	0.0031	0.0025	0.0023	0.0010	0.0697	0.0863	0.0703	1.1991	0.6062	0.3602	0.053
SCOL	0.0043	0.0035	0.0028	0.0023	0.0022	0.0009	0.0672	0.0665	0.1190	0.5835	1.3788	1.1237	0.055
SCOL	0.0043	0.0036	0.0028	0.0023	0.0022	0.0009	0.0673	0.0665	0.1189	0.5835	1.3647	1.1273	0.055
SCOL	0.0043	0.0036	0.0028	0.0023	0.0022	0.0010	0.0673	0.0665	0.1189	0.5789	1.3592	1.1777	0.055
R_4694_Olivine1	0.0043	0.0036	0.0029	0.0023	0.0022	0.0010	0.0679	0.0699	0.1032	0.5832	1.0139	0.3559	0.055
R_4694_Olivine1	0.0044	0.0037	0.0029	0.0023	0.0022	0.0010	0.0676	0.0695	0.1034	0.5759	1.0142	0.3562	0.054
R_4694_Olivine1	0.0044	0.0037	0.0029	0.0023	0.0022	0.0010	0.0675	0.0696	0.1018	0.5933	1.0037	0.3582	0.054
R_4694_Olivine1	0.0044	0.0038	0.0029	0.0024	0.0022	0.0010	0.0684	0.0729	0.0923	0.7663	0.8572	0.3424	0.054
R_4694_Olivine2	0.0043	0.0036	0.0028	0.0023	0.0022	0.0010	0.0678	0.0698	0.1029	0.5884	1.0369	0.3576	0.055
R_4694_Olivine2	0.0043	0.0037	0.0029	0.0023	0.0022	0.0010	0.0678	0.0699	0.1032	0.5883	1.0149	0.3580	0.055
R_4694_Olivine2	0.0044	0.0037	0.0028	0.0023	0.0022	0.0010	0.0676	0.0698	0.1028	0.5902	1.0214	0.3600	0.054
R_4694_Olivine2	0.0043	0.0037	0.0029	0.0023	0.0022	0.0010	0.0678	0.0702	0.1013	0.5886	0.9940	0.3586	0.054
R_4694_Olivine3	0.0043	0.0036	0.0029	0.0023	0.0022	0.0010	0.0675	0.0694	0.1042	0.5611	1.0560	0.3601	0.055
R_4694_Olivine3	0.0043	0.0036	0.0029	0.0023	0.0022	0.0010	0.0676	0.0695	0.1036	0.5722	1.0447	0.3624	0.054
R_4694_Olivine3	0.0043	0.0037	0.0028	0.0023	0.0022	0.0010	0.0675	0.0697	0.1029	0.5824	1.0413	0.3621	0.054
R_4694_Olivine3	0.0044	0.0037	0.0029	0.0024	0.0022	0.0010	0.0679	0.0714	0.0963	0.6763	0.9404	0.3541	0.054
R_4694_Olivine4	0.0044	0.0037	0.0029	0.0023	0.0022	0.0010	0.0675	0.0703	0.1002	0.6282	0.9834	0.3484	0.054
R_4694_Olivine4	0.0044	0.0037	0.0029	0.0024	0.0022	0.0010	0.0674	0.0702	0.1006	0.6312	0.9885	0.3500	0.054
R_4694_Olivine4	0.0044	0.0037	0.0029	0.0023	0.0022	0.0010	0.0675	0.0705	0.0993	0.6429	0.9851	0.3513	0.054
R_4694_Olivine4	0.0044	0.0038	0.0029	0.0023	0.0022	0.0010	0.0675	0.0709	0.0978	0.6561	0.9532	0.3515	0.054
R_4694_Olivine5	0.0044	0.0037	0.0029	0.0023	0.0022	0.0010	0.0675	0.0696	0.1025	0.5924	1.0205	0.3557	0.054
R_4694_Olivine5	0.0044	0.0037	0.0029	0.0023	0.0022	0.0010	0.0675	0.0696	0.1030	0.5949	1.0266	0.3569	0.054
R_4694_Olivine5	0.0044	0.0037	0.0029	0.0023	0.0022	0.0010	0.0677	0.0704	0.1001	0.6187	0.9890	0.3604	0.054
R_4694_Olivine5	0.0044	0.0037	0.0029	0.0023	0.0022	0.0010	0.0676	0.0708	0.0979	0.6625	0.9622	0.3568	0.054
SCOL	0.0043	0.0035	0.0028	0.0023	0.0022	0.0009	0.0671	0.0665	0.1188	0.5801	1.3776	1.1408	0.055
SCOL	0.0043	0.0035	0.0028	0.0023	0.0022	0.0010	0.0671	0.0664	0.1189	0.5766	1.3598	1.1351	0.055
SCOL	0.0043	0.0036	0.0028	0.0023	0.0022	0.0009	0.0671	0.0664	0.1188	0.5823	1.3444	1.1385	0.055
R_4694_Olivine6	0.0043	0.0037	0.0029	0.0023	0.0022	0.0010	0.0675	0.0698	0.1026	0.6057	1.0166	0.3571	0.054
R_4694_Olivine6	0.0044	0.0036	0.0029	0.0023	0.0022	0.0010	0.0672	0.0697	0.1015	0.5945	1.0142	0.3570	0.054
R_4694_Olivine6	0.0044	0.0037	0.0029	0.0023	0.0022	0.0010	0.0675	0.0705	0.0991	0.6308	0.9800	0.3604	0.054
R_4694_Olivine6	0.0043	0.0037	0.0029	0.0023	0.0022	0.0010	0.0676	0.0709	0.0980	0.6612	0.9717	0.3557	0.054
R_4694_Olivine7	0.0043	0.0037	0.0028	0.0023	0.0022	0.0010	0.0672	0.0683	0.1087	0.5419	1.1101	0.3447	0.054
R_4694_Olivine7	0.0044	0.0036	0.0029	0.0023	0.0022	0.0010	0.0676	0.0690	0.1079	0.5521	1.0996	0.3492	0.055
R_4694_Olivine7	0.0044	0.0037	0.0029	0.0024	0.0022	0.0010	0.0679	0.0699	0.1043	0.5819	1.0409	0.3528	0.055
R_4694_Olivine7	0.0044	0.0037	0.0029	0.0024	0.0022	0.0010	0.0682	0.0707	0.1020	0.5961	0.9988	0.3535	0.055
R_4694_Olivine8	0.0044	0.0037	0.0029	0.0024	0.0022	0.0010	0.0680	0.0707	0.0998	0.6218	0.9927	0.3628	0.054
R_4694_Olivine8	0.0044	0.0038	0.0029	0.0024	0.0022	0.0010	0.0681	0.0709	0.0992	0.6364	0.9786	0.3647	0.054

R_4694_Olivine8	0.0044	0.0037	0.0029	0.0024	0.0022	0.0010	0.0681	0.0711	0.0986	0.6510	0.9714	0.3590	0.054
R_4694_Olivine8	0.0044	0.0037	0.0029	0.0024	0.0023	0.0010	0.0682	0.0716	0.0975	0.6792	0.9436	0.3579	0.054
R_4694_Olivine9	0.0044	0.0037	0.0029	0.0023	0.0022	0.0010	0.0680	0.0706	0.1001	0.6283	0.9934	0.3623	0.054
R_4694_Olivine9	0.0044	0.0037	0.0029	0.0024	0.0022	0.0010	0.0680	0.0704	0.1010	0.6095	0.9949	0.3565	0.054
R_4694_Olivine9	0.0044	0.0037	0.0029	0.0023	0.0022	0.0010	0.0681	0.0705	0.1009	0.5985	1.0071	0.3438	0.054
R_4694_Olivine9	0.0044	0.0038	0.0029	0.0024	0.0022	0.0010	0.0681	0.0712	0.0980	0.6546	0.9718	0.3614	0.054
R_4694_Olivine10	0.0044	0.0037	0.0029	0.0023	0.0022	0.0010	0.0678	0.0693	0.1051	0.5638	1.0538	0.3619	0.055
R_4694_Olivine10	0.0044	0.0037	0.0029	0.0024	0.0022	0.0010	0.0681	0.0698	0.1043	0.5722	1.0470	0.3621	0.055
R_4694_Olivine10	0.0044	0.0037	0.0029	0.0023	0.0022	0.0010	0.0678	0.0691	0.1062	0.5565	1.0785	0.3593	0.055
R_4694_Olivine10	0.0043	0.0037	0.0029	0.0023	0.0022	0.0010	0.0680	0.0697	0.1050	0.5672	1.0504	0.3568	0.055
SCOL	0.0043	0.0036	0.0028	0.0023	0.0022	0.0010	0.0674	0.0666	0.1193	0.5833	1.3554	1.1374	0.055
SCOL	0.0043	0.0035	0.0029	0.0023	0.0022	0.0010	0.0673	0.0666	0.1191	0.5801	1.3406	1.1481	0.055
SCOL	0.0043	0.0036	0.0029	0.0023	0.0022	0.0010	0.0673	0.0665	0.1195	0.5826	1.3511	1.1670	0.055
3LV_004_Olivine11	0.0044	0.0037	0.0029	0.0023	0.0022	0.0010	0.0676	0.0692	0.1051	0.5555	1.0726	0.4041	0.054
3LV_004_Olivine11	0.0044	0.0036	0.0029	0.0023	0.0022	0.0010	0.0672	0.0690	0.1071	0.5305	1.0628	0.4977	0.055
SCOL	0.0043	0.0036	0.0028	0.0023	0.0022	0.0010	0.0669	0.0664	0.1186	0.5918	1.3683	1.1294	0.055
SCOL	0.0043	0.0036	0.0028	0.0023	0.0022	0.0010	0.0670	0.0664	0.1188	0.5852	1.3685	1.1352	0.055
SCOL	0.0043	0.0036	0.0028	0.0023	0.0022	0.0009	0.0671	0.0664	0.1187	0.5879	1.3559	1.1365	0.055
3LV_004_Olivine16	0.0043	0.0036	0.0029	0.0023	0.0022	0.0010	0.0675	0.0702	0.1018	0.5874	1.0113	0.2856	0.054
3LV_004_Olivine16	0.0043	0.0037	0.0028	0.0023	0.0022	0.0010	0.0676	0.0702	0.1006	0.5917	1.0020	0.3958	0.054
3LV_004_Olivine16	0.0043	0.0037	0.0029	0.0024	0.0022	0.0010	0.0677	0.0727	0.0929	0.6471	0.9172	0.2226	0.054
3LV_004_Olivine16	0.0044	0.0038	0.0029	0.0024	0.0023	0.0010	0.0678	0.0732	0.0911	0.6783	0.8596	0.5028	0.054
3LV_004_Olivine17	0.0043	0.0037	0.0029	0.0023	0.0022	0.0010	0.0676	0.0711	0.0977	0.6263	0.9790	0.4581	0.054
3LV_004_Olivine17	0.0043	0.0037	0.0029	0.0023	0.0022	0.0010	0.0674	0.0700	0.1016	0.5949	1.0096	0.4486	0.054
3LV_004_Olivine17	0.0043	0.0037	0.0029	0.0023	0.0022	0.0010	0.0676	0.0710	0.0979	0.6165	0.9584	0.4194	0.054
3LV_004_Olivine17	0.0044	0.0038	0.0029	0.0024	0.0022	0.0010	0.0679	0.0740	0.0894	0.6939	0.8427	0.4825	0.054
3LV_004_Olivine18	0.0044	0.0037	0.0029	0.0023	0.0022	0.0010	0.0676	0.0706	0.0992	0.6100	0.9848	0.4855	0.054
3LV_004_Olivine18	0.0044	0.0037	0.0029	0.0023	0.0022	0.0010	0.0675	0.0697	0.1021	0.5723	1.0242	0.3989	0.054
3LV_004_Olivine18	0.0043	0.0037	0.0029	0.0023	0.0022	0.0010	0.0677	0.0702	0.1008	0.5891	0.9889	0.4566	0.054
3LV_004_Olivine18	0.0044	0.0038	0.0029	0.0024	0.0022	0.0010	0.0682	0.0744	0.0878	0.7422	0.8252	0.3986	0.054
3LV_004_Olivine19	0.0043	0.0037	0.0029	0.0023	0.0022	0.0010	0.0677	0.0707	0.1001	0.6131	0.9831	0.3125	0.054
3LV_004_Olivine19	0.0043	0.0037	0.0029	0.0023	0.0022	0.0010	0.0676	0.0716	0.0979	0.6107	0.9578	0.2659	0.054
3LV_004_Olivine19	0.0043	0.0037	0.0029	0.0023	0.0022	0.0010	0.0677	0.0715	0.0979	0.6066	0.9692	0.2755	0.054
3LV_004_Olivine19	0.0043	0.0037	0.0029	0.0023	0.0022	0.0010	0.0678	0.0711	0.0979	0.5968	0.9732	0.3994	0.054
3LV_004_Olivine20	0.0043	0.0036	0.0029	0.0023	0.0022	0.0010	0.0675	0.0700	0.1025	0.5823	1.0154	0.3739	0.055
3LV_004_Olivine20	0.0043	0.0036	0.0028	0.0023	0.0022	0.0010	0.0675	0.0700	0.1025	0.5898	1.0146	0.3608	0.055
3LV_004_Olivine20	0.0043	0.0036	0.0028	0.0023	0.0022	0.0010	0.0674	0.0700	0.1022	0.5897	1.0122	0.3716	0.054
3LV_004_Olivine20	0.0043	0.0037	0.0029	0.0024	0.0022	0.0010	0.0677	0.0721	0.0944	0.6237	0.9273	0.3703	0.054
SCOL	0.0043	0.0035	0.0028	0.0023	0.0022	0.0010	0.0672	0.0665	0.1188	0.5839	1.3416	1.1428	0.055
SCOL	0.0043	0.0035	0.0028	0.0023	0.0022	0.0010	0.0672	0.0665	0.1189	0.5764	1.3378	1.1469	0.055
SCOL	0.0042	0.0035	0.0028	0.0023	0.0021	0.0010	0.0673	0.0666	0.1188	0.5705	1.3213	1.1470	0.055

Mg 2σ Errors	Fe 2σ Errors	Fe 2σ Errors	Ni 2σ Errors	Mn 2σ Errors	Ca 2σ Errors	Fe/Mn 2σ Er	Fo# 2σ Error
0.066	0.116	112	15	35	40	2.61	0.2113
0.066	0.116	112	15	35	40	2.56	0.2112
0.066	0.116	112	15	35	40	2.51	0.2113
0.066	0.094	122	21	39	41	1.77	0.1920
0.065	0.092	123	21	39	40	1.76	0.1895
0.065	0.084	127	21	40	40	1.69	0.1815
0.064	0.067	132	21	44	37	1.25	0.1617
0.066	0.097	121	21	38	42	1.79	0.1948
0.066	0.097	122	21	38	41	1.86	0.1942
0.065	0.093	124	21	39	41	1.73	0.1902
0.064	0.067	133	21	44	38	1.39	0.1613
0.065	0.094	123	21	39	41	1.77	0.1917
0.065	0.093	124	21	39	41	1.72	0.1901
0.065	0.088	126	21	40	40	1.63	0.1847
0.061	0.053	132	21	47	36	1.13	0.1415
0.065	0.095	123	21	39	41	1.74	0.1919
0.065	0.093	124	21	39	41	1.73	0.1904
0.065	0.090	125	21	39	40	1.65	0.1865
0.061	0.052	133	21	48	36	1.11	0.1402
0.065	0.090	125	21	40	41	1.63	0.1867
0.065	0.091	124	21	39	40	1.54	0.1890
0.066	0.118	114	16	35	41	2.54	0.2120
0.066	0.118	114	16	35	41	2.70	0.2120
0.066	0.118	114	15	35	41	2.58	0.2118
0.065	0.096	123	21	38	42	1.78	0.1927
0.065	0.096	123	21	38	42	1.83	0.1927
0.065	0.095	124	21	39	41	1.83	0.1917
0.064	0.072	133	21	44	38	1.28	0.1659
0.065	0.097	122	21	39	41	1.79	0.1939
0.065	0.097	123	21	39	41	1.79	0.1937
0.065	0.090	125	21	40	41	1.56	0.1870
0.065	0.096	123	21	39	42	1.78	0.1928
0.065	0.097	122	21	38	42	1.80	0.1934
0.065	0.091	125	21	39	41	1.68	0.1880
0.063	0.069	133	21	44	39	1.24	0.1632
0.065	0.093	125	21	39	41	1.80	0.1898
0.065	0.091	126	21	39	41	1.76	0.1878
0.065	0.087	127	21	40	40	1.66	0.1835
0.065	0.080	130	21	42	39	1.45	0.1751
0.064	0.075	131	21	42	40	1.53	0.1700
0.064	0.077	131	21	41	39	1.62	0.1725
0.065	0.086	128	22	40	40	1.79	0.1817

0.064	0.070	133	22	43	39	1.43	0.1633
0.066	0.118	114	15	35	41	2.65	0.2119
0.066	0.118	114	16	35	41	2.68	0.2120
0.066	0.118	114	16	35	41	2.52	0.2120
0.065	0.097	123	22	39	41	1.90	0.1937
0.066	0.099	122	21	38	42	1.89	0.1956
0.065	0.089	126	21	40	41	1.84	0.1853
0.061	0.053	134	21	48	39	1.19	0.1418
0.064	0.079	130	22	42	41	1.64	0.1743
0.063	0.063	134	21	45	39	1.38	0.1550
0.060	0.049	132	21	49	38	1.10	0.1348
0.058	0.040	127	21	53	36	0.91	0.1214
0.065	0.086	128	22	41	41	1.67	0.1819
0.065	0.089	127	22	40	41	1.82	0.1858
0.065	0.087	128	22	40	41	1.72	0.1831
0.065	0.080	131	21	42	39	1.54	0.1750
0.064	0.077	132	21	43	40	1.53	0.1716
0.065	0.080	131	21	42	41	1.71	0.1753
0.060	0.048	132	21	50	38	1.10	0.1333
0.065	0.090	126	21	40	41	1.77	0.1863
0.065	0.092	125	21	40	42	1.77	0.1886
0.065	0.087	127	21	40	41	1.83	0.1836
0.063	0.068	133	21	45	39	1.28	0.1615
0.066	0.118	114	15	36	42	2.51	0.2123
0.066	0.118	114	15	36	42	2.46	0.2119
0.066	0.118	114	15	36	42	2.58	0.2123
0.065	0.087	127	21	40	42	1.90	0.1838
0.065	0.094	125	22	40	42	1.85	0.1909
0.065	0.096	124	21	40	43	1.88	0.1929
0.064	0.069	135	21	44	40	1.72	0.1610
0.060	0.045	132	20	50	36	1.22	0.1291
0.065	0.092	125	21	40	42	1.95	0.1881
0.064	0.085	127	20	40	41	1.96	0.1802
0.062	0.061	133	20	47	39	1.20	0.1525
0.062	0.057	134	21	49	38	1.05	0.1471
0.065	0.096	123	21	40	42	1.90	0.1920
0.065	0.094	124	21	40	42	1.88	0.1904
0.065	0.086	127	21	41	42	1.78	0.1816
0.065	0.090	125	21	41	41	1.71	0.1860
0.065	0.087	127	21	42	42	1.70	0.1823
0.064	0.079	130	21	43	41	1.52	0.1737
0.064	0.079	129	21	43	41	1.57	0.1743
0.063	0.069	132	21	45	39	1.40	0.1629

0.066	0.117	113	15	36	43	2.84	0.2108
0.066	0.117	113	15	36	44	2.82	0.2107
0.066	0.117	113	15	37	44	2.78	0.2104
0.065	0.092	124	21	41	43	1.81	0.1878
0.064	0.086	126	21	41	42	1.85	0.1815
0.062	0.060	133	21	47	40	1.36	0.1504
0.065	0.093	123	21	41	43	1.90	0.1886
0.065	0.094	123	21	40	43	1.93	0.1898
0.065	0.094	123	21	40	43	1.94	0.1900
0.064	0.081	128	21	43	42	1.55	0.1767
0.064	0.091	124	21	41	43	1.83	0.1873
0.064	0.091	124	21	41	43	1.89	0.1869
0.063	0.074	130	21	44	42	1.60	0.1680
0.061	0.058	133	21	48	41	1.20	0.1474
0.065	0.095	122	21	41	43	1.91	0.1909
0.065	0.092	124	21	41	43	1.91	0.1881
0.064	0.085	127	21	42	42	1.77	0.1803
0.063	0.070	131	21	46	41	1.36	0.1633
0.065	0.093	123	21	40	44	1.94	0.1893
0.065	0.097	121	21	40	44	2.01	0.1931
0.065	0.094	122	21	41	44	1.94	0.1898
0.064	0.079	129	21	43	42	1.64	0.1736
0.065	0.117	112	15	37	44	2.79	0.2104
0.065	0.117	113	15	37	44	2.91	0.2103
0.065	0.116	113	15	37	44	2.74	0.2099
0.065	0.117	113	15	37	43	2.68	0.2103
0.065	0.117	113	15	37	43	2.71	0.2104
0.065	0.117	113	15	37	43	2.82	0.2105
0.065	0.093	125	22	41	44	1.93	0.1882
0.065	0.092	125	20	41	44	1.99	0.1874
0.064	0.087	127	19	42	43	1.98	0.1814
0.064	0.074	131	21	44	43	1.69	0.1676
0.065	0.093	123	24	41	44	2.02	0.1896
0.065	0.091	125	20	41	44	1.99	0.1869
0.065	0.093	124	18	41	44	1.93	0.1885
0.064	0.091	124	21	41	44	2.02	0.1865
0.064	0.091	124	21	41	44	1.98	0.1869
0.064	0.088	125	20	42	44	1.97	0.1835
0.063	0.070	132	21	45	42	1.60	0.1626
0.062	0.062	134	21	46	40	1.70	0.1523
0.061	0.051	133	20	51	38	1.25	0.1368
0.065	0.117	113	15	37	44	2.81	0.2102
0.065	0.116	113	15	38	44	2.78	0.2098

0.065	0.117	112	15	37	44	2.79	0.2100
0.065	0.116	112	15	35	40	2.53	0.2092
0.065	0.116	113	15	35	40	2.52	0.2091
0.065	0.116	113	15	35	40	2.55	0.2091
0.064	0.084	127	20	40	38	1.52	0.1784
0.064	0.081	129	20	41	38	1.46	0.1749
0.064	0.080	129	20	42	38	1.35	0.1738
0.064	0.077	130	20	42	37	1.29	0.1708
0.065	0.094	123	20	38	40	1.76	0.1899
0.065	0.091	124	20	39	40	1.73	0.1864
0.064	0.089	125	20	39	40	1.68	0.1846
0.064	0.078	129	20	42	38	1.33	0.1723
0.064	0.079	129	20	42	38	1.38	0.1729
0.064	0.083	128	20	41	39	1.52	0.1773
0.064	0.083	128	20	40	39	1.57	0.1779
0.062	0.064	133	20	44	37	1.28	0.1543
0.063	0.069	132	20	44	37	1.20	0.1611
0.063	0.070	132	20	44	37	1.17	0.1624
0.064	0.076	130	20	42	38	1.43	0.1702
0.061	0.057	133	20	47	36	1.05	0.1464
0.064	0.082	128	20	40	38	1.61	0.1765
0.063	0.078	129	20	41	38	1.53	0.1718
0.063	0.079	129	20	41	38	1.49	0.1726
0.063	0.073	131	19	43	38	1.43	0.1656
0.065	0.117	113	14	35	41	2.67	0.2092
0.065	0.117	114	14	35	41	2.53	0.2093
0.065	0.117	114	14	35	41	2.61	0.2094
0.064	0.085	127	20	40	40	1.59	0.1800
0.064	0.086	126	20	40	40	1.59	0.1811
0.063	0.071	132	20	43	38	1.33	0.1632
0.062	0.064	133	20	46	37	1.10	0.1543
0.064	0.085	127	20	41	40	1.55	0.1794
0.063	0.081	128	20	41	39	1.48	0.1752
0.063	0.082	128	20	41	40	1.43	0.1759
0.063	0.078	129	20	43	39	1.36	0.1714
0.064	0.086	126	20	40	40	1.61	0.1806
0.063	0.078	129	20	42	39	1.42	0.1714
0.062	0.069	131	20	44	38	1.32	0.1615
0.060	0.052	132	19	49	37	1.00	0.1386
0.064	0.091	123	20	39	40	1.80	0.1861
0.064	0.088	125	20	40	40	1.78	0.1826
0.063	0.087	125	20	40	40	1.65	0.1817
0.062	0.073	130	20	43	39	1.38	0.1660

0.064	0.091	123	20	40	41	1.65	0.1857
0.064	0.085	127	20	41	40	1.58	0.1795
0.064	0.086	127	20	41	41	1.68	0.1811
0.063	0.079	129	20	43	40	1.40	0.1728
0.065	0.117	114	15	36	42	2.48	0.2093
0.065	0.117	114	14	36	42	2.63	0.2092
0.065	0.117	113	14	36	42	2.53	0.2092
0.063	0.076	130	20	42	40	1.53	0.1703
0.063	0.076	130	20	43	40	1.50	0.1693
0.063	0.074	131	19	43	40	1.53	0.1676
0.062	0.063	133	19	45	39	1.31	0.1536
0.063	0.079	129	20	42	40	1.49	0.1734
0.063	0.081	128	20	42	41	1.54	0.1753
0.062	0.063	133	19	45	40	1.29	0.1538
0.060	0.054	132	19	48	39	1.15	0.1417
0.064	0.084	127	20	41	41	1.64	0.1793
0.064	0.084	127	20	41	40	1.59	0.1788
0.060	0.052	132	20	48	37	1.16	0.1392
0.059	0.045	130	20	51	36	0.96	0.1286
0.064	0.089	125	20	40	42	1.76	0.1844
0.063	0.084	127	20	41	40	1.60	0.1781
0.064	0.088	125	20	40	41	1.66	0.1825
0.063	0.075	130	20	43	40	1.40	0.1683
0.064	0.087	126	20	41	41	1.63	0.1815
0.064	0.087	126	20	40	41	1.67	0.1815
0.064	0.082	129	20	41	40	1.57	0.1758
0.061	0.057	133	20	48	38	1.11	0.1452
0.065	0.117	113	14	36	42	2.62	0.2087
0.065	0.117	113	14	36	42	2.61	0.2090
0.065	0.117	114	14	36	42	2.72	0.2089
0.064	0.085	127	20	41	41	1.53	0.1793
0.064	0.084	128	19	42	40	1.48	0.1782
0.064	0.082	128	20	42	41	1.57	0.1765
0.062	0.067	132	20	45	38	1.34	0.1585
0.064	0.090	125	20	40	42	1.74	0.1846
0.064	0.089	125	20	40	42	1.79	0.1835
0.064	0.087	126	20	40	41	1.64	0.1817
0.062	0.069	131	20	44	39	1.37	0.1618
0.064	0.090	124	20	40	42	1.76	0.1852
0.064	0.088	126	20	40	42	1.73	0.1827
0.064	0.085	127	20	41	41	1.69	0.1795
0.063	0.073	131	20	44	40	1.35	0.1658
0.064	0.095	122	20	39	42	1.79	0.1900

0.064	0.094	123	20	40	42	1.77	0.1889
0.064	0.091	124	20	40	42	1.70	0.1857
0.063	0.076	130	20	43	41	1.49	0.1694
0.064	0.083	128	20	41	41	1.61	0.1772
0.062	0.068	132	20	45	39	1.23	0.1603
0.063	0.071	131	20	44	39	1.27	0.1632
0.059	0.048	131	20	50	37	1.03	0.1337
0.065	0.116	113	14	36	42	2.68	0.2090
0.065	0.116	113	14	36	42	2.63	0.2089
0.065	0.116	113	14	36	42	2.60	0.2089
0.064	0.095	123	20	40	42	1.73	0.1904
0.064	0.095	122	20	39	42	1.73	0.1906
0.064	0.093	122	20	39	42	1.74	0.1884
0.064	0.081	129	20	42	39	1.45	0.1746
0.064	0.095	123	20	39	42	1.83	0.1900
0.064	0.095	122	20	40	42	1.74	0.1904
0.064	0.095	122	20	39	42	1.78	0.1898
0.064	0.093	123	20	40	42	1.72	0.1877
0.064	0.096	121	20	39	42	1.87	0.1917
0.064	0.096	122	20	39	42	1.85	0.1908
0.064	0.095	122	20	39	42	1.86	0.1899
0.064	0.086	126	20	41	40	1.66	0.1807
0.064	0.091	123	20	40	41	1.71	0.1863
0.064	0.092	123	20	40	41	1.72	0.1869
0.064	0.090	124	20	40	41	1.75	0.1850
0.064	0.088	124	20	40	40	1.66	0.1830
0.064	0.094	122	20	39	42	1.78	0.1894
0.064	0.095	122	20	39	42	1.79	0.1901
0.064	0.091	124	20	40	41	1.73	0.1861
0.064	0.088	125	20	40	40	1.70	0.1829
0.065	0.116	113	15	36	42	2.68	0.2088
0.065	0.116	113	15	36	41	2.60	0.2088
0.065	0.116	113	15	36	42	2.56	0.2087
0.064	0.094	122	20	39	41	1.77	0.1895
0.064	0.093	122	20	39	41	1.79	0.1881
0.064	0.090	124	20	40	41	1.73	0.1847
0.064	0.088	125	20	40	40	1.73	0.1832
0.064	0.102	118	20	38	43	1.95	0.1974
0.065	0.101	120	20	39	43	1.93	0.1965
0.065	0.096	122	20	39	42	1.81	0.1918
0.065	0.093	124	20	40	42	1.72	0.1886
0.064	0.091	125	20	40	41	1.76	0.1855
0.064	0.090	126	20	40	41	1.72	0.1847

0.064	0.089	126	20	40	41	1.71	0.1838
0.064	0.087	127	20	41	40	1.63	0.1822
0.064	0.091	125	20	40	41	1.76	0.1860
0.064	0.092	124	20	40	42	1.74	0.1872
0.064	0.092	125	20	40	42	1.79	0.1871
0.064	0.088	126	20	40	41	1.74	0.1830
0.064	0.098	122	20	39	43	1.85	0.1928
0.065	0.097	123	20	39	43	1.84	0.1917
0.065	0.099	121	20	39	43	1.90	0.1941
0.065	0.097	122	20	39	43	1.83	0.1926
0.065	0.117	114	15	36	42	2.59	0.2093
0.065	0.117	114	15	36	42	2.54	0.2090
0.065	0.117	113	15	36	42	2.57	0.2095
0.064	0.098	121	19	38	42	1.93	0.1927
0.064	0.100	119	18	39	43	1.82	0.1956
0.065	0.116	113	15	36	42	1.55	0.1969
0.065	0.116	113	15	35	42	1.62	0.2008
0.065	0.116	113	15	35	41	1.62	0.2011
0.064	0.093	122	22	39	42	1.78	0.1893
0.064	0.092	124	19	39	42	1.64	0.1833
0.063	0.081	127	26	41	41	2.93	0.1900
0.063	0.079	129	18	42	40	3.00	0.1893
0.064	0.088	125	18	40	41	2.79	0.1943
0.064	0.093	123	18	39	42		
0.064	0.088	125	19	40	41		
0.063	0.076	129	18	42	40		
0.064	0.090	124	18	40	41		
0.064	0.094	122	19	39	42		
0.064	0.092	124	18	39	42		
0.063	0.074	130	19	43	39		
0.064	0.091	124	21	40	42		
0.064	0.087	124	23	40	42		
0.064	0.087	124	23	40	42		
0.064	0.088	125	19	40	42		
0.064	0.094	122	20	39	42		
0.064	0.094	122	20	39	42		
0.064	0.093	122	20	39	42		
0.063	0.083	126	20	40	41		
0.065	0.116	113	15	36	42		
0.065	0.116	113	15	36	42		
0.065	0.116	113	15	36	42		

Table 6 Olivine phenocryst and standard statistics

	Chromian Augite, NMNH 164905			Kakanui Pyrope, USNM 143968			Augite 209		
	Average (N=8)	1 Sigma	ublished**	Average (N=9	Sigm	Published*	Average (N=9)	1 Sigma	Published*
SiO2	50.18	0.12	50.48	40.80	0.15	41.46	47.39	0.17	47.9
MgO	17.15	0.04	17.32	18.67	0.09	18.51	12.73	0.09	12.67
FeO	4.67	0.02	4.69	10.52	0.05	10.68	8.22	0.04	8.18
NiO2	0.049	0.006	n.a.	0.008	###	n.a.	0.008	0.005	n.a.
MnO	0.124	0.008	0.12	0.320	###	0.28	0.177	0.008	0.18
CaO	Standard	n.a.	17.30	5.11	0.02	5.17	18.51	0.07	18.36

	San Carlos Olivine, USNM 111312/44			
	Average (N=48)	1 Sigma		Published*
SiO2 %	40.85	0.09	0.17	40.81
MgO %	48.89	0.06	0.12	49.42
FeO %	9.70	0.04	0.08	9.55
NiO %	0.357	0.003	0.01	0.37
MnO %	0.131	0.002	0.00	0.14
CaO %	0.063	0.001	0.00	0.05
Fo #	90.0	0.03	0.06	90.2
Fe (ppm)	75409	299	597.06	74233
Mn (ppm)	1013	16	32.59	1084
Ni (ppm)	2808	20	40.38	2907
Ca (ppm)	452	7	14.69	357
Fe/Mn	74.5	1.11	2.23	68.5

Primary Standards:	
Si	Synthetic Ni2SiO4 (Boyd)
Mg	Synthetic Forsterite (Takei)
Fe	Synthetic Fayalite (Takei)
Ni	Synthetic Ni2SiO4 (Boyd)
Mn	Synthetic Tephroite (Takei)
Ca	Chromian Augite, USNM 164905

*Jarosewich et al., 1980
** All analyses of the RU SCOL standard at high currents and long count times over the last 4 years
***Jarosewich et al., 1987

Table 7 Standards used in olivine analysis

Sample Name	Citation	Classification	SiO2*	TiO2*	Al2O3*	Cr2O3*	FeO*	MnO*	MgO*	CaO*	Na2O*	K2O*
CS5	Callegaro et al. (2013)	Southern CAMP	47.28	1.00	15.11	0.05	12.69	0.19	9.82	9.49	2.47	0.62
CS8	Callegaro et al. (2013)	Southern CAMP	46.76	0.86	15.57	0.05	12.35	0.18	11.11	9.37	2.40	0.44
CS33	Callegaro et al. (2013)	Southern CAMP	48.00	0.54	15.47	0.09	10.73	0.18	10.76	11.41	1.78	0.13
CS49	Callegaro et al. (2013)	Southern CAMP	50.23	0.53	16.60	0.08	8.40	0.16	9.12	11.79	2.04	0.36
NEW136C	Merle et al. (2014)	Transitional CAMP	48.43	0.70	9.36	0.09	13.78	0.21	16.82	8.28	1.28	0.30
NEW136D	Merle et al. (2014)	Transitional CAMP	47.22	0.76	9.22	0.06	13.74	0.21	18.38	7.39	1.24	0.36
NEW17	Merle et al. (2014)	Transitional CAMP	50.44	0.90	11.37	0.12	10.90	0.18	12.91	10.06	1.62	0.58
OF 26	Callegaro et al. (2014)	Europe	49.97	0.81	13.34	0.07	9.80	0.17	10.90	11.98	1.51	0.34
OF 27	Callegaro et al. (2014)	Europe	49.97	0.91	13.10	0.06	10.43	0.18	10.62	11.66	1.46	0.42
GCY342	this study	Southern CAMP	47.49	0.58	16.23	0.08	10.34	0.18	10.62	10.59	1.91	0.36
GDH-271	this study	Southern CAMP	46.82	0.55	16.10	0.09	10.18	0.18	11.30	10.17	1.82	0.44
GDH-831	this study	Southern CAMP	47.07	0.53	15.53	0.11	10.52	0.18	13.21	9.90	1.72	0.37
R-4693	this study	Southern CAMP	47.40	0.56	16.32	0.10	10.60	0.18	11.92	10.37	1.88	0.32
SPY681/150812-4	this study	Southern CAMP	47.10	0.54	15.71	0.11	10.68	0.18	13.24	10.01	1.79	0.29

* original sample composition

Table 8 Original sample compositions used for calculated primary magmas

Sample Name	SiO2	TiO2	Al2O3	Cr2O3	FeO	MnO	MgO	CaO	Na2O	K2O	H2O	Fe2O3	Total	Fo	final mass relative to original mass	Olivine added %
CS5	48.31	0.73	9.24	0.00	12.17	0.21	19.31	6.88	1.08	0.53	0	1.50	99.95	0.89	1.00	0.4
CS8	52.43	0.85	12.90	0.00	8.38	0.15	11.48	10.54	1.73	0.50	0	0.95	99.92	0.89	1.06	6.3
CS33	48.23	0.60	13.95	0.00	9.81	0.17	14.20	9.43	1.93	0.38	0	1.16	99.86	0.89	1.04	3.9
CS49	46.93	0.52	14.28	0.00	10.44	0.18	14.99	9.31	1.78	0.33	0	1.17	99.93	0.89	1.09	8.8
NEW136C	50.25	0.85	10.99	0.00	10.19	0.17	14.54	9.58	1.60	0.59	0	1.14	99.89	0.89	1.09	9.2
NEW136D	47.82	0.75	8.73	0.00	12.56	0.20	19.76	7.04	1.13	0.46	0	1.49	99.94	0.89	1.05	4.6
NEW17	48.14	0.65	8.74	0.00	12.40	0.20	19.14	7.74	1.20	0.28	0	1.43	99.91	0.89	1.08	7.7
OF 26	47.57	0.74	9.01	0.00	12.47	0.21	19.67	7.22	1.21	0.35	0	1.49	99.94	0.89	1.04	3.7
OF 27	50.43	0.87	10.99	0.00	9.94	0.17	14.46	9.72	1.57	0.56	0	1.17	99.89	0.89	1.04	4.3
GCY342	47.64	0.54	15.26	0.00	9.61	0.17	13.53	9.95	1.79	0.34	0	1.08	99.92	0.89	1.08	8.0
GDH-271	47.50	0.54	15.61	0.00	9.48	0.17	13.48	9.86	1.76	0.43	0	1.10	99.91	0.89	1.06	5.5
GDH-831	47.30	0.52	15.37	0.00	9.56	0.18	13.93	9.80	1.70	0.36	0	1.16	99.89	0.89	1.02	1.8
R-4693	47.15	0.53	15.51	0.00	9.66	0.17	13.82	9.86	1.79	0.30	0	1.12	99.91	0.89	1.05	5.4
SPY681/150812-4	47.06	0.52	15.39	0.00	9.66	0.18	14.07	9.80	1.75	0.29	0	1.16	99.89	0.89	1.02	2.3

Table 9 Calculated primary magma